MULTIVARIABLE CONTROL FOR THE GE T700 ENGINE USING THE LQG/LTR DESIGN METHODOLOGY

by

WILLIAM H. PFEIL

B.S. UNIVERSITY OF TEXAS, ARLINGTON

(1980)

SUBMITTED IN PARTIAL FULFILLMENT

OF THE REQUIREMENTS FOR THE

DEGREE OF MASTER OF SCIENCE

at the

MASSACHUSETTS INSTITUTE OF TECHNOLOGY

JULY 1984

Signature of Author.....
Department of Mechanical Engineering, July 1984

Certified by.....
Professor M. Athans
Thesis Supervisor

Certified by.....
Professor H. A. Spang
Thesis Co-Supervisor

Accepted by.....
Chairman, Department Committee on Graduate Students

MULTIVARIABLE CONTROL FOR THE GE T700 ENGINE USING THE LQG/LTR DESIGN METHODOLOGY

by

WILLIAM H. PFEIL

Submitted to the Department of Mechanical Engineering on July 31, 1984 in partial fulfillment of the requirements for the degree of Master of Science in Mechanical Engineering.

ABSTRACT

The LQG/LTR design methodology is presented and applied to the control problem defined by the GE T700 turboshaft engine coupled to a helicopter rotor system. A series of linear models are presented and analized. Robustness and performance specifications are posed in the frequency domain. A SISO LQG/LTR compensator is derived and a performance comparison made with the current controller. The performance comparison displays the potential for significant performance improvement. The use of frequency dependent plots of the singular values of loop transfer function matrices are utilized in deriving and evaluating LQG/LTR compensators for two MIMO system definitions. Linear and selected non-linear transient evaluations of the compensated MIMO systems are presented. The evaluations demonstrate the applicability of the LQG/LTR design methodology to MIMO controller design and the utilization of the coordinated control of several variables to achieve performance not realizeable with conventional scalar controls.

THESIS SUPERVISORS: Dr. M. Athans, Professor of Systems Science and Engineering
Dr. H. A. Spang III, Adjunct Professor of Electrical Engineering

ACKNOWLEDGEMENTS

Without the patience, understanding and dedication of Professors Michael Athans and H. Austin Spang III, this thesis would not have been written. I thank them unendingly. I also want to acknowledge the considerable direction provided by the unsolicited help of Professor Gunter Stein, whose keen insight was key in providing direction and understanding. And to Samir Sayegh, of the General Electric Company, who made this research realizeable, and to Cindy Avagianos, for an excellent typing job, I convey my upmost appreciation.

Above all, I want to thank Margie, Emily and Andy - to whom I was all too often a stranger during the course of this work.

This research was carried out at the MIT Laboratory for Information and Decision Systems. Financial support was provided by the Aircraft Engine Group of the General Electric Company and the General Electric Corporate Research and Development Center.

TABLE-OF-CONTENTS

TABLE OF CONTENTS (cont'd)

LIST OF FIGURES

LIST OF TABLES

1. INTRODUCTION AND SUMMARY

1.1 Background

The control of turbine engines based on optimization techniques has received significant attention in the past decade [1,2]. A major portion of the attention has been focused on turbofan engine applications [3,4,5,6]. The most extensively studied turbofan engine is the Pratt & Whitney F100. While the potential for improved system performance has been amply demonstrated for turbofan engines, the utilization of optimization techniques for feedback control synthesis as applied to the turboshaft engine control problem has been limited [7], with no consideration given to a multivariable control law requiring the dynamic coordination of several control variables. The formulation of an optimal controller for a turboshaft engine, the GE T700, using the Linear Quadradic Gaussian/Loop Transfer Recovery (LQG/LTR) methodology, both for a single-input-single-output and multi-input-multi-output (referred to henceforth as SISO and MIMO respectively) system definition is presented in this work.

The definition "optimal" is often misleading. It is stressed at the outset that any controller will be optimal only in the sense that the designer specifies it to be. Fundamental physical laws and system constraints cannot be ignored or a mathematically "optimal" controller could be dangerous to the health of those in close proximity to the controlled system. The LQG/LTR methodology provides the necessary flexibility required in linear control design to meet system specifications while achieving recognized stability and

robustness properties [8,9,10]. The evaluation of the MIMO design on a conventional frequency domain basis utilizing singular value analysis of loop transfer function matrices and the application of the principle of robustness recovery, are instrumental in the utilization of the LQG/LTR methodology as a control synthesis tool for linear time-invariant multivariable feedback control systems.

The motivation for the exploration into a new control law for the GE T700 engine is that some limitations of the current SISO controller are becoming increasingly apparent. Emphasis on nap-of-the-earth helicopter maneuverability and pilot workload concerns have delineated a need for system performance improvement. Nap-of-the-earth maneuverability, which is critical to the success of military attack helicopter missions, involves obstacle avoidance at low altitude and high forward velocity. The pilot workload must be optimally split between payload deliverance and attention to helicopter maneuvering. Poor engine performance, or slow power supply by the engines to satisfy the helicopter power demand will degrade the maneuvering capability or handling quality of the helicopter. The helicopter pilot can overcome some maneuvering degradation by strict attention to the helicopter maneuvering controls. However, excessive pilot time spent on maneuvering due to poor engine performance renders a mission ineffective. Several studies [11,12] have begun to explore the important relationships between engine control and helicopter handling qualities. Gas turbine cycle limitations are also being challenged to the extent that more advanced control approaches are required to

achieve specified performance in the face of seemingly conflicting operational goals.

1.2 Research Scope

This research will apply the LQG/LTR design methodology to the turboshaft engine control problem. The control problem will be defined, a series of linear models formulated and analized, robustness and performance criteria defined, several controllers designed, and transient simulations performed on both a linear and non-linear basis. Performance comparisons between the current SISO controller design and a controller designed using the LQG/LTR methodology will be made. The resulting controller designs are not intended as final engineering designs, but rather as a feasibility study so as to display the applicability of the LQG/LTR methodology to the turboshaft engine and aircraft gas turbines in general, and support the need for further research.

1.3 Contributions

The primary intent and contribution of this thesis is to present a detailed example of the LQG/LTR methodology as applied to a gas turbine engine problem definition (both SISO and MIMO). This approach adopted is wholistic, i.e. it encompasses the entire design process from model formulation to compensator design and evaluation.

The first step, that of model formulation, is presented in terms of providing a nominal linear model representation that describes the low frequency system dynamics. The concept of frequency-dependent singular value

plots of a system transfer function matrix and some of the analytical tools available for examining the nominal linear model representation are introduced.

A novel method to quantify modeling error is presented. The modeling error is formulated as a frequency domain robustness test. Performance requirements are also posed on a frequency domain basis to be consistent with the LQG/LTR design methodology which heavily utilizes frequency domain interpretations of frequency-dependent singular value plots of a system transfer function matrix.

Finally, the feasibility of the LQG/LTR design methodology is demonstrated through actual compensator design and linear and non-linear transient simulations of the resulting feedback control systems.

Thus, the major theme of this thesis, which is to present the applicability of the LQG/LTR design methodology as applied to a gas turbine engine, is systematically developed and demonstrated.

1.4 Outline

In Chapter 2, the turboshaft engine/helicopter system is described in detail. A series of nominal linear models of the system are presented.

In Chapter 3, the system definitions and the specific design models to be utilized in controller design are presented. The concept of frequency-dependent singular value plots of a system transfer function matrix is introduced. The nominal linear model is examined in detail at specific operating conditions utilizing eigenvalue/eigenvector analysis, modal decomposition and the singular value decomposition. The quantification of

modeling error and the posing of performance requirements in the frequency domain are also presented in Chapter 3.

Chapter 4 introduces the LQG/LTR design methodology. Controller designs for each of the system definitions are presented. Linear and non-linear transient simulations for each system definition controller design are also presented in Chapter 4.

Finally, Chapter 5 contains a summary and some directions for further research.

2. SYSTEM DESCRIPTION AND MODEL FORMULATION

2.1 Introduction

The turboshaft engine/helicopter system is characterized by complex dynamics. These dynamics do vary across the operational envelope due to changes in engine power level and helicopter flight condition. The formulation of a linear time-invariant description of this coupled system as a prerequisite to the application of the LQG/LTR methodology is presented in this chapter. The rationale and procedure for the posing of a simplified dynamic model for controller design is stressed.

A description of the system is presented in Section 2.2. This will motivate the design process and clarify the performance requirements and specifications imposed on the system as outlined in Chapter 3.

The system model is best formulated by considering each subsystem separately. Section 2.3 begins with a brief description of the GE T700 turboshaft engine and its operational characteristics. The remainder of this section pertains to the turboshaft engines' state-space model formulation. The helicopter rotor subsystem is detailed in Section 2.4 which concludes with the coupled system description.

Thus, this chapter focuses on the important dynamic characteristics of the open-loop system and its modeling.

2.2 System Description

A conventional helicopter, as shown in Figure 2.1, utilizes a single main

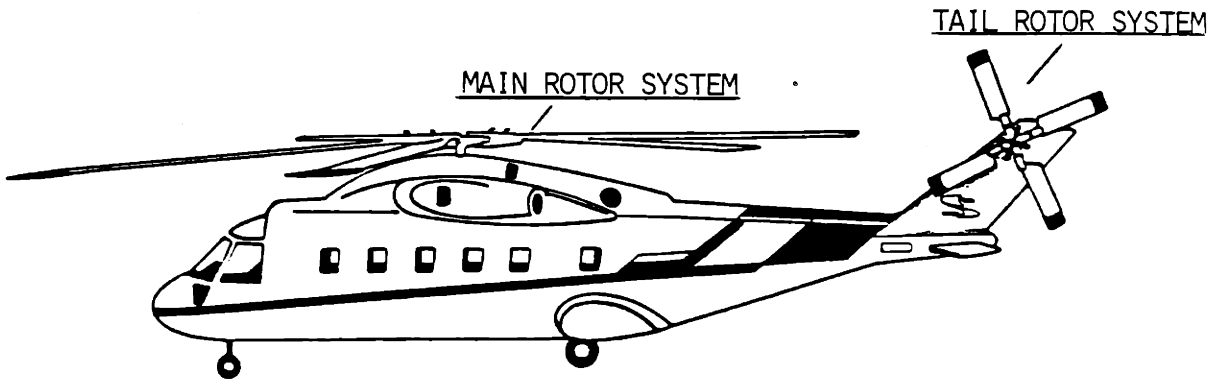

FIGURE 2.1: CONVENTIONAL SINGLE MAIN ROTOR HELICOPTER

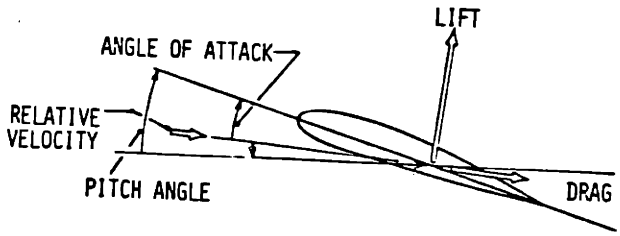

FIGURE 2.2: AIRFOIL AND VARIABLE DEFINITIONS

rotor primarily for lift and a tail rotor for torque reaction and directional control in the yaw degree of freedom. The use of two engines is common due to survivability motivations.

The main and tail rotor blades, the number and design of which vary from application to application, are airfoils that provide lift or thrust according to the laws of aerodynamics. As shown in Figure 2.2, an airfoil provides lift as a function of its angle of attack and relative velocity, among other things (i.e. air density, chord length, etc.). The helicopter is unique in aviation in that the airfoils rotate continuously, thus changing the relative velocity about the azimuth. This effect is compensated for in the main rotor by the introduction of flexible dynamics [13]. The flexible dynamics equilibrate the angles of attack of the main rotor blades and, therefore, lift about the azimuth. These flexible compliant "flapping" dynamics, as they are commonly referred to, are underdamped. The engine can excite rotor compliant dynamics because the engine is directly coupled to the drive train of which the rotors are a part of.

The summation of the lift emanating from all main rotor blades can be considered to be characterized by a single lift vector originating at the main rotor hub. This same generalization is made for the tail rotor system, where the composite vector is considered to be a thrust vector because of its principle line of action. The depiction of this generalized system is shown in Figure 2.3.

A pilot maneuvers the helicopter in six degrees of freedom by modulating the lift and thrust vector magnitudes and the lift vector orientation. A

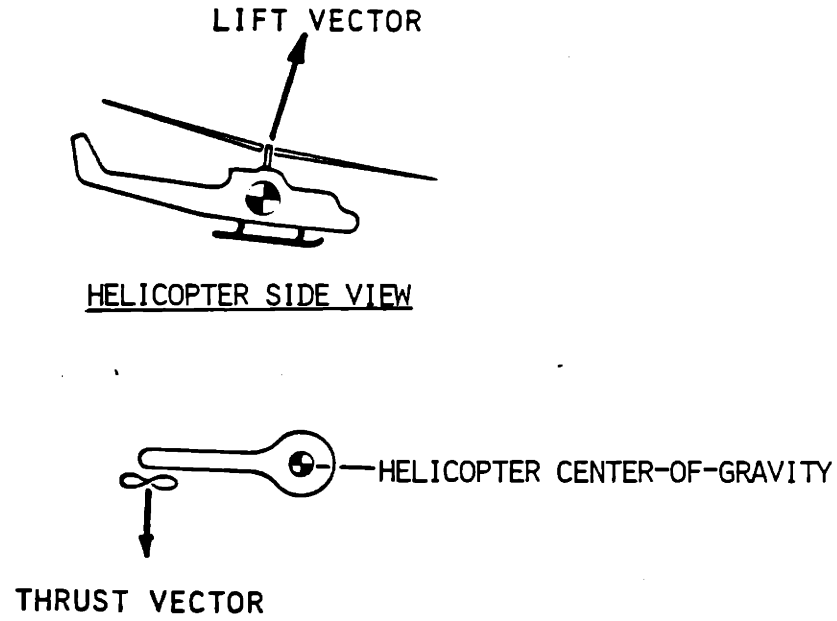

FIGURE 2.3: HELICOPTER LIFT AND THRUST VECTORS

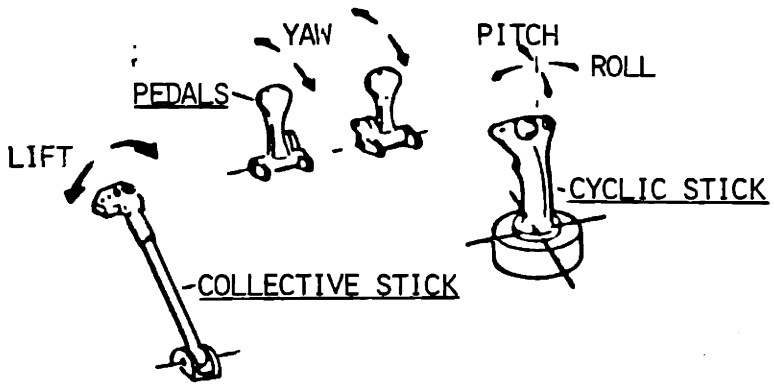

FIGURE 2.4: HELICOPTER PILOT CONTROLS

conventional helicopter provides three control interfaces to the pilot as shown in Figure 2.4. The collective stick position changes the pitch or effective angle of attack of the main rotor blades and thus the magnitude of the lift vector. The cyclic stick position changes the lift vector orientation by tilting the entire rotation plane of the main rotor. Directional control in the yaw degree of freedom is provided by a change in magnitude of the tail rotor thrust vector by changing tail rotor blade pitch via a differential pedal input. A helicopter pilot is a very busy person relying on instinct ingrained through intense training. The pilot is the loop closer on an inherently unstable open-loop system.

Purposely glossed over until the present discusson was elaboration of the fact that both lift and thrust is directly influenced by the relative speed of the airfoils. The "and" is applicable because the main and tail rotors are directly geared to the engines and cannot rotate independently. The pilot will influence the speed of the airfoils indirectly through his maneuvering control interfaces by demanding changes in the lift and/or thrust vector magnitudes. A pilot demand for a change in the lift or thrust vector magnitude is equivalent to producing a load disturbance on the rotor systems. It is desireable to provide constant rotor speed control independent of pilot attention because of his workload situation. The engines must provide constant speed control within the compliant rotor system constraints, basic gas turbine cycle limitations and in the presence of upsetting load disturbances to the main and tail rotor systems produced by pilot demands for

changes in the lift or thrust vector magnitudes or from sources such as wind gusts. A "fast" or "tight" speed control will prevent degradation in lift, directional control and coincidentally, component and pilot stress levels.

2.3 Turboshaft Engine Model

2.3.1 GE T700 Engine Description

The engine utilized in this stuay is the GE T700, shown in Figure 2.5, as representative of a recent technology turboshaft engine in current production. All gas turbines convert the energy of expanding gases created by a compression/combustion process into useful work through turbomachinery. The thermodynamic description of this process is given by the Brayton Cycle [14]. In general, any energy not required to sustain the compression/combustion process is converted into useful work. The turboshaft engine recovers the useful energy in the form of shaft horsepower to drive the helicopter main and tail rotor systems.

A simplified cross-section of the GE T700 turboshaft engine is shown in Figure 2.6. The engine has two turbo-machinery components, the gas generator and the free turbine. The gas generator extracts energy from the hot gas stream using a high pressure turbine to rotate a compressor thus providing the high pressure air for the combustor. The free turbine enjoys a one-way coupling to the gas turbine cycle (i.e. it only extracts energy). It is the free turbine, when directly coupled to the helicopter rotor system, that recovers the useful work of the gas turbine cycle. The responsibility of the gas generator is to supply the power requested by the helicopter rotor system at a specified free turbine speed.

The turboshaft engine is required to run efficiently in a steady-state condition from idle to full power over a wide range of air densities and temperatures. Efficient operation is most often defined as minimum fuel

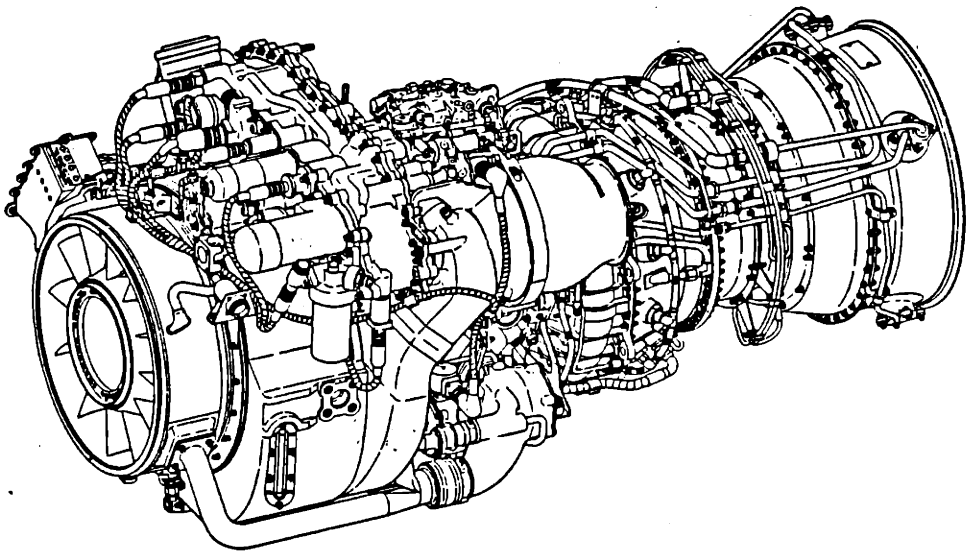

FIGURE 2.5: GE T700 TURBOSHAFT ENGINE

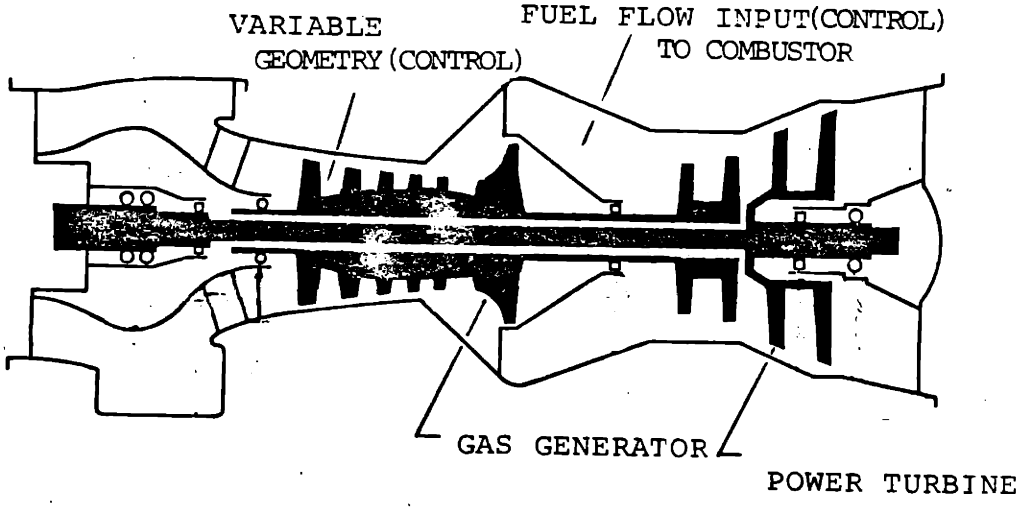

FIGURE 2.6: GE T700 SIMPLIFIED CROSS SECTION

consumption at a given power level. The range of ambient conditions over which an engine must operate, and the requirements on engine efficiency demand engine cycle changes that are most often realized by variation of compressor geometry. A small turboshaft engine, such as the GE T700, may have several stages of axial compressor stator variable geometry. This variable geometry control variable modulates the effective nozzle area as shown in Figure 2.7, thus realizing a variation in engine efficiency by changing airflow characteristics. The location of this variable geometry on the engine is displayed in Figure 2.6. This location, near the inlet of the engine, controls mass airflow. The variable geometry provides a powerful tool over cycle efficiency, and its effect, as reflected in several parameters, identifies a potential control variable in addition, of course, to the fuel flow control variable.

The turboshaft engine, in common with the operational requirements of all aircraft gas turbines, must accelerate and decelerate rapidly without experiencing stall or surge phenomena. Any occurance of stall may be accompanied by a loss in power and the potential for engine component and structural damage. Stall boundaries are approximately defined and engine transient operation in close proximity to these boundaries is prevented by hard control limits.

Modern gas turbine engines operate close to their thermal and material limits. Excursions above defined temperature limits and excessive turbine speeds will quickly lead to engine destruction. Aviation applications must be

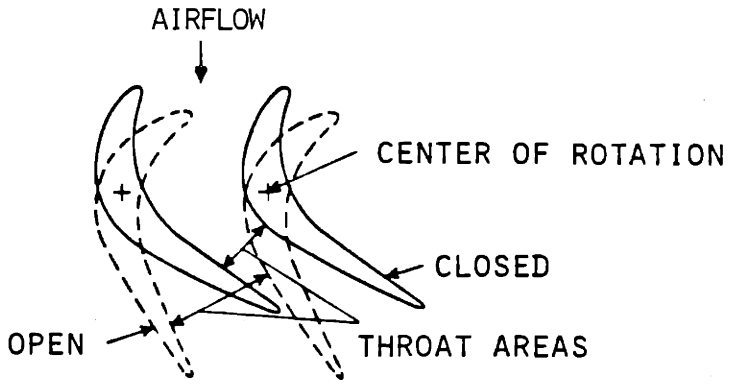

FIGURE 2.7: VARIABLE STATOR COMPRESSOR GEOMETRY

particularly sensitive to these constraints, as the potential for loss of life is a real possibility.

The operational requirements for the free turbine engine are summarized below. The engine must

1. Maintain constant power turbine speed in the presence of load disturbances*1 to the helicopter rotor system,
2. Not provide input energy to excite helicopter drive train torsional modes,
3. Maintain adequate stall margin,
4. Limit temperature, turbine speeds, torque, and
5. Operate at peak efficiency.

This research will examine the feasibility of the LQG/LTR methodology in the formulation of a control system that meets the above operational requirements.

---

*1 Load disturbances occur, as detailed earlier, because of pilot maneuvering or aerodynamic disturbances such as wind gusts.

2.3.2 Engine Model Formulation

Turbine engine dynamics are described by non-linear equations relating state variables $\underline{x}(t)$, control variables $\underline{u}(t)$, output and ambient variables $\underline{\theta}$ in the form,

$$\frac{d}{dt}\ \underline{x}(t) = \underline{f}(\underline{x}(t),\underline{u}(t),\underline{\theta}) \tag{2.1a}$$

$$\underline{y}(t) = \underline{g}(\underline{x}(t),\underline{u}(t),\underline{\theta}) \tag{2.1b}$$

The state variables are associated with energy storage elements and for the gas turbine system are temperatures, pressures and inertia terms. The control inputs for a gas turbine are fuel flows and variable geometries. The outputs are generally turbine speeds, pressures, pressure ratios and gas temperatures. The ambient variables are ambient pressure and temperature ratios.

Prior to the formulation of an LQG/LTR controller, the non-linear dynamic description given by Eq(2.1) must be converted to a linear dynamic model. A linearization will provide a linear time-invariant model pertinent to operation about an equilibrium operating condition. This equilibrium condition is characterized by $\underline{\theta}$ and the steady-state values of the state, control and output variables ($\underline{x}_o$, $\underline{u}_o$, $\underline{y}_o$). The linear, time invariant, constant coefficient model utilized in this research is of the form

$$\frac{d}{dt}\ \delta\underline{x}(t) = \underline{A}\delta\underline{x}(t) + \underline{B}\delta\underline{u}(t) \tag{2.2a}$$

$$\delta\underline{y}(t) = \underline{C}\delta\underline{x}(t) + \underline{D}\delta\underline{u}(t) \tag{2.2b}$$

where

$$\underline{A} = \frac{\partial \underline{f}}{\partial \underline{x}}\bigg|_{\substack{\underline{x}_o \\ \underline{u}_o}} ; \quad \underline{B} = \frac{\partial \underline{f}}{\partial \underline{u}}\bigg|_{\substack{\underline{x}_o \\ \underline{u}_o}}$$

$$\underline{C} = \left.\frac{\partial \underline{g}}{\partial \underline{x}}\right|_{\underline{x}_o} \quad ; \quad \underline{D} = \left.\frac{\partial \underline{g}}{\partial \underline{u}}\right|_{\underline{u}_o}$$

and

$$\delta\underline{x}(t) = \underline{x}(t) - \underline{x}_o$$
$$\delta\underline{y}(t) = \underline{y}(t) - \underline{y}_o$$
$$\delta\underline{u}(t) = \underline{u}(t) - \underline{u}_o$$

The partial derivative coefficient matrices in Eq(2.2) were calculated on an unbalanced torque basis using a full non-linear component simulation of the GE T700 engine provided by the Aircraft Engine Division of the General Electric Company of Lynn, Ma. This was accomplished by satisfying engine cycle constraints for suitable state and input pertubation magnitudes realized in succession while holding all other state and input variables fixed at their constant steady-state values. The partial derivatives are approximated by

$$\frac{\partial q}{\partial r} \simeq \frac{\Delta q}{\Delta r}$$

Where q = dependent variable

r = independent or perturbed variable.

The GE T700 state-space description realized in this manner is given in Table 2.1.

The objective in model formulation is to establish a nominal representation of the open-loop system, or plant, in the low frequency region where performance specifications are imposed. Coincident with this is the

TABLE 2.1: LINEAR ENGINE STATE DESCRIPTION

$$\frac{d}{dt}\begin{bmatrix} N_g(t) \\ N_p(t) \end{bmatrix} = \begin{bmatrix} \frac{\partial Q_g}{\partial N_g}\frac{1}{J_g} & \frac{\partial Q_g}{\partial N_p}\frac{1}{J_g} \\ \frac{\partial Q_p}{\partial N_g}\frac{1}{J_{pt}} & \frac{\partial Q_p}{\partial N_p}\frac{1}{J_{pt}} \end{bmatrix}\begin{bmatrix} N_g(t) \\ N_p(t) \end{bmatrix} + \begin{bmatrix} \frac{\partial Q_g}{\partial W_f}\frac{1}{J_g} & \frac{\partial Q_g}{\partial V_g}\frac{1}{J_g} \\ \frac{\partial Q_p}{\partial W_f}\frac{1}{J_{pt}} & \frac{\partial Q_p}{\partial V_g}\frac{1}{J_{pt}} \end{bmatrix}\begin{bmatrix} W_f(t) \\ V_g(t) \end{bmatrix}$$

$$\underline{Y}(t) = \begin{bmatrix} N_g(t) \\ N_p(t) \\ P_3(t) \\ T_{4.5}(t) \end{bmatrix} = \begin{bmatrix} 1 & 0 \\ 0 & 1 \\ \frac{\partial P_3}{\partial N_g} & 0 \\ \frac{\partial T_{4.5}}{\partial N_g} & 0 \end{bmatrix}\begin{bmatrix} N_g(t) \\ N_p(t) \end{bmatrix} + \begin{bmatrix} 0 & 0 \\ 0 & 0 \\ \frac{\partial P_3}{\partial W_f} & \frac{\partial P_3}{\partial V_g} \\ \frac{\partial T_{4.5}}{\partial W_f} & \frac{\partial T_{4.5}}{\partial V_g} \end{bmatrix}\begin{bmatrix} W_f(t) \\ V_g(t) \end{bmatrix}$$

VARIABLE DEFINITIONS

N_g = Gas Generator Speed, RPM

N_p = Power Turbine Speed, RPM

Q_g = Gas Generator Gas Torque, ft-lbs

Q_p = Power Turbine Gas Torque, ft-lbs

J_g = Gas Generator Inertia, ft-lb-sec/RPM

J_{pt} = Power Turbine Inertia, ft-lb-sec/RPM

W_f = Fuel Flow Input, lb/hr

V_g = Variable Geometry Input, degrees

P_3 = Compressor Discharge Pressure, psi

$T_{4.5}$ = Inter-turbine Gas Temperature, degrees R

quantification of the model uncertainty errors that become dominant at high frequencies. This uncertainty description will be presented in Chapter 3, and is crucial in the design process in order to guarantee the closed-loop stability of the actual system and not only of the nominal mathematical model.

To achieve a practical and implementable design, the order of the design model was determined by analysis of the desired controller function as compared to the dominant system dynamics. To pursue this goal, dynamics in the frequency range of 0-40 rad/sec were examined for inclusion in the model. Two control variables, fuel flow, W_f, and compressor variable geometry, V_g, were used, to independently control two output variables (to be discussed later).

For small pertubations, the low frequency (<10 rad/sec) GE T700 engine dynamics are dominated by the gas generator and power turbine dynamics. Pressure and temperature dynamics appearing in the flow equations are typically "fast" for a small turboshaft engine and are included in the model only as outputs thus neglecting their dynamics. The temperature and pressure outputs considered are $T_{4.5}$, inter-turbine gas temperature, and P_3, compressor discharge pressure. These variables are measured variables on the GE T700 engine and were thus chosen as outputs. Turbine metal case and blade temperature dynamics, although low frequency in nature (~2-5 rad/sec), were excluded due to their uncertain description and generically uncoupled behavior [15]. The reduced engine state vector for design purposes is thus given simply by the two turbine speeds, denoted by N_p and N_g.

The specific output definitions for various control schemes will be presented in Chapter 3. The linear model described by Table 2.1 is valid for small pertubations about a defined equilibrium condition. Linear models were generated at six (6) equilibrium conditions representing engine operation from flight idle to maximum continous power. The operating conditions are characterized by engine output power level as denoted by percent of design gas generator speed. The operating conditions used for model generation are 73.7, 83., 90., 95., 97.2 and 100% N_g. The numerical results of the model generation are given in Appendix A1. The effect of operating point changes on controller design and performance will be demonstrated in Chapter 4.

Variable geometry actuation dynamics are modeled by a first order lag at 10 rad/sec. Fuel flow metering valve dynamics were fast (>50 rad/sec) with respect to the frequency range of interest and, hence, are neglected in the design model. The $T_{4.5}$ sensor dynamics are modeled as a first order lag with a changing time constant dependent on operating conditions. The $T_{4.5}$ sensor time constant is tabulated in Appendix A2.

2.4 Helicopter Drive Train Model Formulation

The helicopter drive train compliant dynamics must be represented in the system model because they are present in the desired engine response bandpass (≤ 10 rad/sec). A representative helicopter drive train is shown isometrically in Figure 2.8. The lumped parameter, spring-mass-damper representation of this system is shown in Figure 2.9. This lumped parameter model can be considerably simplified through eigenvalue/ eigenvector analysis.

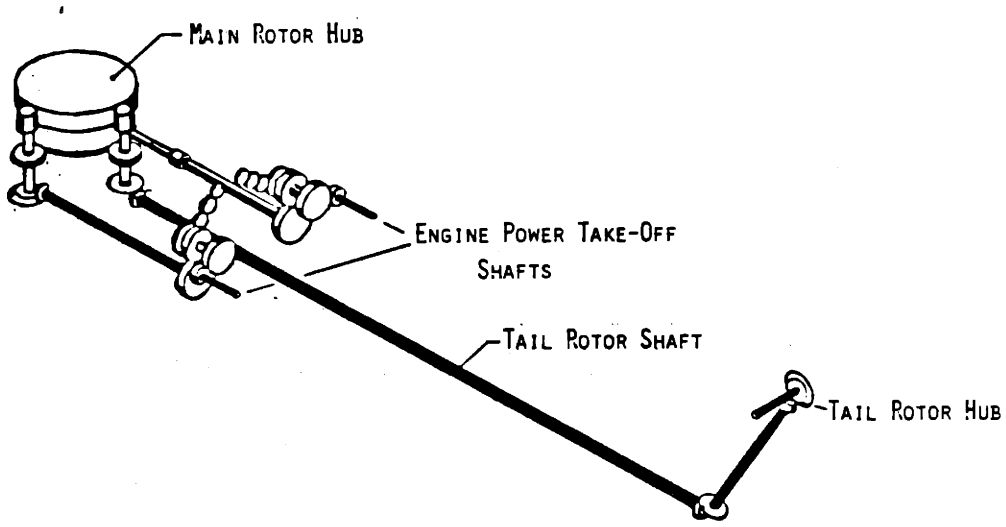

FIGURE 2.8: HELICOPTER DRIVE TRAIN ISOMETRIC DIAGRAM
(MAIN AND TAIL ROTOR BLADES NOT SHOWN)

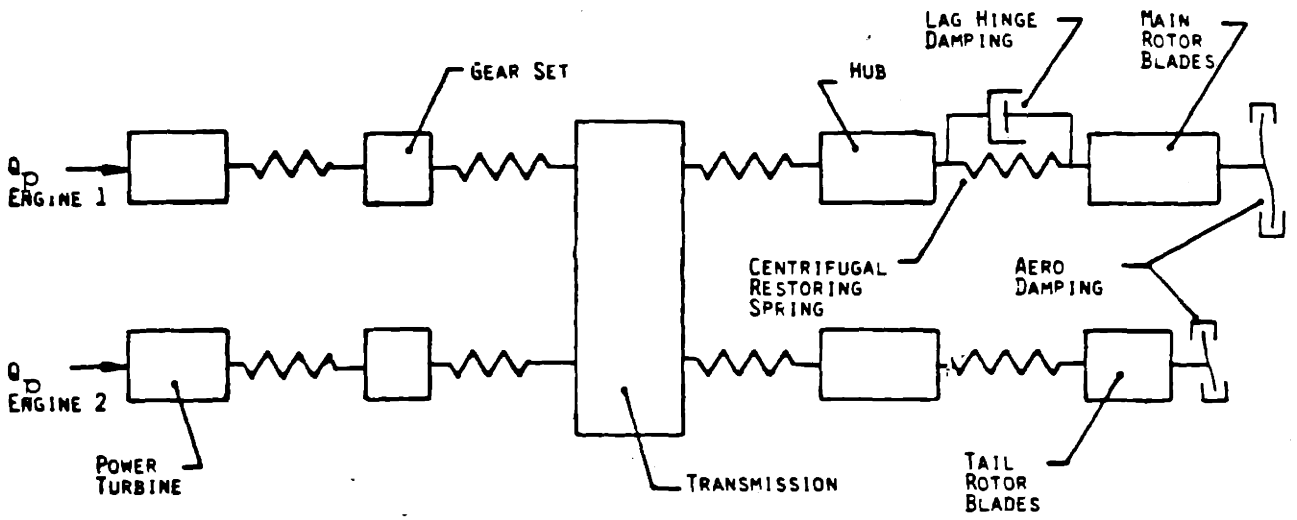

FIGURE 2.9: LUMPED PARAMETER ROTOR SYSTEM REPRESENTATION OF SYSTEM IN FIG. 2.8

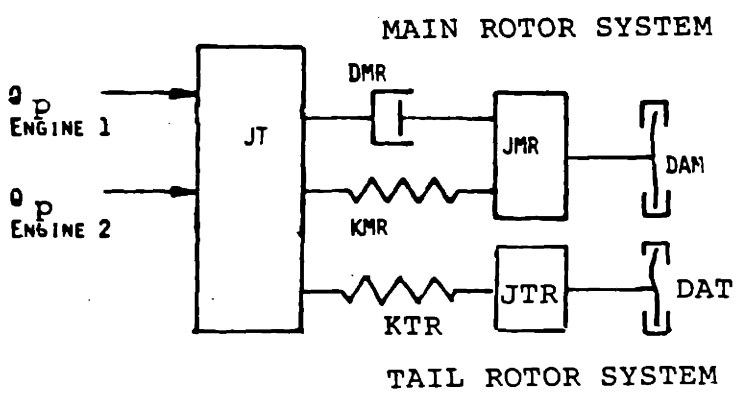

FIGURE 2.10: REDUCED MODEL OF FIG. 2.9

An eigenvalue/eigenvector analysis identifies high frequency rotor system dynamics and the associated spring and inertia elements. The springs associated with high frequency dynamics are relatively stiff and can be neglected. The connected inertia elements are collapsed, or summed, and the low frequency dynamics are faithfully represented. The dynamics of the rigid shaft and main and tail rotor resonant modes are preserved in the design model. The resultant model is presented in Figure 2.10. The numerical values of the rotor system parameters utilized for model generation are given in Appendix A3.

2.5 Turboshaft Engine/Helicopter Drive Train Model

The helicopter drive train model utilized in this research incorporates two turboshaft engines. The helicopter drive train is coupled at the turboshaft engines only through the gas path. The gas path connection is shown in Figure 2.10 as Q_p, which is the gas torque produced by the engine and applied at the power turbine. Q_p is defined by the linear model of the turboshaft engine which is presented in Table 2.1. The power turbines are directly connected to the rotor system and both power turbine inertias are represented in the lumped inertia J_T. The separate representations of the turboshaft engine and helicopter drive train can be combined into the parametric description of the coupled system presented in Table 2.2. A block diagram representation of the coupled system is shown in Figure 2.11.

TABLE 2.2: COUPLED SYSTEM STATE DESCRIPTION

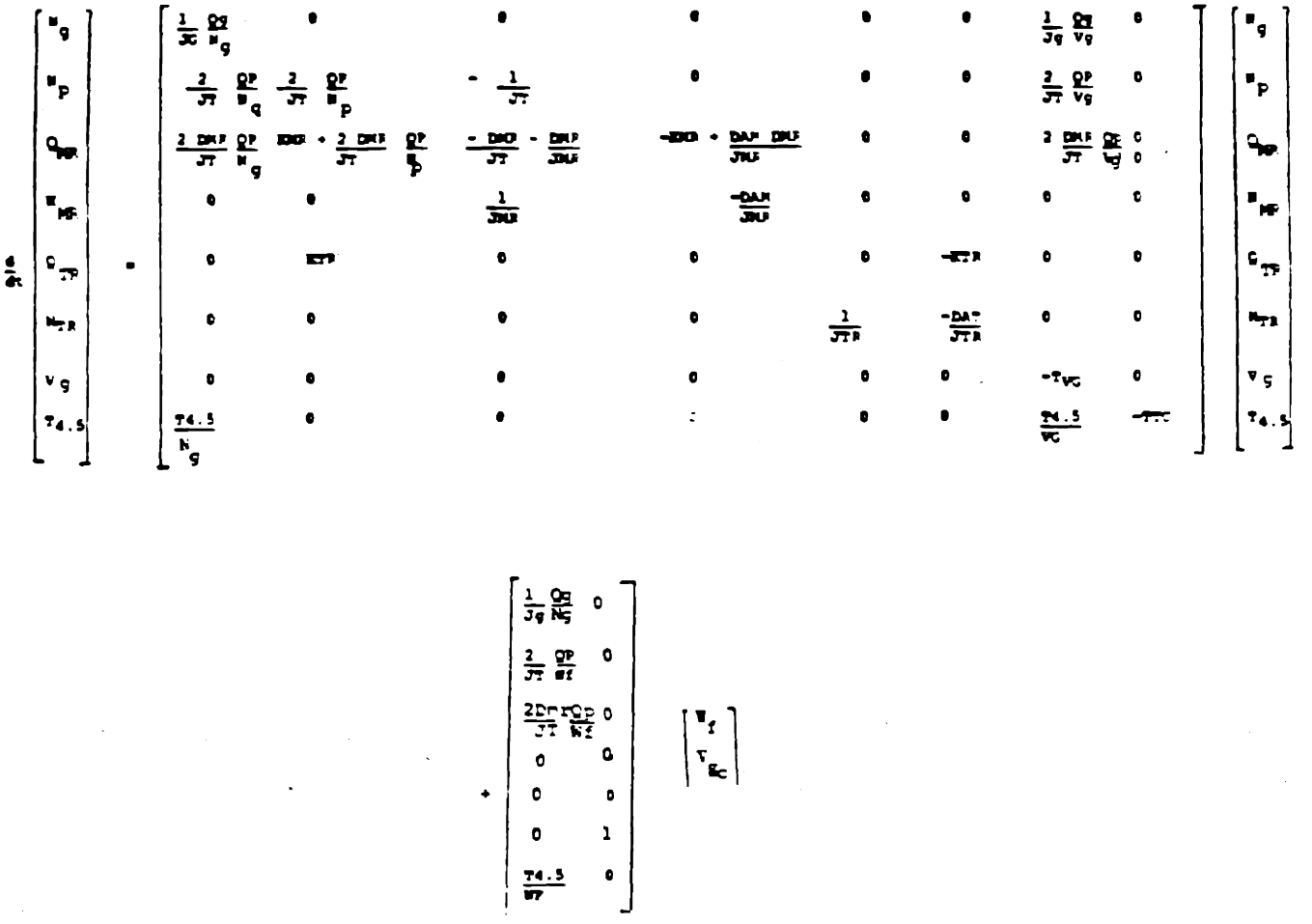

VARIABLE DEFINITIONS

N_g = Gas Generator Speed, RPM

N_p = Power Turbine Speed, RPM

W_f = Fuel Flow, lb/hr

V_g = Variable Geometry Position, degrees

Q_{MR} = Main Rotor Torque, ft-lbs

N_{MR} = Main Rotor Speed, RPM

Q_{TR} = Tail Rotor Torque, ft-lbs

N_{TR} = Tail Rotor Speed, RPM

$T_{4.5}$ = Interturbine Gas Temperature, degrees R

Q_g = Gas Generator Gas Torque, ft-lbs

Q_p = Power Turbine Gas Torque, ft-lbs

J_g = Gas Generator Inertia, ft-lb-sec/RPM

J_T = Lumped Drive Train Inertia, ft-lb-sec/RPM

D_{MR} = Main Rotor Damping, ft-lbs/RPM

K_{MR} = Main Rotor Spring Constant, ft-lbs/RPM-sec

J_{MR} = Main Rotor Inertia, ft-lb-sec/RPM

D_{AT} = Tail Rotor Aerodynamic Damping, ft-lbs/RPM

D_{AM} = Main Rotor Aerodynamic Damping, ft-lbs/RPM

K_{TR} = Tail Rotor Spring Constant, ft-lbs/RPM-sec

T_{VG} = Variable geometry Actuator Time Constant, 1/sec

T_{TC} = Thermocouple Time Constant, 1/sec

V_{gc} = Variable Geometry Input Command, degrees

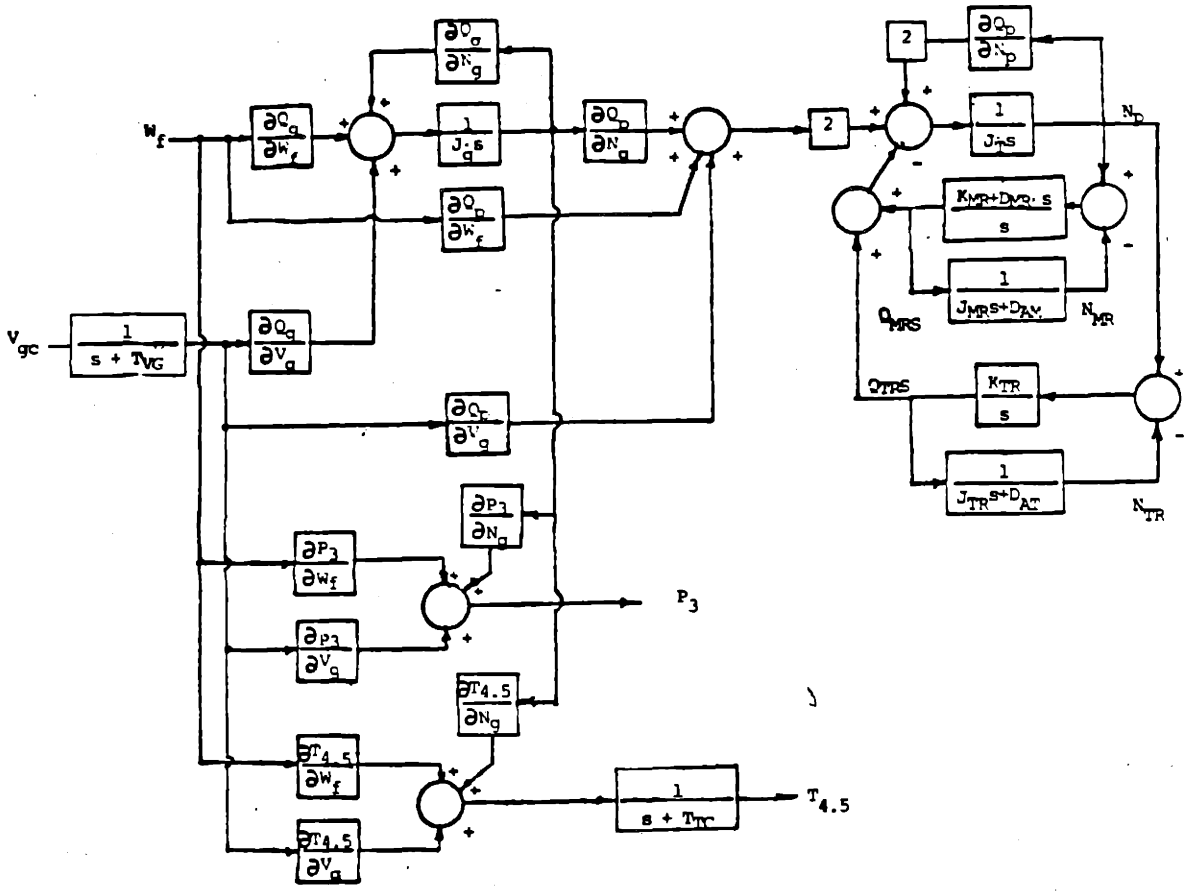

FIGURE 2.11: BLOCK DIAGRAM REPRESENTATION OF COUPLED SYSTEM

2.6 Summary

The turboshaft engine/helicopter system has been described in this Chapter. The presentation of the total system, and the separate description of the helicopter rotor and turboshaft engine subsystems has provided insight into the physical requirements on system operation. The operational requirements of the turboshaft engine/helicopter system were defined. The physical insight obtained in this chapter motivates the posing of realistic design specifications which will be developed in Chapter 3.

The formulation of a series of nominal low frequency linear models of the turboshaft engine representing the full range of operating conditions was accomplished. The linear turboshaft engine model was coupled to a representative helicopter drive train model to provide a design model that captures the low frequency (< 40 rad/sec) dynamics of the system.

Chapter 3 will examine in detail the nominal linear model representation and modeling errors to further explore the nature of the physical system and to understand the implications of a closed-loop control law.

3. MODEL ANALYSIS, ROBUSTNESS REQUIREMENTS AND DESIGN SPECIFICATIONS

3.1 Introduction

The modeling procedure decomposes a non-linear, infinite-dimensional and inherently uncertain physical process into a linear, finite-dimensional nominal design model valid over a defined frequency range. The control problem is to take this necessarily simple design model and provide closed-loop stability of the physical system (not just the mathematical model!) while achieving increased system performance [16]. This chapter will provide the basis for the derivation of a meaningful control law through the detailed analysis and interpretation of the linear models presented in Chapter 2. Performance specifications will also be posed.

The nominal linear model will be analyzed in Section 3.2. The input-output definitions will be presented. The use of eigenvalue/eigenvector analysis, matrix residue expansion and an interpretation of the singular value decomposition are shown to provide insight into the nature of the physical process. The limitations of the linear model will be examined in Section 3.3 and appropriate bounds on the modeling errors in the frequency domain will be generated. Design specifications are delineated in Section 3.4.

3.2 Linear Model Analysis

3.2.1 Input-Output Definitions

Three system definitions will be examined in this research. The first is a conventional SISO system with scalar fuel flow control and a single scalar output, the power turbine speed. With two available control inputs, fuel flow and variable geometry position, control over two distinct output variables is realizable. The second system definition (MIMO System I) explores the control of power turbine speed and gas generator speed. The third system definition (MIMO System II) represents an exploration into the simultaneous control of power turbine speed and inter-turbine gas temperature.

The control of power turbine speed is required to satisfy the fundamental system requirement of a commanded power supply to the helicopter rotor systems. The simultaneous control of both the power turbine and gas generator speeds is undertaken to explore the utilization of this control system definition for both input and output disturbance rejection as compared to a SISO controller. The simultaneous control of turbine temperature allows a potential handle on dynamic engine operational efficiency and provides some latitude in temperature limiting.

The input-output definitions are summarized in Table 3.1. Linear controller design will be performed for each system definition in Chapter 4. The linear model utilized for each design, as denoted by the power level or % N_g, is also presented in Table 3.1. The 90% N_g power level was chosen as the SISO Design Model because it is representative of normal operating power.

TABLE 3.1: SYSTEM DEFINITIONS

DESCRIPTION	CONTROLS	OUTPUT	OPERATING CONDITION(S) FOR DESIGN MODEL
SISO (see Appendix B1)	W_f Only	N_p Only	90% N_g (SISO)
MIMO SYSTEM I (see Appendix B2)	W_f and V_g	N_p and N_g	83% N_g (MIMO)
MIMO SYSTEM II (see Appendix B3 and B4)	W_f and V_g	N_p and $T_{4.5}$	90%, 95% N_g (MIMO)

The 83% N_g Design Model was used for the MIMO System I design to examine the implications of a MIMO control law at a low power level. The 90 and 95% N_g Design Models were chosen for MIMO System II because they are representative of normal operating power. The numerical state-space description of the design models are presented in Appendix B.

3.2.2 Pole-Zero Structure of Design Models

The poles and zeros of each design model are tabulated in Table 3.2. The zeros for the multivariable system definitions are the transmission zeros [17].

The non-minimum phase transmission zero in the 90% N_g MIMO System II Design Model at .199 rad/sec will be shown in Chapter 4 to present a fundamental system performance restriction.

3.2.3 Open-loop Frequency Response of Design Models

It is now necessary to introduce notion of singular values of a n x n complex valued matrix $\underline{A}$, denoted by $\sigma_i(A)$, i =1,2...n. The singular values are defined as

$$\sigma_i(\underline{A}) = \sqrt{\lambda_i(\underline{A}^H \underline{A})} \qquad (3.1)$$

and they are all non-negative. The "H" in Eq(3.1) signifies the Hermitian or complex conjugate transpose.

TABLE 3.2: POLE-ZERO STRUCTURE OF DESIGN MODELS

SYSTEM DEFINITIONS	DESIGN MODEL	POLES	ZEROS
SISO	90% N_g (SISO)	- .526 -3.64 -5.07 $\pm$j15.8 - .62$\pm$j404	-7.37 -.86$\pm$j6.84 -.18$\pm$j34.2
MIMO SYSTEM I	83% N_g (MIMO)	- .482 -1.92 -10.0 -4.97$\pm$j15.8 - .56$\pm$j40.4	- .84$\pm$j6.85 - .18$\pm$j34.2
MIMO SYSTEM II	90% N_g (MIMO)	- .526 -2.2 -3.64 -10.0 -5.07$\pm$j15.8 - .62$\pm$j40.4	.199 -.85$\pm$j6.85 -.18$\pm$j34.2
	95% N_g (MIMO)	- .602 -2.0 -6.23 -10.0 -5.25$\pm$j15.7 - .70$\pm$j40.4	-1.42 - .98$\pm$j7.74 - .18$\pm$j34.2

Consider the time domain description of a MIMO system.

$$\frac{d}{dt}\underline{x}(t) = \underline{A}\,\underline{x}(t) + \underline{B}\,\underline{u}(t) \tag{3.2a}$$

$$\underline{y}(t) = \underline{C}\,\underline{x}(t) + \underline{D}\,\underline{u}(t) \tag{3.2b}$$

The control-to-output transfer function matrix $\underline{G}(s)$ is

$$\underline{G}(s) = \underline{C}(s\underline{I}-\underline{A})^{-1}\underline{B} + \underline{D} \tag{3.3}$$

In the frequency domain ($s=j\omega$) the singular values of $\underline{G}(j\omega)$ characterize the input-to-output behavior of the system. A complete development of the singular value concept is outside the scope of this work and the reader is referred to an extensive development presented by Athans [18]. Concisely, a frequency dependent plot of the singular values of a MIMO system transfer function is an extension of a Bode plot used for SISO systems. The minimum and maximum singular values, as defined by Eq(3.1) of a MIMO system transfer function, provide magnitude bounds on the input-to-output relationship. This is a fact that will be elaborated on in Section 3.4 in posing performance specifications.

Singular value plots (frequency-dependent) of the open-loop transfer functions of the design models are shown in Figures 3.1 - 3.4. These singular value plots depict open-loop dynamics.

The singular value plot for the SISO system definition shown in Figure 3.1 is simply the magnitude portion of a Bode plot. The effect of the main and tail rotor dynamics are clearly shown in Figure 3.1 as typical resonant peaks.

Figure 3.2 is the singular value depiction of the open-loop transfer function of MIMO System I, 83% N_g Design Model (MIMO). Two separate singular value plots are depicted in Figure 3.2 since the transfer function matrix is of second order (i.e. two input-two output). The helicopter rotor dynamics are evident in both singular values.

The singular value plot of the open-loop transfer function for MIMO System II 90% N_g Design Model (MIMO) is shown in Figure 3.3. The helicopter rotor dynamics are evident in the maximum singular value of Figure 3.3. A comparison of Figures 3.3 and 3.4, which are singular value plots of the open-loop transfer function matrices for the same MIMO system definition but different design models, display a difference in system gain for both singular values after .1 rad/sec. The difference is attributable to the presence of a non-minimum phase zero in the 90% N_g Design Model (MIMO) at .199 rad/sec which accounts for the magnitude increase after .1 rad/sec shown in Figure 3.3 as compared to Figure 3.4. Since this is a magnitude plot only, the phase degradation associated with the non-minimum phase zero is not apparent. The resulting performance limitations will become all too apparent, however, and will be discussed in Chapter 4.

The frequency-dependent singular value plots of the open-loop transfer functions of the design models are thus shown to depict the system open-loop dynamics. The use of frequency-dependent singular value plots of a loop

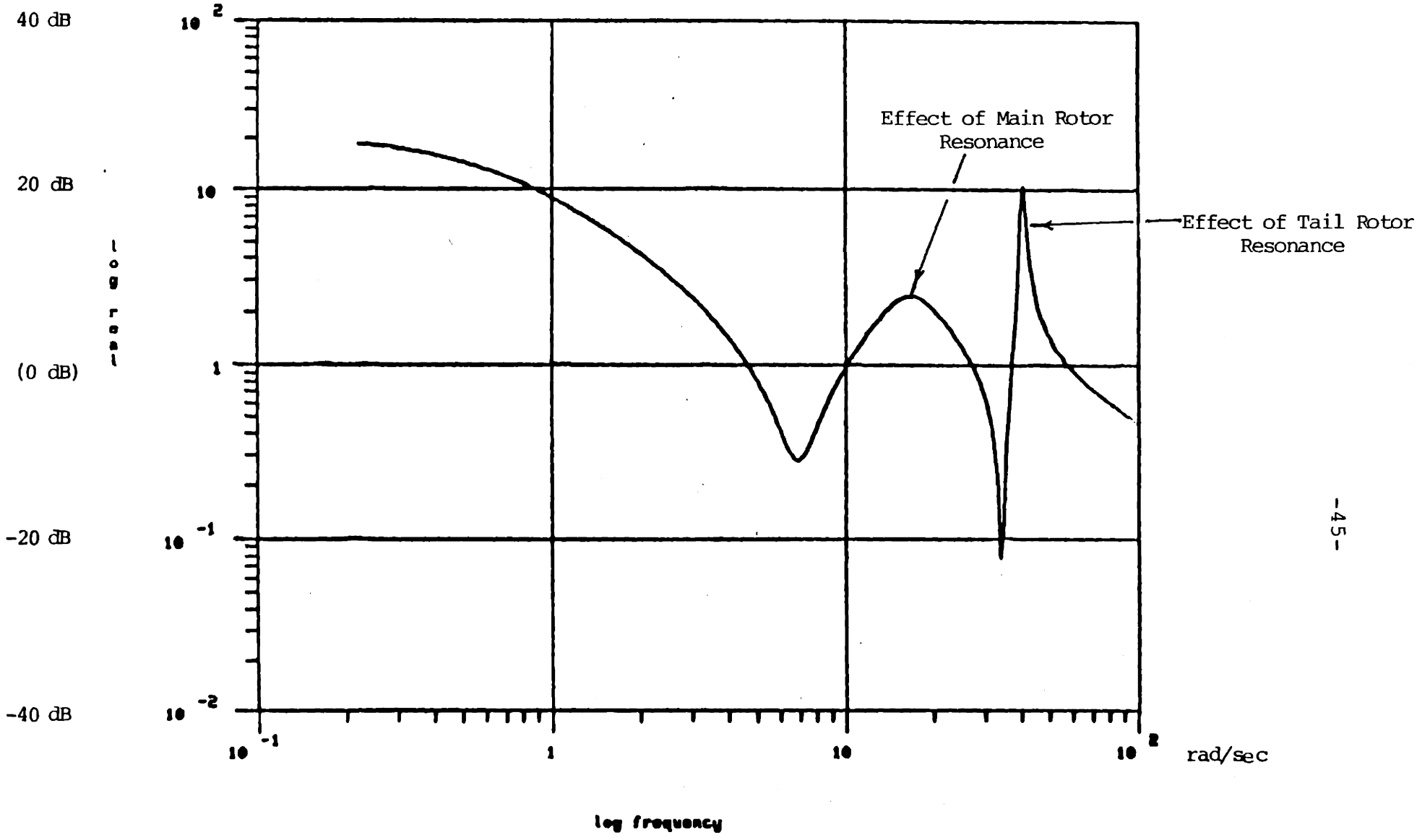

FIGURE 3.1: MAGNITUDE BODE PLOT OF OPEN-LOOP TRANSFER FUNCTION SISO - 90% N_g DESIGN MODEL (SISO)

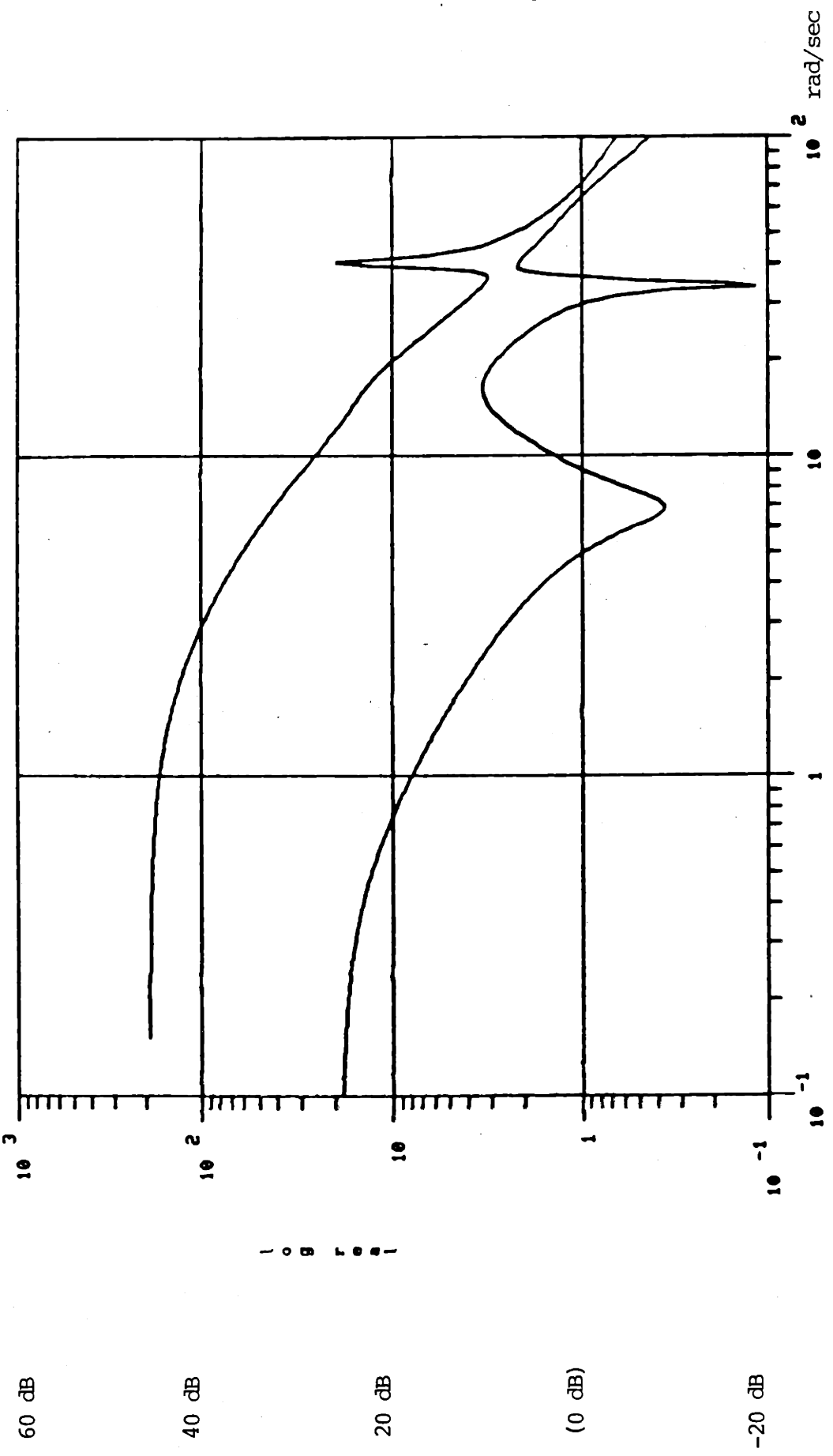

FIGURE 3.2: SINGULAR VALUE PLOT OF OPEN-LOOP TRANSFER FUNCTION

MIMO SYSTEM I - 83% N_g DESIGN MODEL (MIMO)

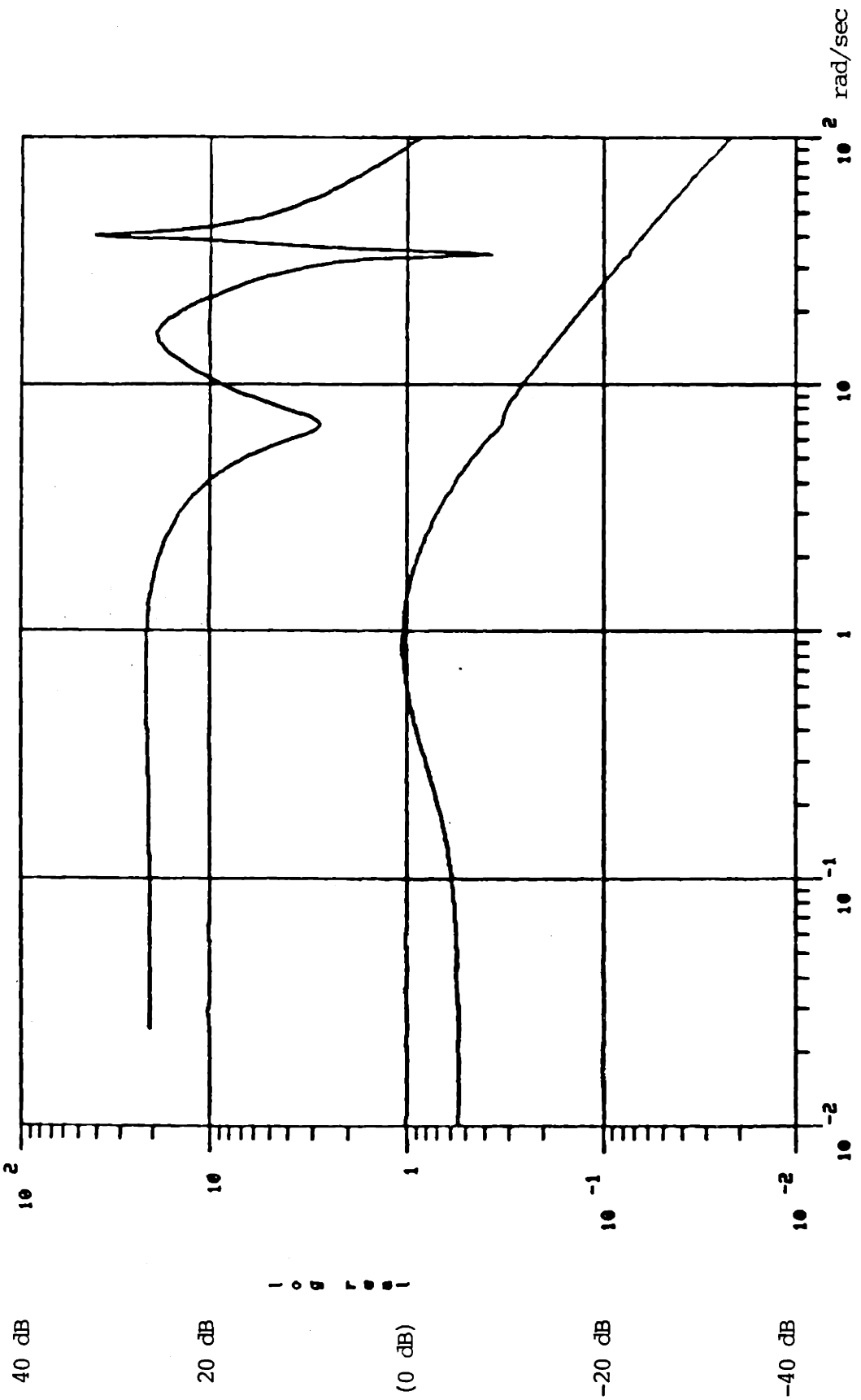

FIGURE 3.3: SINGULAR VALUE PLOT OF OPEN-LOOP TRANSFER FUNCTION MIMO SYSTEM II - 90% N_g DESIGN MODEL (MIMO)

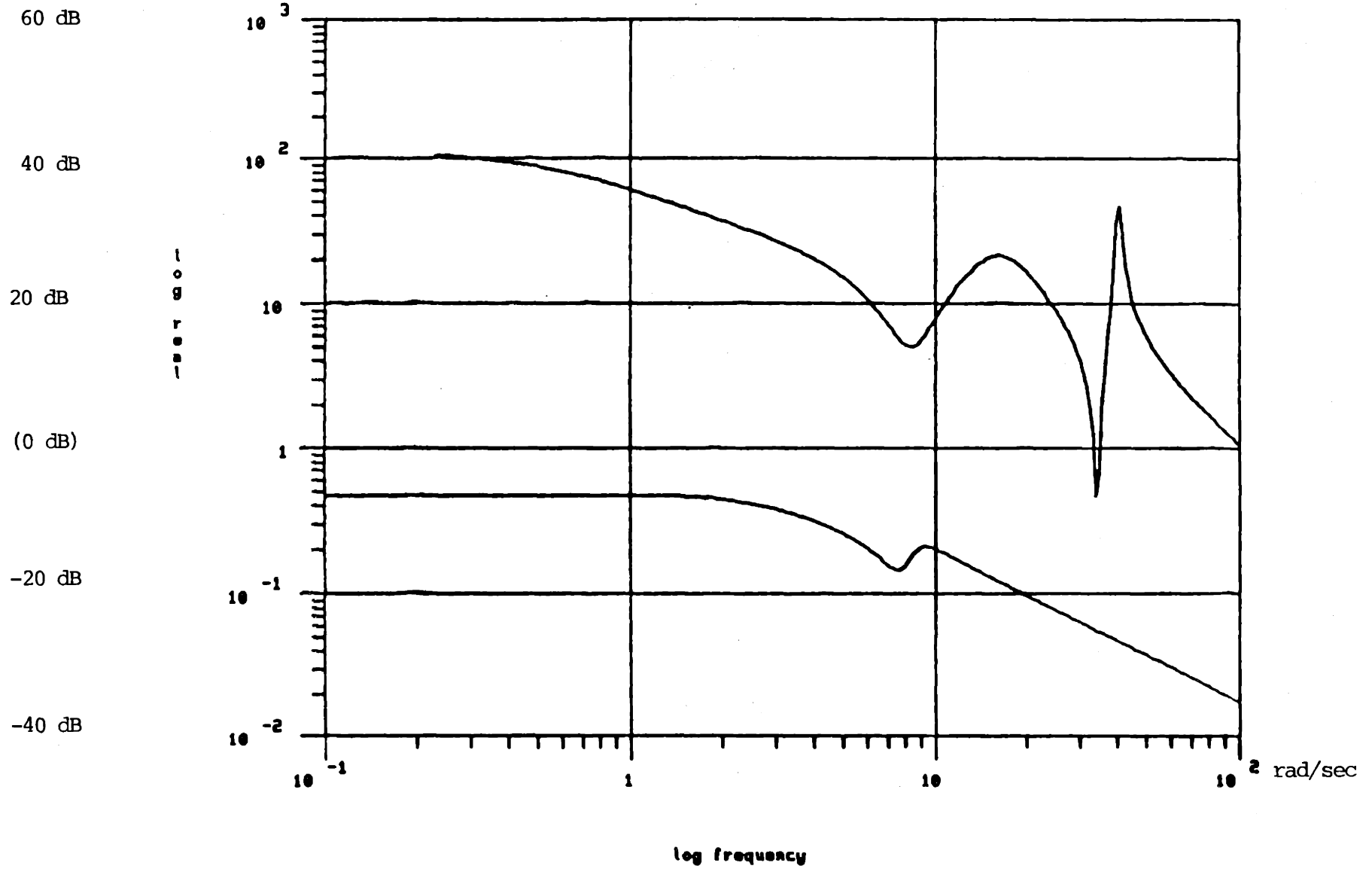

FIGURE 3.4: SINGULAR VALUE PLOT OF OPEN-LOOP TRANSFER FUNCTION MIMO SYSTEM II - 95% N_g DESIGN MODEL (MIMO)

transfer function matrix, as introduced in this section, will be extensively utilized in compensator design and evaluation.

3.2.3 Eigenvalue/Eigenvector Analysis

The free or unforced response of the linear model characterizes the open-loop plant dynamics. The linear model as formulated in Chapter 2, is of the form

$$\frac{d}{dt}\ \underline{x}(t) = \underline{A}\ \underline{x}(t) + \underline{B}\ \underline{u}(t) \tag{3.4a}$$

$$\underline{y}(t) = \underline{C}\ \underline{x}(t) + \underline{D}\ \underline{u}(t) \tag{3.4b}$$

The free response is described by the model $\underline{A}$ matrix [19]. The n_1 distinct, real eigenvalues and the n_2 complex eigenvalue pairs define $n_1 + n_2$ system modes. The corresponding eigenvectors display the participation of the individual states in each mode. Through the examination of the relative magnitudes of the eigenvector elements, insight into physical system behavior and a basis for model reduction is provided.

The model formulated for the turboshaft engine/helicopter system was analized in detail for an intermediate power setting. This power setting, denoted by 90% N_g, was singled out for analysis because it is representative of system behavior for the full range of operating conditions and does not represent an operating extreme. The particular model utilized is the 90% N_g (SISO) Design Model. This model is not augmented with sensor or actuator dynamics which facilitates the physical interpretation of the open-loop system. A display of the relative magnitudes of the eigenvector elements for each mode at this power setting is shown in Figure 3.5.

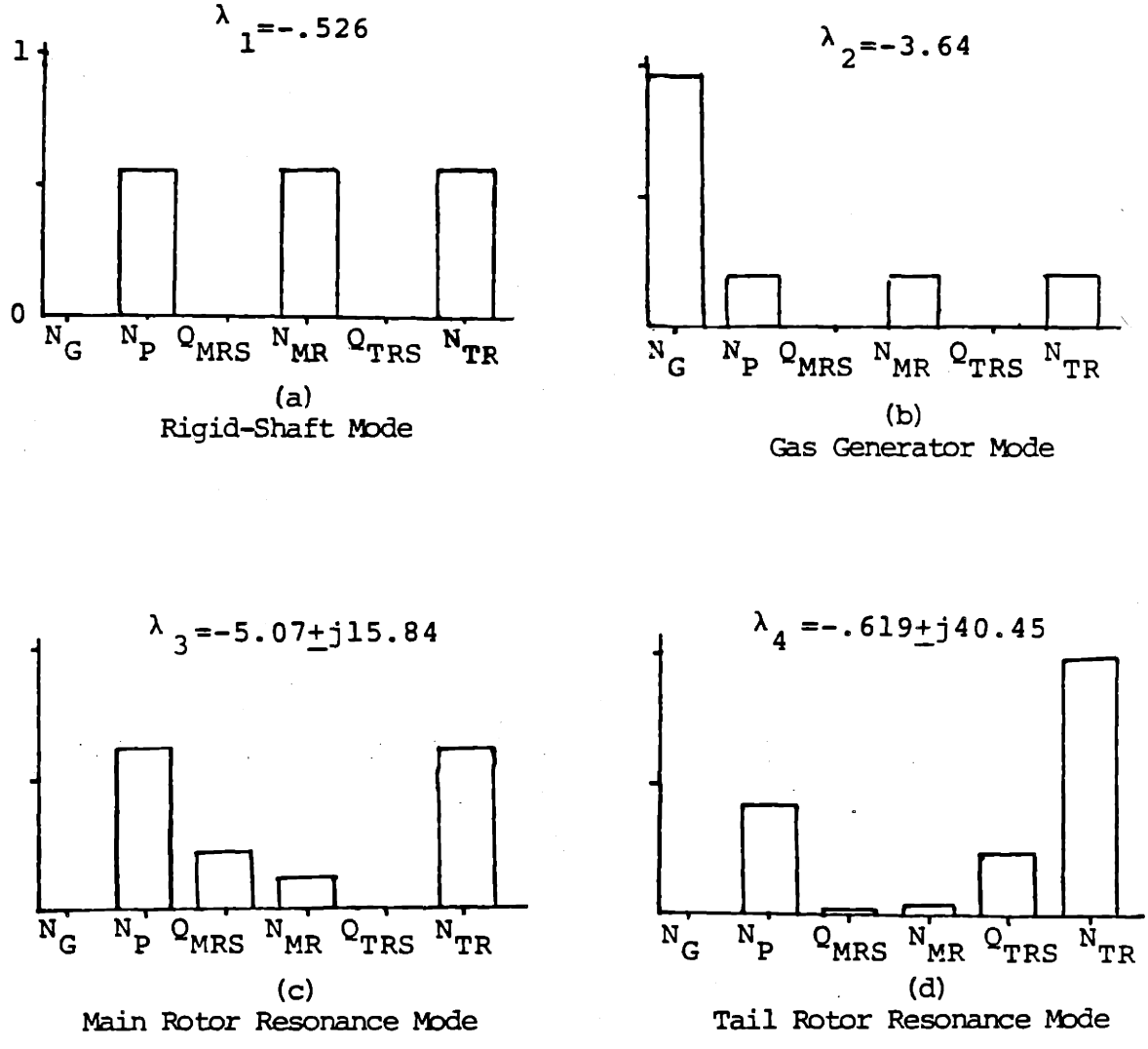

FIGURE 3.5: MODE SHAPES

(The variables N_G, N_p, Q_{MRS}, N_{MR}, Q_{TRS}, and N_{TR} are the state variables defined in TABLE 2.2)

The first eigenvector (Fig. 3.5a) associated with the first eigenvalue at $\lambda_1 = -.526$ rad/sec corresponds to the three drive train inertias, J_{PT}, J_{MR} and J_{TR} rotating in unison. This rigid-shaft mode, characterized by no intermediate shaft twist, can be derived by considering the first-order equation or motion of the total drive train inertia rotating against the main and tail rotor aerodynamic and power turbine damping elements.

The second eigenvector (Fig. 3.5b) corresponding to the eigenvalue at $\lambda_2 = -3.64$ rad/sec is dominated by the gas generator speed N_g. This mode is the gas generator mode. The contribution of the remaining speed states to this mode is due to the effect of the power turbine differentially rematching to the gas generator turbine through the gas flow path. With an increase in gas generator speed, less unbalanced torque is available to accelerate the power turbine (i.e. the gas generator consumes the available unbalanced gas torque to accelerate and power turbine speed decreases). Since this mode is relatively low frequency and low energy in nature, the drive train inertias rotate in unison and negligible shaft torque is generated. The eigenvalue of this mode is often labeled the "gas generator time constant" and is given by

$$\frac{\partial Q_g / \partial N_g}{J_g} \tag{3.5}$$

The final two system modes are helicopter drive train resonant modes and are described by the second order dynamics

$$s^2 + 2\zeta \omega_n s + \omega_n^2 \quad .$$

and for the respective modes,

$$\zeta_3 = .32, \quad \omega_n = 15.84 \text{ rad/sec}$$

and

$$\zeta_4 = .015, \quad \omega_n = 40.45 \text{ rad/sec.}$$

The first of these is commonly labeled the main rotor resonance (Fig. 3.5c) because of the motion of the power turbine and tail rotor relative to the heavy inertia main rotor. The highest frequency mode represented by the model is the second drive train or tail rotor resonant mode (Fig. 3.5d) and is characterized by power turbine and main rotor rotation relative to the tail rotor.

The eigenvalue/eigenvector analysis presented in this section is invaluable in providing insight into the physical nature of the system dynamics. In particular, the interaction of the elements of the rotor system in the resonant modes has been displayed. The coupling of the gas generator to the rotor system through the gas path was also presented.

3.2.2 Modal Decomposition

Consider the time domain description of a MIMO System

$$\frac{d}{dt}\ \underline{x}(t) = \underline{A}\ \underline{x}(t) + \underline{B}\ \underline{u}(t) \tag{3.7a}$$

$$\underline{y}(t) = \underline{C}\ \underline{x}(t) \tag{3.7b}$$

with dim $\underline{x}(t)=n$, dim $\underline{u}(t)=$dim $\underline{y}(t)=m$.

The control-to-output transfer function matrix $\underline{G}(s)$ is

$$\underline{G}(s) = \underline{C}(s\underline{I}-\underline{A})^{-1}\underline{B} \tag{3.8}$$

Let λ_i denote the i^{th} eigenvalue (pole) of $\underline{A}$, i=1, 2, ...,n. Let $\underline{u}_i$ denote the corresponding right eigenvector (column vector), and let $\underline{v}_i$ th denote the corresponding left eigenvector (row vector), i.e.

$$\underline{A}\,\underline{u}_i = \lambda_i\underline{u}_i \tag{3.9a}$$

$$\underline{v}_i^T\underline{A} = \lambda_i\underline{v}_i^T \tag{3.9b}$$

The MIMO transfer function $\underline{G}(s)$ in Eq(3.7) can be written in a MIMO residue representation, or partial fraction expansion, as follows (assuming the poles λ_i are distinct).

$$\underline{G}(s) = \sum_{i=1}^{n} \frac{\underline{R}_i}{s-\lambda_i} = \sum_{i=1}^{n} \frac{\underline{R}_i/\lambda_i}{s/\lambda_i-1} \tag{3.10}$$

The mxm matrices (in general complex) $\underline{R}_i$ are called the residue matrix at the pole s= λ_i. They are computed as follows using the time-domain system representation of Eq(3.7).

$$\underline{R}_i = \underline{C}\,\underline{u}_i\underline{v}_i^T\underline{B} \tag{3.11}$$

The residue term for a SISO system definition is simply the partial fraction coefficient.

The larger the residue term, $\underline{R}_i / \lambda_i$, the larger the contribution of the corresponding pole to the response of the system. A convenient measure of residue matrix size is provided by its maximum singular value, i.e. spectral norm

$$\sigma_{max}(\underline{R}_i/\lambda_i) = \sqrt{\lambda_{max}(R_i/\lambda_i)^H(\underline{R}_i/\lambda_i)} \tag{3.12}$$

The residue matrices and their maximum singular value norms are presented in Table 3.3. The residue expansion was performed only at the 90% N_g power level. Actuator and sensor dynamics were not considered. The expansion was performed at this particular power level because the 90% N_g power level is representative of normal operating power.

There are two important interpretations to be obtained from the residue analysis presented in Table 3.3. The first interpretation is obtained by examining the relative values of the maximum singular value norms for all system definitions. The relative magnitude of the maximum singular value norm for the fourth mode or tail rotor resonant mode is small. It could be interpreted that the effect of this mode on system response is negligible thus providing a basis for model reduction. However, the tail rotor resonant mode will <u>not</u> be deleted in this research because it is desired to examine the effect of this underdamped resonance on system response.

The second interpretation is obtained by examining the individual residue matrix coefficients of the MIMO system definitions. Note that the residue matrices for the MIMO system definitions have zeros in the second row for all

TABLE 3.3: RESIDUE ANALYSIS

	SISO		MIMO SYSTEM I*2			MIMO SYSTEM II*2		
MODE*1	r/λ_i	σ_{max}	$\underline{R}_i/\lambda_i$		σ_{max}	$\underline{R}_i/\lambda_i$		σ_{max}
1	22	22	22	32.6	39.3	- SAME AS -		-
			0	0		SYSTEM I		
2	-2.2	2.2	-2.2	-35	204	-2.2	-35	38
			12.4	201		-.819	-13.3	
3	.2+ j.7	.72	.2+ j.7	2.5+ j12.6	12.8	- SAME AS -		-
			0	0		SYSTEM I		
4	-.04+ j.167	.17	-0.4+ j.167	1.+ j2.51	2.73	- SAME AS -		-
			0	0		SYSTEM I		

*1 MODE	λ_i
1	- .526
2	-3.64
3	$-5.07 \pm j15.84$
4	$-.619 \pm j40.45$

*2 See Table 3.1

modes except for the second mode or the gas generator mode. The zeros in the second row display how the control input contribution to the second output for either MIMO system definition (i.e. N_g or $T_{4.5}$) is effective only in the gas generator mode. This result is not surprising. Examination of the mode shapes, presented in the previous section, displayed that modes 1, 3 and 4, are rotor system modes and that the gas generator is uncoupled from these modes except through the gas path. It is expected then that the gas generator speed and inter-turbine gas temperature output, being engine and not rotor system variables, would only be represented in the residue matrices in the gas generator mode.

The residue analysis presented in this section has quantified the effect of each system mode on the total system response. Physical insight, in terms of the nature of the engine/helicopter rotor system coupling was provided by examination of the residue matrix coefficients.

3.2.6 Singular Value Analysis of Input-to-Output Structure

The relative contribution of the inputs to each output variable for a MIMO system definition can be examined using the Singular Value Decomposition (SVD) of the system open-loop transfer function. The SVD of a complex valued matrix is defined as follows [18,20]. Given any complex n x n complex valued matrix $\underline{A}$, then there exists unitary matrices $\underline{U}$ and $\underline{V}$ such that

$$\underline{A} = \underline{U}\,\underline{\Sigma}\,\underline{V}^H = \sum_{i=1}^{n} \sigma_i(\underline{A})\underline{u}_i\underline{v}_i^H \tag{3.13}$$

Where $\underline{\Sigma}$ is a diagonal matrix of the singular values, $\sigma_i(\underline{A})$, the $\underline{u}_i$ are the column vectors of $\underline{U}$, i.e.

$$\underline{U} = [\underline{u}_1, \underline{u}_2, \ldots, \underline{u}_n] \tag{3.14}$$

and the $\underline{v}_i$ are the column vectors of $\underline{V}$, i.e.

$$\underline{V} = [\underline{v}_1, \underline{v}_2, \ldots, \underline{v}_n] \tag{3.15}$$

The $\underline{v}_i$ are the right singular vectors of $\underline{A}^H\underline{A}$ because

$$\underline{A}^H\underline{A}\ \underline{v}_i = \sigma_i^2(\underline{A})\underline{v}_i \tag{3.16}$$

The $\underline{u}_i$ are called the left singular vectors of $\underline{A}^H\underline{A}$ because

$$\underline{u}_i^H\ \underline{A}^H\underline{A} = \sigma_i^2(\underline{A})\underline{u}_i^H \tag{3.17}$$

Consider the open-loop transfer function matrix of a system in the frequency domain, $\underline{G}(j\omega)$. For $\omega = 0$, the elements of $\underline{G}(j0)$ are real and are the steady-state or DC gains of the system.

Defining the linear transformations

$$\underline{u}' = \underline{V}^H\underline{u} \tag{3.18a}$$

$$\underline{y}' = \underline{U}^{-1}\underline{y} \tag{3.18b}$$

facilitates the interpretation of the system open-loop, steady-state transfer function presented in Figure 3.6. Figure 3.6 can be viewed as a series of linear transformations relating the input vector $\underline{u}$ to the output vector $\underline{y}$. It is evident from Figure 3.6 that a given input contributes to the system

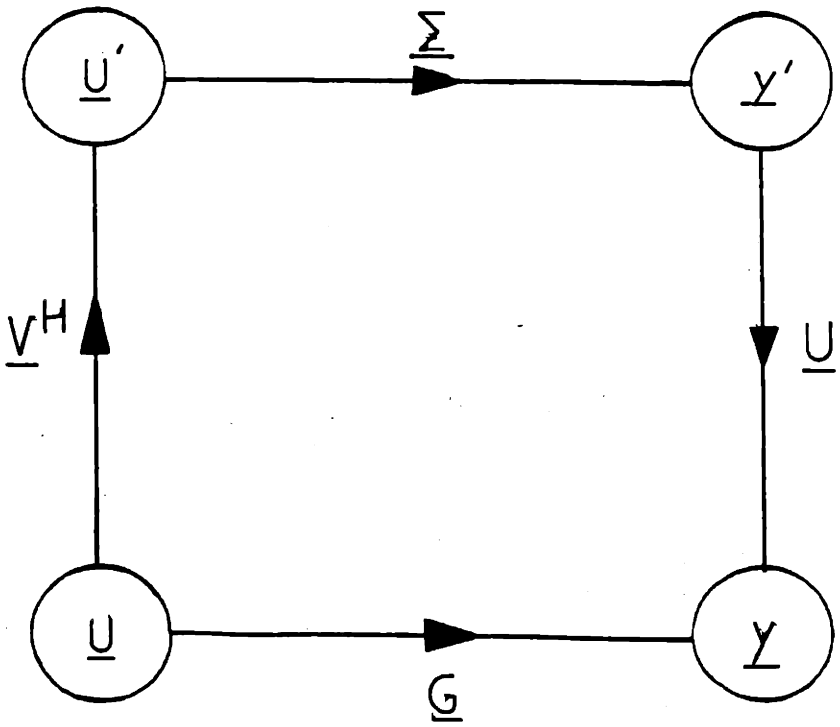

FIGURE 3.6: SINGULAR VALUE DECOMPOSITION (SVD) INTERPRETATION OF A SYSTEMS INPUT-TO-OUTPUT RELATIONSHIP

response as determined by the relative values of the individual row elements of $\underline{V}^H$. A given output is affected by the input as determined by the relative values of the individual row elements of $\underline{U}^{-1}$. The singular values act as weighting factors.

The above interpretation of the SVD is attributable to Kapasouris [4] and presents a powerful tool in examining the input-to-output structure of a MIMO system definition.

The elements of $\underline{G}(j0)$ are unit dependent and must be scaled (i.e. made dimensionless) to form a basis for numerical comparison. The scaling is performed by redefining the output and input variables as

$$\underline{y} = \underline{N}_y \, \underline{y}_n \tag{3.19a}$$

$$\underline{u} = \underline{N}_u \, \underline{u}_n \tag{3.19b}$$

where $\underline{N}_y$ and $\underline{N}_u$ are square, diagonal matrices.

The matrix $\underline{G}(j0)$ is scaled in this research by utilizing 1% of the steady-state or equilibrium values of the outputs of each MIMO design model and 1% of the expected deviations of the control variables of 100 lb/hr of fuel flow and 10 degrees of variable geometry motion. The scaled and unscaled $\underline{G}(j0)$ for each MIMO system definition, along with the applicable scaling matrices are presented in Appendix C.

The relative contributions of the inputs to the outputs are best viewed as percentages, thus the individual elements of the row vectors of $\underline{U}^{-1}$ and $\underline{V}^H$ are expressed as percentages of the total row value.

The SVD was performed in this manner for each MIMO system definition. The results are depicted in Figure 3.7. Figure 3.7a depicts the results of

FIGURE 3.7: SVD REPRESENTATION OF INPUT-TO-OUTPUT STRUCTURE OF MIMO DESIGN MODELS

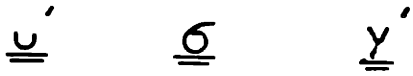

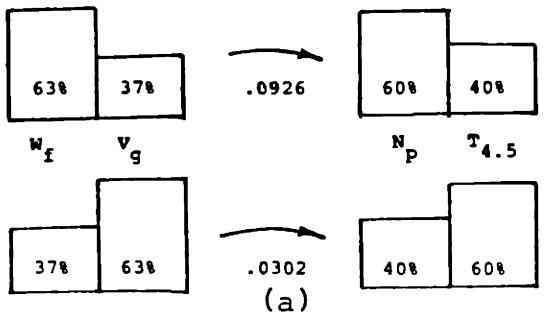

(a)
MIMO SYSTEM I
83% N_G DESIGN MODEL (MIMO)

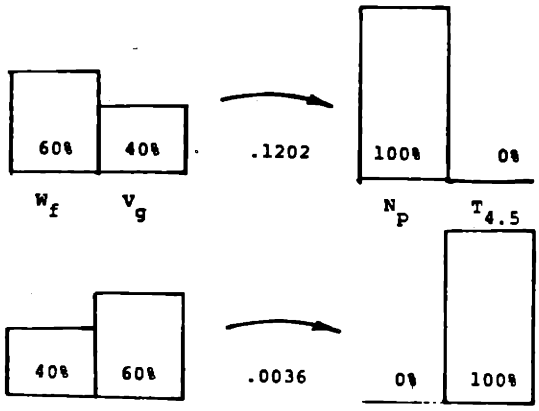

(b)
MIMO SYSTEM II
90% N_G DESIGN MODEL (MIMO)

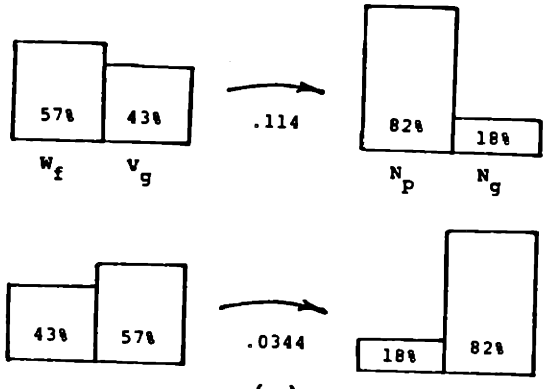

(c)
MIMO SYSTEM II
95% N_G DESIGN MODEL (MIMO)

the SVD analysis of MIMO System I, 83% N_g Design Model (MIMO). The coupled nature of the system is displayed. Both input variables are shown in Figure 3.7a to contribute to both output variables, thus the system is not decoupled, or each input does not affect only single output.

Figure 3.7b displays the SVD analysis as applied to MIMO System II, 90% N_g Design Model (MIMO). Note that the singular values or weighting factors depict that $T_{4.5}$ is a weak output as compared to N_p. The same input-to-output characterization, as applied to MIMO System II, 95% N_g Design Model (MIMO) is shown in Figure 3.7c. The strong coupling between input and output is evident by noting that the singular values are not widely skewed as they were in the 90% N_g Design Model (MIMO) and that both output variables are represented in each singular value weighting.

The analysis presented in this section is not only valuable in examining the input-to-output structure of a MIMO system definition, but provides an analysis tool that is applicable in formulating MIMO system definitions. The effect of various inputs on chosen outputs for a high order MIMO system can be evaluated and the optimum system definition formulated.

3.3 Modeling Errors and Robustness Criteria

The dominant high-frequency uncertainty in the linear model is in the description of the helicopter rotor dynamics. The rotor system lumped parameter model does not portray the functional relationships of the main rotor spring and damping coefficients with helicopter flight condition, rotor

coning angle, etc. The posing of a maximum realizable range of coefficient variation, while not capturing the explicit functional relationships, will acknowledge their presence and provide the basis for a conservative, stable design.

The actual plant transfer function matrix, $\underline{\tilde{G}}(s)$[*1], will be assumed to be related to the nominal linear model $\underline{G}_p(s)$, by the multiplicative relationship

$$\underline{\tilde{G}}(s) = \underline{L}(s)\underline{G}_p(s) \tag{3.20}$$

This relation reflects the model uncertainty quantified by $\underline{L}(s)$ to the system output variables as shown in Figure 3.8. The output of the turboshaft engine/helicopter system is a physically meaningful point at which disturbances, such as load disturbances to the helicopter rotor systems, and modeling errors, such as uncertainties in the description of the helicopter rotor dynamics may be reflected. The specific location in the loop where error, as well as performance and disturbance rejection specifications are reflected in a MIMO system is important because matrices in general do not commute. This consideration is of no particular significance in a SISO system. A feedback system such as that defined in Figure 3.13, is guaranteed to be stable for the error definition given by Eq(3.20) if the inequality

$$\sigma_{max}[\underline{L}(j\omega)-\underline{I}] \leq \sigma_{min}[\underline{I}+(\underline{G}_p(j\omega)\underline{K}(j\omega))^{-1}] \tag{3.21}$$

is satisfied for all ω[10], where $\underline{K}(j\omega)$ is the compensator transfer function matrix.

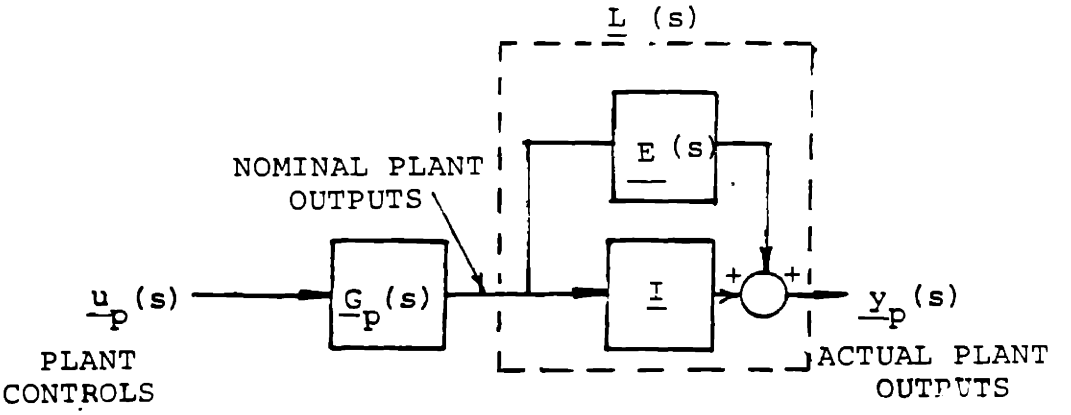

FIGURE 3.8: MODELING ERROR DEFINITION

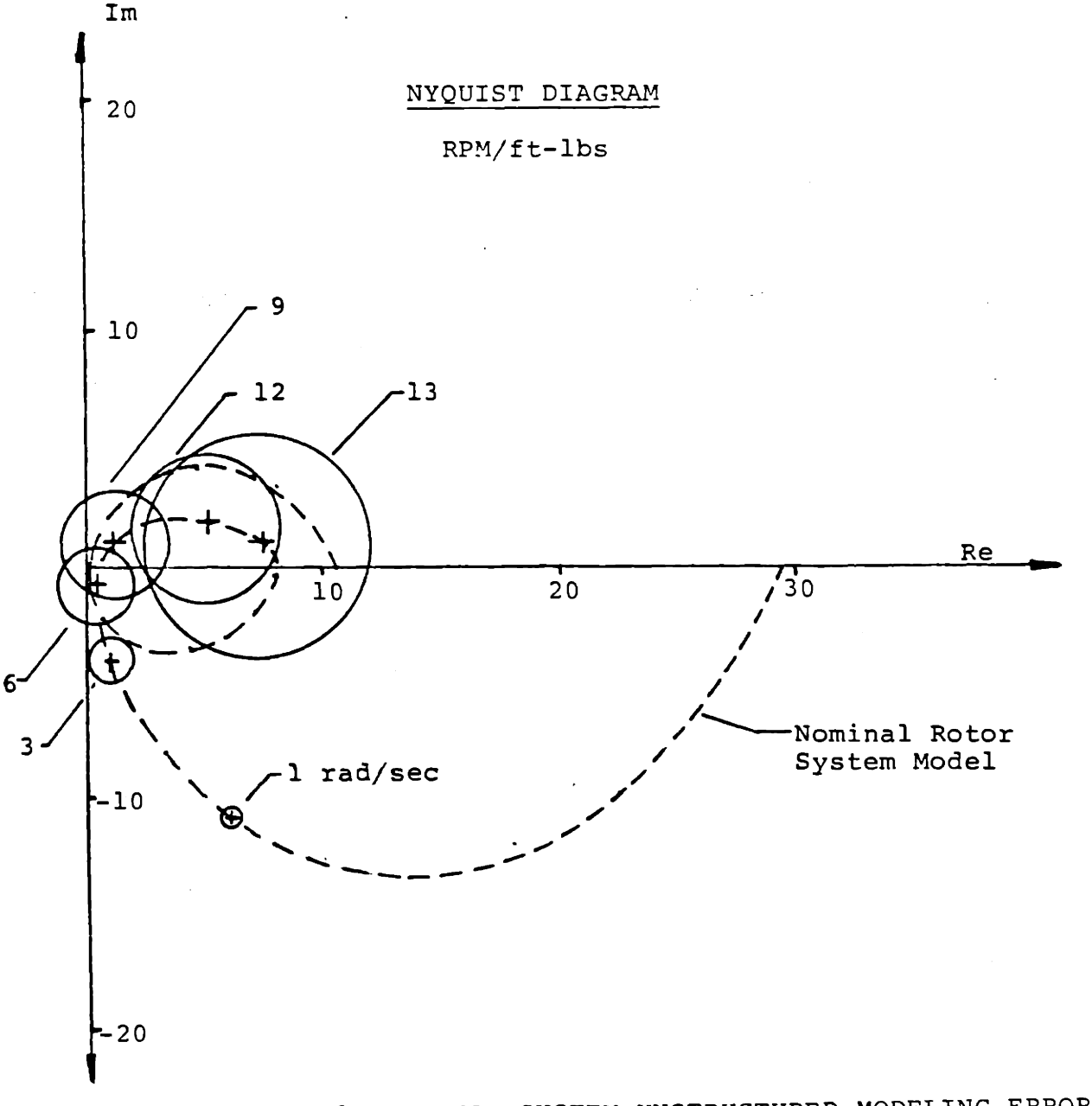

FIGURE 3.9: ROTOR SYSTEM UNSTRUCTURED MODELING ERROR

The error matrix, $\underline{L}(s)$, for this system will be assumed to be of the form

$$\underline{L}(j\omega) = \underline{I} + \underline{E}(j\omega) = \underline{I} + \text{diag}[e_r(\omega), e_e(\omega)] \tag{3.22}$$

where $e_r(\omega)$ = rotor system error

$e_e(\omega)$ = engine error.

This error structure will reflect the uncertainty of the high frequency rotor system description to the power turbine speed output. The error in the low frequency engine description will be assumed to be zero small and we will let $e_e(\omega)=0$. This assumption is valid based on the confidence in the low frequency engine description and in the dominant nature of the rotor system uncertainty. For the SISO system definition, Eq(3.22) becomes

$$\ell(j\omega) = 1+e(j\omega) = 1+e_r(\omega) \tag{3.23}$$

The construction of $e_r(\omega)$ to quantify rotor system parametric variations is best visualized on a polar plot (Nyquist diagram) of the open-loop rotor system transfer function as shown in Figure 3.9. The rotor system dynamics are present in the system transfer function matrix for power

---

*1 The robustness theory is presented here in general matrix form. Note that a SISO system definition can be considered a special case (i.e. one-dimensonal) of the n-dimensional MIMO system.

turbine speed output and for both control variables W_f and V_g. Rotor system parameter variations will perturb the nominal representation on the polar or Nyquist plot by changing the gain and phase characteristics. It is necessary to quantify the effect of realizable rotor system parametric variations so that the compensated system will not realize a change in the number of encirclements of the critical point on the Nyquist plot. A change in the number of encirclements is indicative of instability, and will be avoided if the inequality presented by Eq(3.21) is satisfied for the multiplicative error quantified through this procedure. The physical realizable variations of $\pm$20% of nominal equivalent main rotor spring constant and $\pm$50% of nominal main rotor damping are the pertubations considered. The changes in the main rotor spring constant will change the location of the main rotor resonant peak and the changes in the main rotor damping change the magnitude of both the main rotor resonant peak and the anti-resonance "trough".

A circle of radius r and center coincident with the nominal model encompassing the family of perturbed plants at several frequencies is shown in Figure 3.9. The functional relationship of the magnitude of r with frequency establishes $e_r(\omega)$. The function $e_r(\omega)$ thus relates the maximum magnitude deviations of the system open-loop transfer function for the rotor system variations considered to frequency. This error description is "unstructured".

The above error description is additive in nature but is easily transformed into a multiplicative or relative error format as demanded by Eq(3.21) by normalizing by the nominal gain at each examined frequency. The

multiplicative character of $\underline{L}(j\omega)$ given by Eq(3.20) is best illustrated on the logarithmic plot shown in Figure 3.10. The error characterization shown in Figure 3.10 displays the confidence in the model in the low frequency region and the growing uncertainty with increasing frequency where the main rotor system dynamics become dominant. Note that the dynamics at frequencies above the main rotor resonant frequency show little error. This is because variations in only the main rotor dynamics were considered as these dynamics will provide the lower frequency bound for guaranteed robustness. The higher frequency dynamics will undoubtedly be inherently more uncertain. A logarithmic plot of $e_r(\omega)$ is shown explicitly in Figure 3.11. This function is equivalent to

$$\sigma_{max}[\underline{L}(j\omega)-\underline{I}] \tag{3.24}$$

and will be used as the robustness criteria for design acceptance.

3.4 Design Specifications

It is necessary to transition the operational requirements outlined in Chapter 2, with due consideration given to modeling error, into frequency domain performance specifications to provide the basis for the LQR/LTR based controller formulation. The implication of specifications is to achieve good performance in terms of

1. command following,
2. disturbance rejection, and
3. insensitivity to modeling errors through the introduction of feedback.

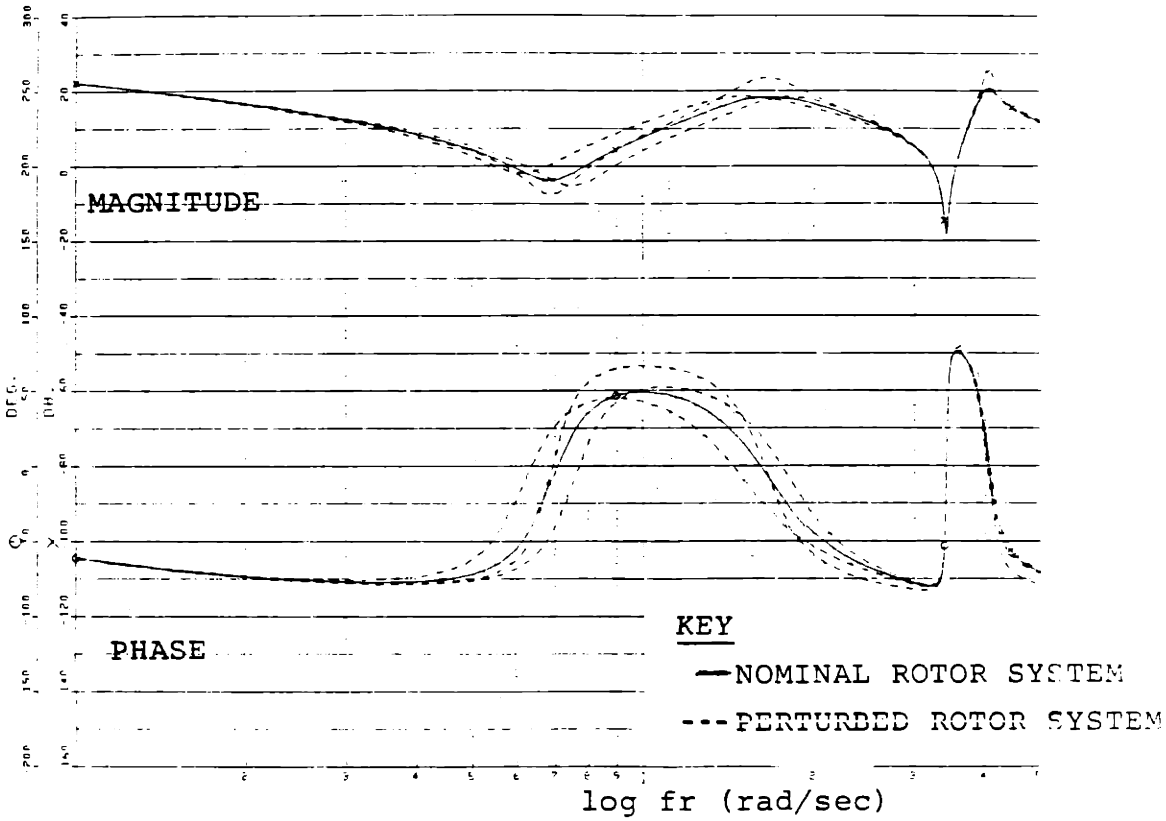

FIGURE 3.10: BODE PLOT OF NOMINAL AND PERTURBED ROTOR SYSTEM TRANSFER FUNCTION

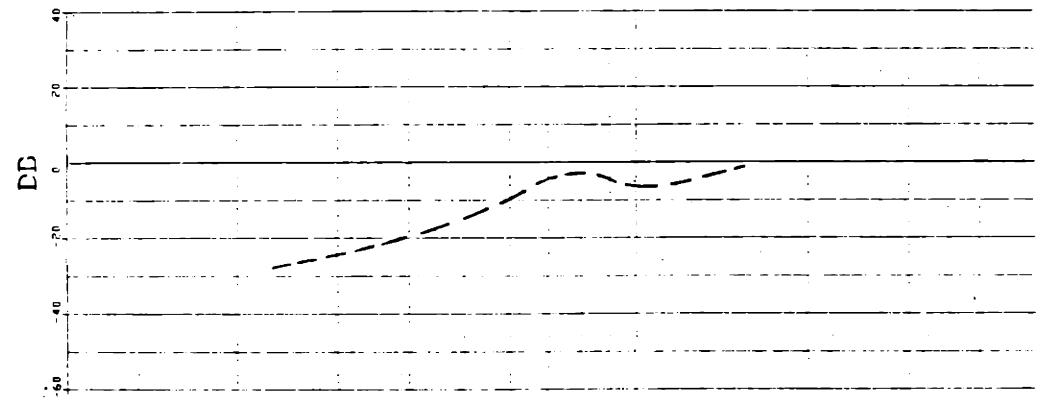

FIGURE 3.11: ROBUSTNESS CRITERIA FOR DESIGN ACCEPTANCE GIVEN BY Eq(3.24)

The primary controller requirement for any system definition is to provide isochronous power turbine speed governing. Integral augmentation is thus required to achieve zero steady-state error to a reference value on the power turbine speed output variable. Isochronous power turbine speed governing is the primary requirement for the SISO system definition.

MIMO System I is required to provide isochronous power turbine and gas generator speed governing.

MIMO System II is required to provide both isochronous power turbine speed governing and zero steady-state error to a referenced inter-turbine gas temperature. Specifically, it will be required that the system provide isochronous power turbine speed governing while simultaneously allowing the inter-turbine gas temperature to be trimmed to a desireable level as predetermined by efficiency calculations or to hold the gas temperature at a constant value to provide a limiting function. The trim requirement is less demanding on system performance than the limiting function because of the characteristically low frequency content of a trim signal.

Output disturbances on power turbine speed occur because of load disturbances to the helicopter rotor systems. These load disturbances are reflected through the rotor system dynamics to power turbine speed. The frequency spectrum of these rotor dynamics, derived in Appendix D, is shown in Figure 3.12. It is required that the controllers reject power turbine speed disturbances while maintaining isochronous power turbine speed control and not

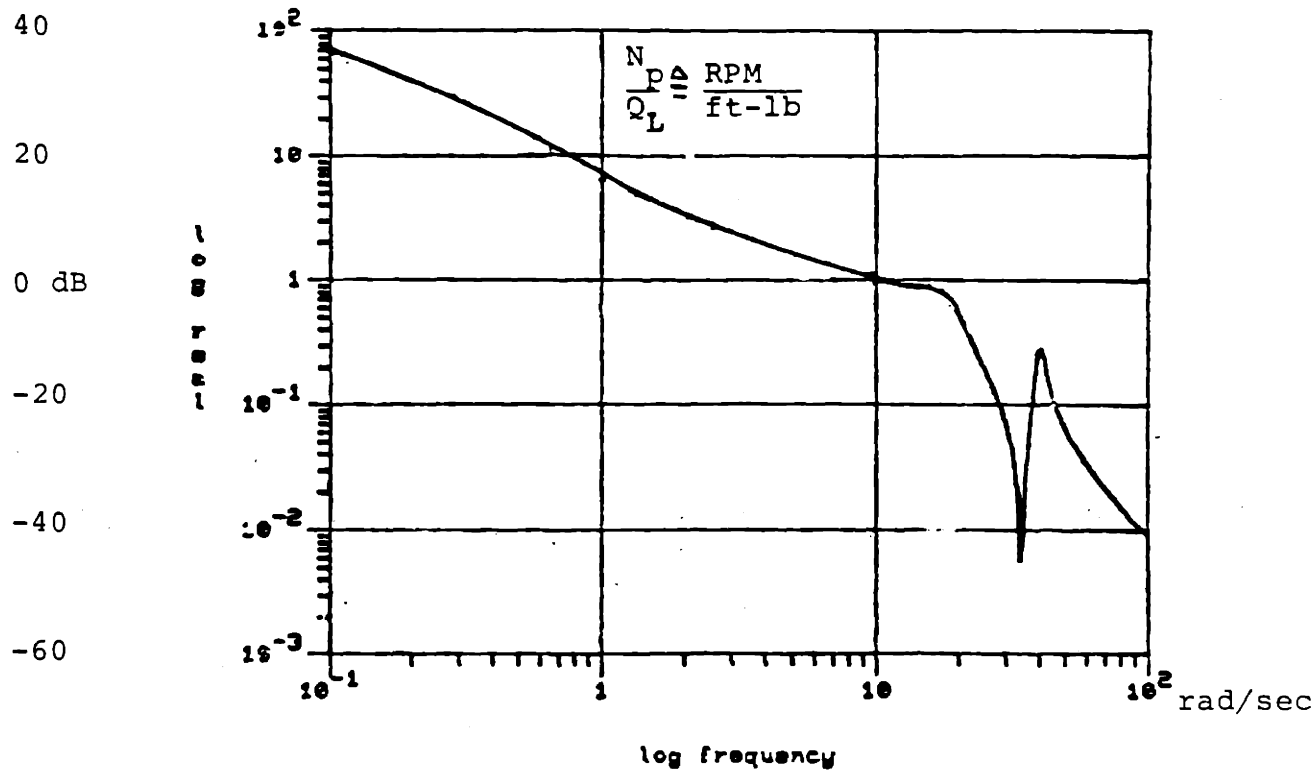

FIGURE 3.12: FREQUENCY SPECTRUM OF HELICOPTER ROTOR SYSTEM LOAD DISTURBANCES TO POWER TURBINE SPEED OUTPUT

provide input energy to support potentially divergent drive train resonant modes. Disturbances to the engine output variables (i.e. $T_{4.5}$ and N_g) will be assumed to be small as compared to the load disturbance spectrum.

To realize these command following and disturbances rejection expectations, it is necessary to examine the generalized feedback system shown in Figure 3.13. The relationship of the error signal, $\underline{e}(s)$, to the system command signals and output disturbances, $\underline{r}(s)$ and $\underline{d}_o(s)$, is given by

$$\underline{e}(s) = [\underline{I}+\underline{T}(s)]^{-1}[\underline{r}(s)-\underline{d}_o(s)] \tag{3.25}$$

where $\underline{T}(s) = \underline{G}_p(s)\underline{K}(s)$ = Loop Transfer Functions Matrix (LTFM)

$[\underline{I}+\underline{T}(s)]$ = Return Difference Transfer Function Matrix (RDTFM).

If $\underline{e}(s)$ is to be "small" (i.e. if the system is to follow commands or reject disturbances) in the presence of some "not-so-small" $\underline{r}(s)$ and/or $\underline{d}_o(s)$, then the RDTFM must intuitively be "large". This matrix cannot be made arbitrarily "large" for all frequencies, but it must be of sufficient magnitude in those frequency ranges where $\underline{r}(s)$ and $\underline{d}_o(s)$ contain energy in order to meet the aforementioned performance goals. The measure of matrix size utilized is provided by its singular values. Note that

A matrix is "large" if its <u>minimum</u> singular value is "large" ($\sigma_{min} >> 1$).

A matrix is "small" if its <u>maximum</u> singular value is "small" ($\sigma_{max} << 1$).

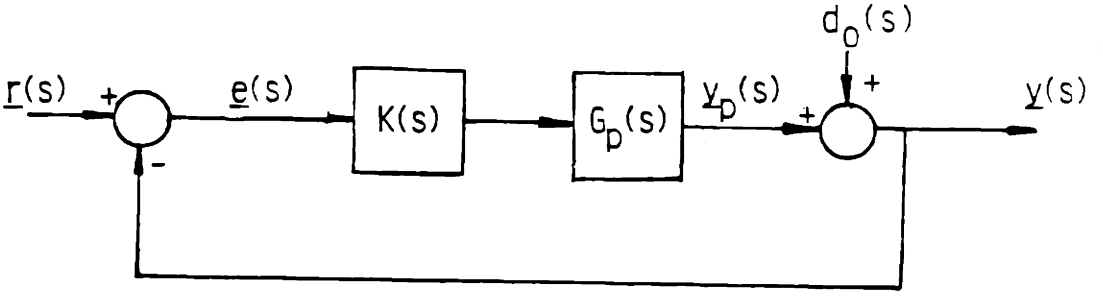

FIGURE 3.13: FEEDBACK SYSTEM

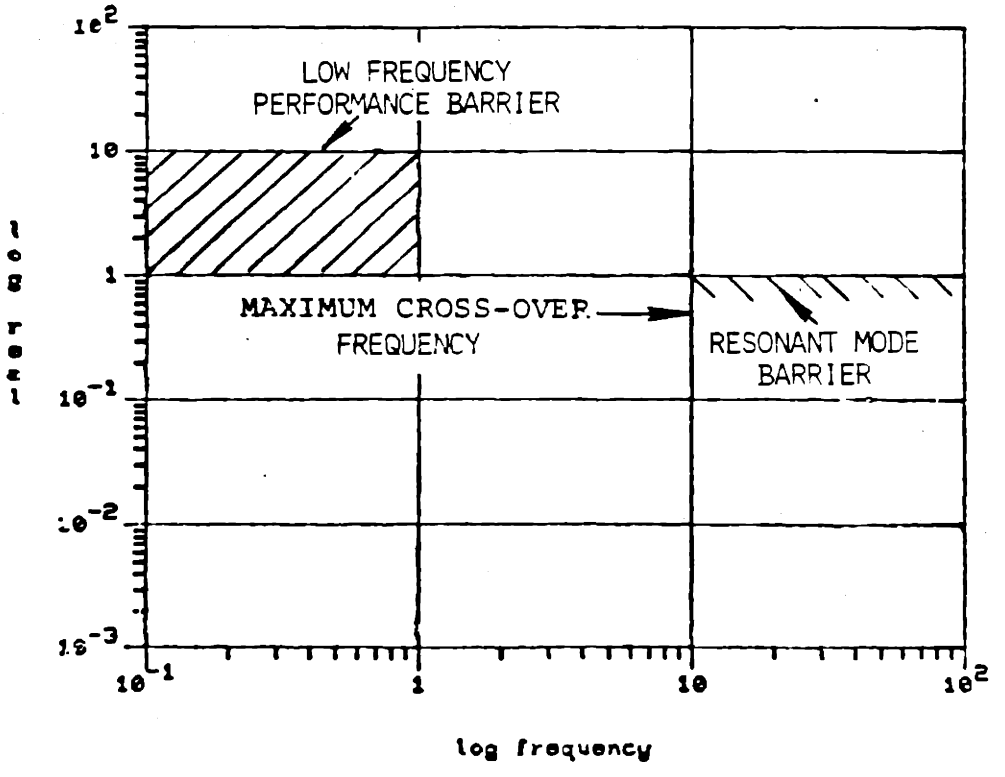

FIGURE 3.14: DESIGN SPECIFICATIONS

The maximum error magnitude at a given frequency, ω_o, for unit magnitude commands and output disturbances is given by

$$||\underline{e}||_2 = \frac{1}{\sigma_{min}[\underline{I}+\underline{T}(j\omega_o)]} \tag{3.26}$$

If $\sigma_{min}\ \underline{T}(j\omega_o)>>1$, then Eq. (3.26) is nearly

$$||\underline{e}||_2 \leq \frac{1}{\sigma_{min}\ \underline{T}(j\omega_o)} \tag{3.27}$$

The frequency range for which $\sigma_{min}\ \underline{T}(j\omega)$ is to be "large" as well as how "large" is "large" must be tempered with a system bandwidth consideration. The presence of a non-minimum phase zero in the desired system bandpass will severely limit the frequency range for which $\sigma_{min}\ \underline{T}(j\omega)$ can be made "large". A desirable crossover frequency for this system (i.e. when $\sigma_{max}\ \underline{T}(j\omega)=1$), derived from pilot evaluations [12] is about 10 rad/sec. This bandwidth restriction will provide drive train resonant mode attenuation which will preclude the possibility that the engine could provide input energy into potentially divergent mode*1.

To provide maximum command following and disturbance rejection performance, it is desired that $\sigma_{min}\underline{T}(j\omega)$ be "large" over the widest possible frequency range. Considering the bandwidth restriction and LQG/LTR typical slopes at crossover of approximately -20dB/dec, it is not unreasonable to impose the requirement that

$$\sigma_{min}\ \underline{T}(j\omega) > 20dB\forall\ \ \omega \leq 1 \text{ rad/sec} \tag{3.28}$$

---

*1 This could occur if $\sigma_{max}\underline{T}(j\omega)= 1$ at either drive train resonant mode due to disturbances reflected to the command input.

Figure 3.14 summarizes the performance specifications for command following and disturbance rejection. Robustness will be achieved through satisfaction of the inequality presented in Eq(3.21).

3.5 Summary

The present Chapter has accomplished the prerequisites necessary for a successful design. The obvious first step was the definition of the desired controller functions. Three system definitions, one SISO and two MIMO, were presented. The pole-zero structures of the design models to be utilized in controller design were examined. The concept of frequency-dependent singular value plots of a system transfer function matrix was presented. As utilized in this Chapter, the singular value plots depicted the open-loop dynamics of each design model.

Several of the tools available for examining a nominal model representation were presented in this Chapter. An eigenvalue/eigenvector analysis was particularly useful in unfolding the physical behavior of the open-loop plant. A modal decomposition, or partial fraction expansion strengthened the physical interpretation provided by the eigenvalue/eigenvector analysis and provided a relative comparison of the effects of each of the system modes to the total system response. A unique interpretation of the Singular Value Decomposition (SVD) was particularly useful in unfolding the input-to-output structure of a MIMO system definition. This unique interpretation of the SVD, as applied to the MIMO system definitions proposed in this research, displayed the relative effects of the contributions of the inputs to the outputs.

A helicopter drive train modeling error description, which represents the dominant error in the nominal model, was quantified. The error description was presented as a robustness criterion pertinent to the physically meaningful output loop break point.

Finally, design requirements and specifications for all system definitions were posed. Design specifications were posed in the frequency domain to be consistent with the use of frequency-dependent plots of the singular values of a system transfer function matrix. Singular value plots (frequency-dependent) of a system transfer function matrix will be extensively utilized in compensator design and evaluation, which will be presented in the following Chapter.

4. CONTROLLER DESIGN

4.1 Introduction

The preceeding chapters have provided the groundwork for meaningful SISO and MIMO feedback control system designs. In summary, the system operational characteristics have been examined, a series of simplified linear models has been derived and analized, and performance specifications outlined on a frequency domain basis.

In this chapter, the LQG/LTR methodology is presented and applied to the synthesis of several controllers. Section 4.2 is dedicated to a brief description of the LQG/LTR design methodology. Section 4.3 will fix the notation and control structure to be utilized. In Section 4.4, a controller formulation for the SISO system definition is presented. A comparison of the performance of the LQG/LTR SISO controller with the current design is performed. Section 4.5 addresses the scaling issue as it relates to MIMO controller design. Controller formulations for the MIMO system definitions are presented in Sections 4.6 and 4.7. The transient responses of the controlled systems are examined using both linear and non-linear simulations.

This Chapter will thus serve to highlight how desired control characteristics can be attained and evaluated through the systematic application of the frequency domain approach embodied in the LQG/LTR design methodology. The comparison of the LQG/LTR SISO controller with the current controller is particularly useful in illustrating, on a *conventional* SISO frequency domain basis, how increased system performance is *attained*. The SISO presentation

sets the stage for three MIMO system controller designs. The frequency domain interpretations pertinent to system performance which were presented for the SISO system are extended to the MIMO system definitions through the utilization of frequency-dependent plots of the singular values of a system transfer function matrix.

The first MIMO system design (MIMO System I) provides for the coordinated control of the engine power turbine and gas generator speeds. The utilization of this MIMO system definition, as compared to the SISO system definition, in providing increased disturbance rejection is presented. This comparison is useful in illustrating that the coordinated control of several variables can be utilized to attain a performance that is beyond the capabilities of scalar control.

The final two MIMO designs (MIMO System II) provide for the coordinated control of the engine power turbine speed and inter-turbine gas temperature. The MIMO controller designs for this system definition illustrate further the LQG/LTR design methodology and, in the first design model of this system definition, how the presence of a non-minimum phase zero within the desired control bandwidth presents a fundamental system performance restriction.

A concept emphasized in all the MIMO system designs presented in this Chapter is that desireable performance and disturbance rejection capabilities are provided at a specific point in the loop, i.e. at the plant output. Obtaining a "good" loop shape *simultaneously* at both the plant input and output is still of current research interest.

4.2 LQG/LTR Design Methodology Overview

A Model-Based Compensator (MBC) in a feedback control implementation, as presented by Athans [21] is shown in Figure 4.1. The linear model description given by the $\underline{A}$, $\underline{B}$ and $\underline{C}$ matrices is reproduced within the compensator, hence the Model-Based designation. It can be shown that there exists several values of the filter gain matrix $\underline{H}$, and the control gain matrix $\underline{G}$, that yield a nominally stable feedback control system. What distinguishes an LQG compensator from a MBC is in the specific way that the $\underline{H}$ and $\underline{G}$ matrices are computed.

The LQG proceedure begins with the nominal linear model state space description.

$$\frac{d}{dt}\, x(t) = \underline{A}\, \underline{x}(t) + \underline{B}\, \underline{u}(t) + \underline{L}\, \underline{\xi}(t) \tag{4.1a}$$

$$\underline{y}(t) = \underline{C}\, \underline{x}(t) + \underline{\theta}(t) \tag{4.1b}$$

which includes process white noise, $\underline{\xi}(t)$, and sensor white noise, $\underline{\theta}(t)$. The intensity matrices of $\underline{\xi}(t)$ and $\underline{\theta}(t)$ are assumed to be given by $\underline{I}$ and $\underline{\Theta}$, respectively.

The open-loop plant transfer function is

$$\underline{G}_p(s) = \underline{C}(s\underline{I}-\underline{A})^{-1}\underline{B} \tag{4.2}$$

and the MBC transfer function is

$$\underline{K}(s) = \underline{G}(s\underline{I}-\underline{A}+\underline{B}\ \underline{G}+\underline{H}\ \underline{C})^{-1}\underline{H} \tag{4.3}$$

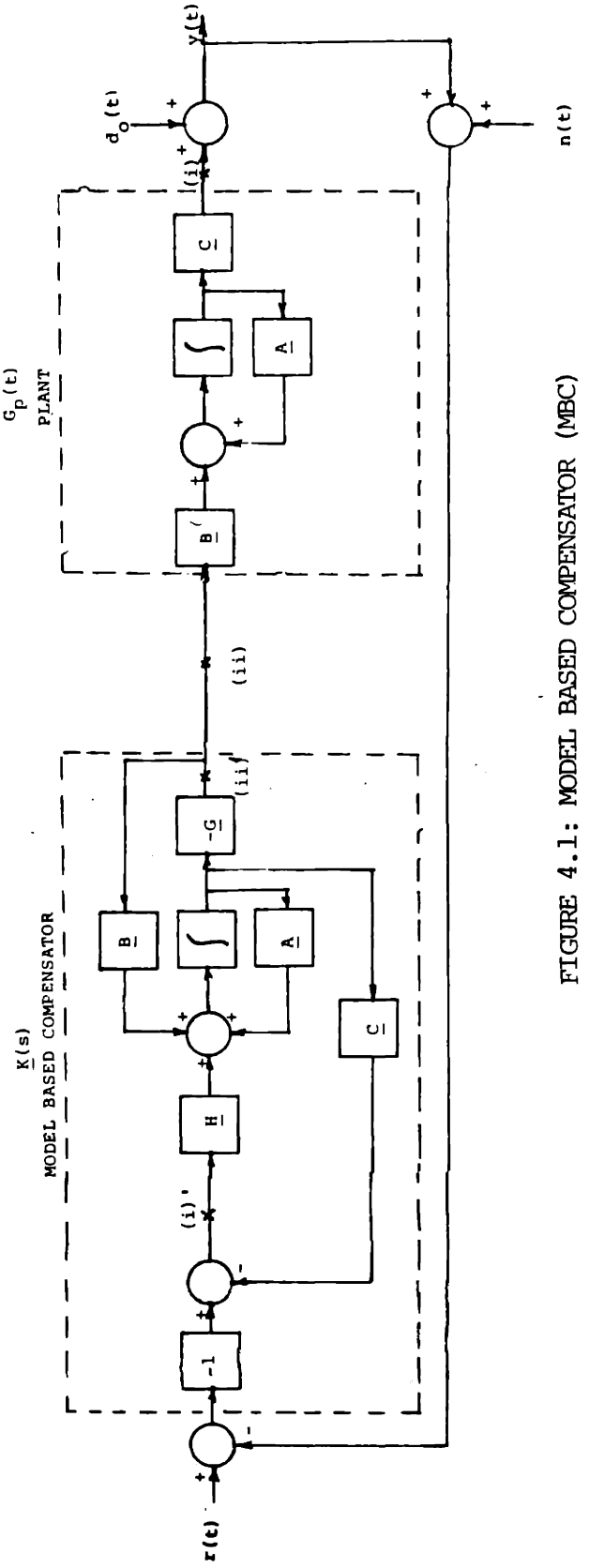

FIGURE 4.1: MODEL BASED COMPENSATOR (MBC)

FEEDBACK CONTROL IMPLIMENTATION

The gain matrices, $\underline{H}$ and $\underline{G}$ in Eq(4.3) are computed from:

Filter Gain: $\underline{H} = \underline{\Sigma}\,\underline{C}^T\underline{\Theta}^{-1}$

Control Gain: $\underline{G} = \underline{R}^{-1}\underline{B}^T\underline{P}$

Where $\underline{\Sigma}$ and $\underline{P}$ are the solutions to the Algebraic Riccati Equations (ARE):

Filter Alegebraic Riccati Equation (FARE)

$$\underline{A}\,\underline{\Sigma} + \underline{\Sigma}\,\underline{A}^T + \underline{L}\,\underline{L}^T - \underline{\Sigma}\,\underline{C}^T\underline{\Theta}^{-1}\,\underline{C}\,\underline{\Sigma} = 0 \tag{4.4a}$$

Control Algebraic Riccati Equation (CARE)

$$\underline{A}^T\underline{P} + \underline{P}\,\underline{A} + \underline{Q} - \underline{P}\,\underline{B}\,\underline{R}^{-1}\underline{B}^T\underline{P} = 0 \tag{4.4b}$$

The optimal estimation interpretation of the Kalman Filter will be discarded. The noise parameters $\underline{L}$ and $\underline{\Theta}$, in conjunction with the state and control weighting matrices $\underline{Q}$ and $\underline{R}$, will be used as design parameters to achieve desireable system frequency response characteristics.

The Loop Transfer Functions (LTF) at points (i)' and (ii)' in Figure 4.1 are:

$$\text{LTF at (i)'} = \underline{C}\Phi(j\omega)\underline{H} = \underline{G}_{KF}(j\omega) \tag{4.5}$$

$$\text{LTF at (ii)'} = \underline{G}\Phi(j\omega)\underline{B} = \underline{G}_{LQ}(j\omega) \tag{4.6}$$

where $\underline{\Phi}(j\omega) = ((j\omega)\underline{I} - \underline{A})^{-1}$.

Using the design parameters applicable to the solution of the respective Algebraic Riccati Equation, it is possible to shape $\underline{G}_{KF}(j\omega)$ and $\underline{G}_{LQ}(j\omega)$ in the frequency domain. The frequency domain properties of $\underline{G}_{KF}(j\omega)$, or

$\underline{G}_{LQ}(j\omega)$, as depicted by singular value plots, and their "goodness" in relation to the degree to which they conform to the frequency domain performance specifications presented in Chapter 3 is the criteria for design acceptance.

For the MIMO system definitions presented in this research, it is required to achieve a "good" LTF at the plant output, or point (i) in Figure 4.1. This was the motivation for reflecting robustness and disturbance rejection requirements to the plant output in Chapter 3. A "good" loop shape at the output will also insure good command following. Insuring a "good" loop shape simultaneously at the plant input is of current research interest.

An LQG controller, although providing a nominally stable design, is in general irrelevant to the feedback control design problem because it provides desireable frequency response characteristics within the MBC compensator structure (i.e. at points (i)' and ($\hat{i}$)') and not at the interface with the physical world where various command inputs, disturbances and uncertainties are presented. The application of Loop Transfer Recovery (LTR), or robustness recovery, used in conjunction with the LQG formulation, is shown in the following discussion to provide an integrated design tool, the LQG/LTR methodology needed to provide a meaningful control law.

The LQG/LTR methodology, applied to the MIMO system definitions in this research is to:

1. Shape $\underline{G}_{KF}(j\omega)$ in the frequency domain to satisfy performance and robustness specifications, then

2. solve the CARE for a specific $\underline{G} = \underline{G}_q$ using the following definition of the design parameters:

$$\underline{R} = \underline{I} \tag{4.7a}$$

$$\underline{Q} = q\underline{C}^T\underline{C} \tag{4.7b}$$

As $q \to \infty$, the system LTF at point $(^{ii})$ in Figure 4.1 will approach $\underline{G}_{KF}(j\omega)$ pointwise in ω

$$\underline{C}\ \underline{\Phi}(j\omega)\underline{B}\ \underline{G}_q[\Phi^{-1}(j\omega)+\underline{B}\ \underline{G}_q+\underline{H}\ \underline{C}]^{-1}\underline{H} \to \underline{C}\ \underline{\Phi}(j\omega)\underline{H} \tag{4.8}$$

if the plant contains no non-minimum phase zeros.

The recovery proceedure breaks down in the frequency range of a non-minimum phase zero. The presence of a non-minimum phase zero within the desired system bandwidth restricts the frequency range for which $\sigma_{min}\ \underline{I}(j\omega)$ can be made "large", thus limiting achievable performance. This restriction is generic in nature and should not be considered an indictment of the LQG/LTR methodology.

The dual of the recovery proceedure presented above is to shape $\underline{G}_{LQ}(j\omega)$ in the frequency domain, and to recover this loop shape at the plant input. This dual proceedure will be demonstrated for the SISO system definition controller design, which will be presented in Section 4.4. Desireable frequency response characteristics were more easily obtained using the dual proceedure for the SISO case.

4.3 Control Structure

Prior to initiating the design sequence, it is necessary to fix the system notation and control structure to be utilized. The control structure

is shown in Figure 4.2. To satisfy the performance requirements presented in Chapter 3, integrators are augmented at the plant input on each control channel. The integrators, although they will be physically built within the compensator, are considered to be part of the nominal plant for design purposes. The relation between the nominal plant for design purposes, $\underline{G}_D(s)$, the integral augmentation, $\underline{G}_a(s)$, and the nominal linear model $\underline{G}_p(s)$, is

$$\underline{G}_D(s) = \underline{G}_p(s)\underline{G}_a(s) \tag{4.9}$$

where $\underline{G}_a(s) = \underline{I}/s$.

The compensator derived using the LQG/LTR methodology is denoted by $\underline{K}_D(s)$. The resulting LTF for the loop broken at the output is defined by

$$\underline{T}(s) = \underline{G}_D(s)\underline{K}_D(s) = \frac{\underline{I}}{s}\underline{G}_p(s)\underline{K}_D(s) \tag{4.10}$$

For the scalar case, the corresponding forms of Eqs(4.9) and (4.10) are

$$g_d(s) = g_p(s)g_a(s) \tag{4.11}$$

where $g_a(s) = 1/s$, and

$$\begin{aligned} t(s) &= g_d(s)K_D(s) \\ &= \frac{1}{s}\ g_p(s)K_D(s) \end{aligned} \tag{4.12}$$

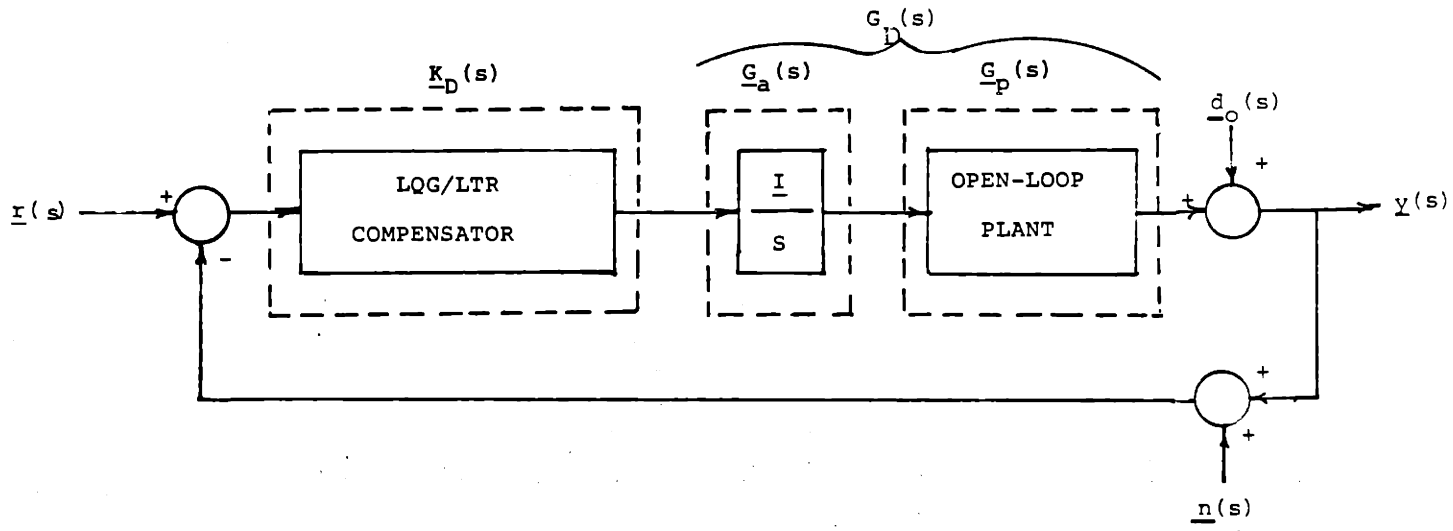

FIGURE 4.2: CONTROL STRUCTURE

4.4 SISO Controller Design

4.4.1 Loop Shaping in the Frequency Domain

The SISO system definition will provide scalar fuel flow control over a single output, the power turbine speed. The 90% N_g design model (SISO) with integral augmentation, required to provide isochronous power turbine speed governing, is utilized for this design.

The dual of the LQG/LTR methodology presented in section 4.2 will by utilized. This dual proceedure consists of shaping the LTF $g_{LQ}(j\omega)$ in the frequency domain and then recovering this loop shape at the plant input. The loop shape at this break point is not unique for a SISO system. The same loop shape is obtained from the same design sequence by breaking the loop at the output. The justification for using the dual proceedure is that the desired frequency response characteristics were easily obtained and interpreted for this particular design sequence.

The dual proceedure is presented here as applied to the SISO system definition. The design sequence is:

1. shape $g_{LQ}(j\omega)$ in the frequency domain to satisfy performance specifications, then
2. solve the FARE for a specific $\underline{H} = \underline{H}_q$ using the following definition of the design parameters.

$$\Theta = 1 \tag{4.13a}$$

$$\underline{L} = q\underline{B} \tag{4.13b}$$

As $q \to \infty$, the overall LTF, $t(j\omega)$ will approach $g_{LQ}(j\omega)$ pointwise in ω

$$\underline{G}[\underline{\Phi}^{-1}(j\omega) + \underline{B}\ \underline{G} + \underline{H}_q\underline{C}]^{-1}\ \underline{H}_q\underline{C}\ \underline{\Phi}(j\omega)\underline{B} \to \underline{G}\ \underline{\Phi}(j\omega)\underline{B} \tag{4.14}$$

provided that the plant contains no non-minimum phase zeros. The 90% N_g Design Model (SISO) contains no non-minimum phase zeros, so we can expect the LTR method to work.

The LTF, $g_{LQ}(j\omega)$ is shaped in this research using the following definition of the design parameters:

$$\underline{Q} = \underline{h}^T\underline{h} \tag{4.15a}$$

$$\underline{R} = r = \rho \tag{4.15b}$$

The design $g_{LQ}(j\omega)$, representing the design to be recovered, is shown in Figure 4.3 in relation to the performance specifications and with the numerical values of the design parameters.

The recovered loop shape, $t(j\omega)$, is shown in Figure 4.4. The recovery proceedure produced convergence in the low frequency region but was less successful in the frequency range of the tail rotor resonance range of the tail rotor resonance as indicated by the sharp notch at about 35 rad/sec. Recovery at this frequency could be assured by increasing q, but the "notch" characteristic is not detrimental to control operation.

The frequency response of the LQG/LTR compensator $k_D(s)$ is shown in Figure 4.5. The state space description of $k_D(s)$ is given in Appendix E. The recovery proceedure performance an approximate inversion of the open-loop plant dynamics in order to achieve the desired loop shape. This result can be proved rigorously [22], but is clearly demonstrated in this design by

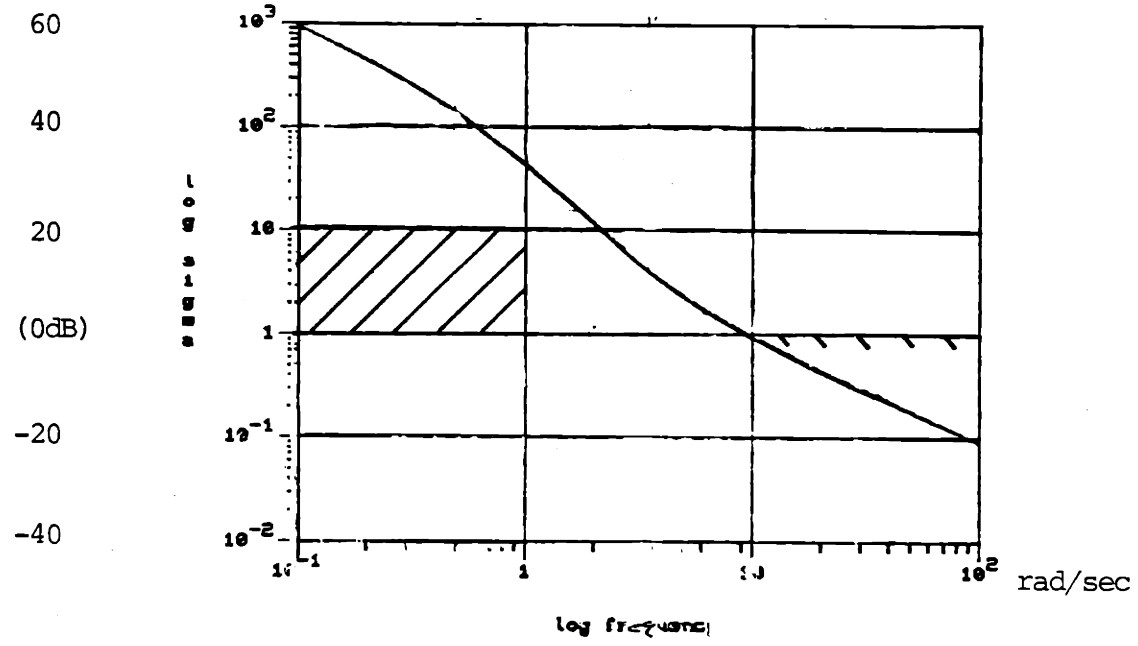

FIGURE 4.3: g_{LQ} FOR h=[0001001] ; r=.05.

MAGNITUDE vs. FREQUENCY

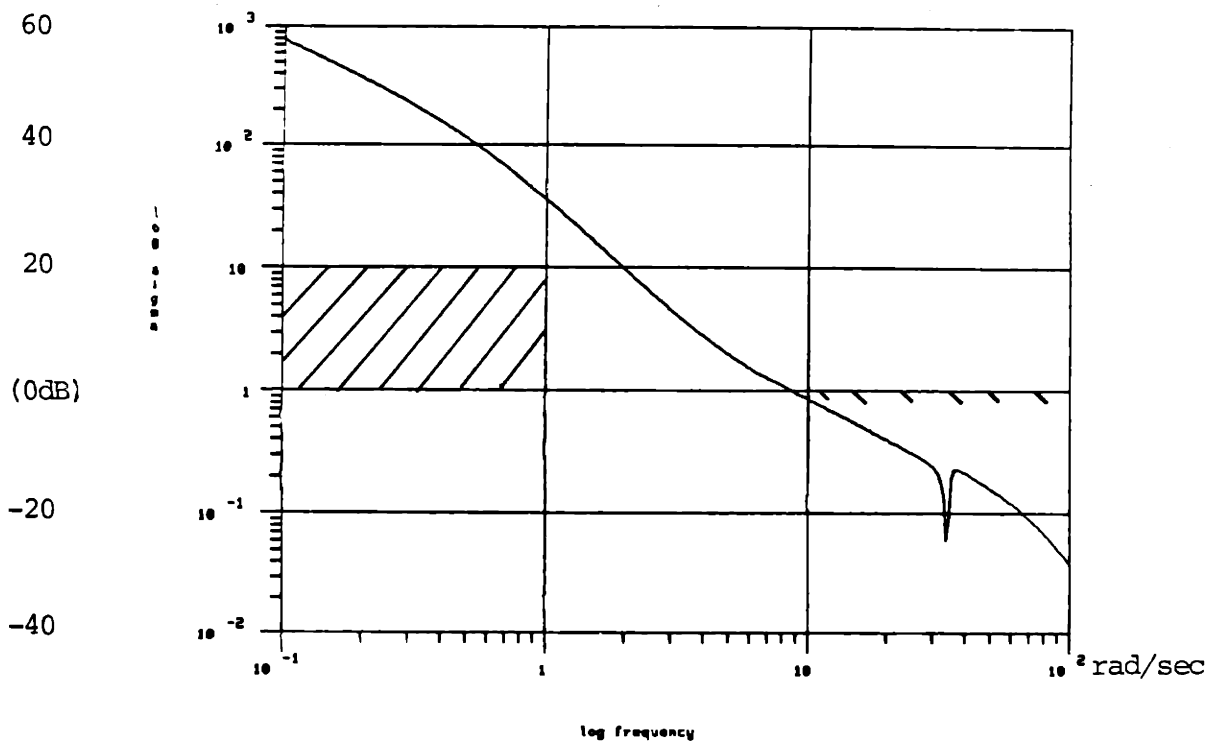

FIGURE 4.4: LOOP TRANSFER RECOVERY; q=100

MAGNITUDE vs. FREQUENCY

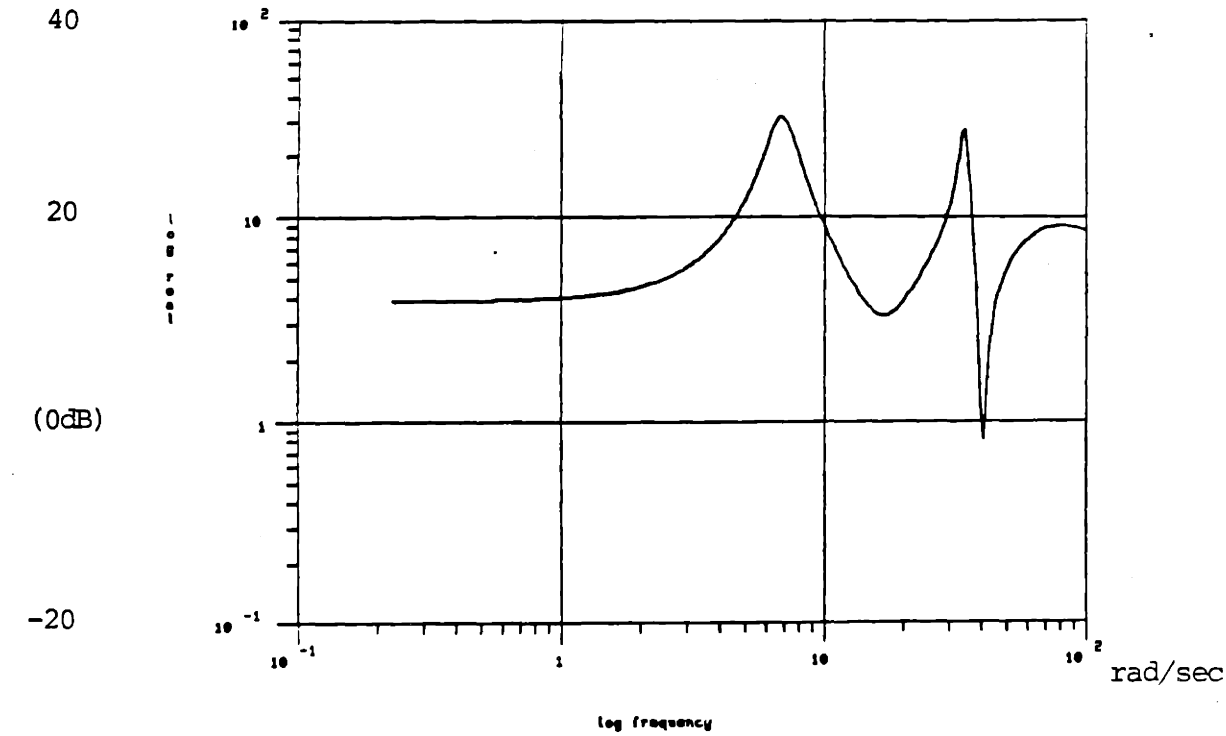

FIGURE 4.5: SISO LQG/LTR COMPENSATOR $k_D(j\omega)$

MAGNITUDE vs. FREQUENCY

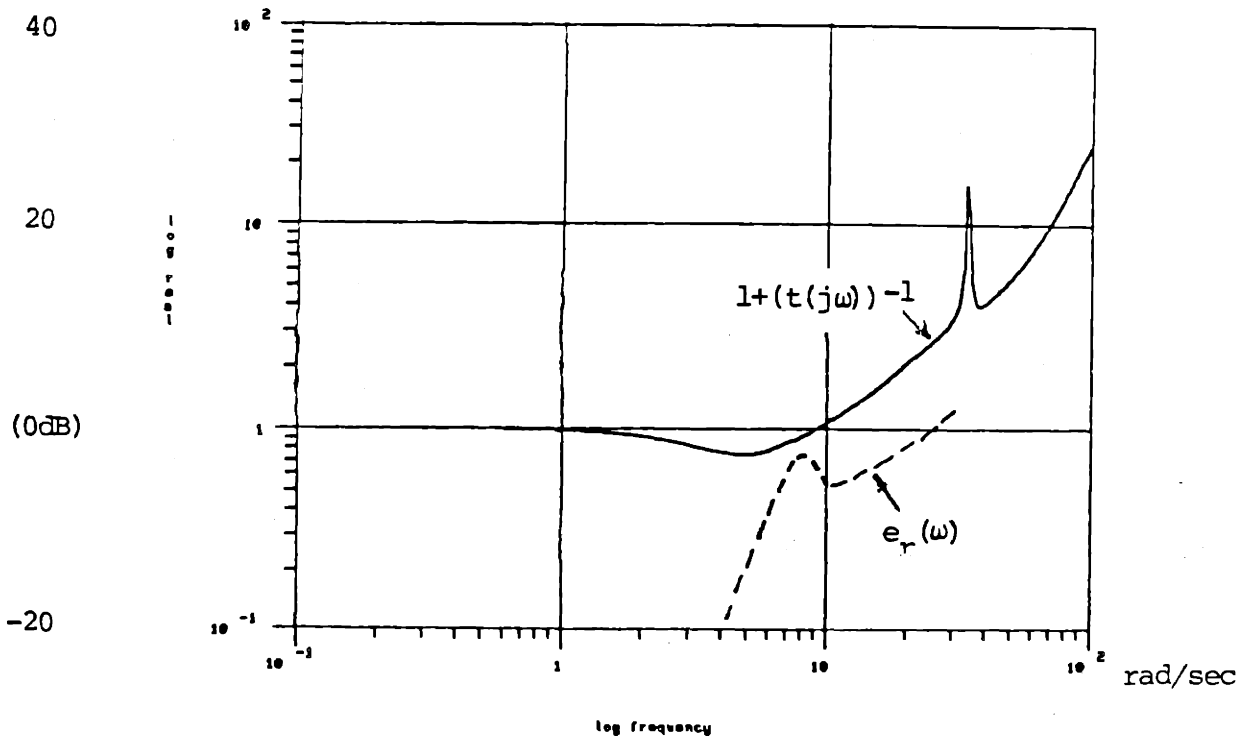

FIGURE 4.6: ROBUSTNESS REQUIREMENT PLOT

$e_r(\omega) < 1+(t(j\omega))^{-1}$

MAGNITUDE vs. FREQUENCY

comparing the compensator transfer function in Figure 4.5 to the open-loop plant transfer function shown in Figure 3.1. The LQG/LTR derived compensator, $k_D(s)$ is recognized as the approximate inverse of the open-loop plant. The inverse is obtained in the compensator through tne use of underdamped complex pole and zero pairs to cancel the helicopter rotor system dynamics.

Robustness, for the modeling errors defined in Chapter 3, is assured as shown in Figure 4.6. The closed-loop transfer function, shown in Figure 4.7, displays how the input-output behavior approximates that of an underdamped ($\xi \cong .45$) second order system. The inverse of the return difference transfer function, also called the sensitivity transfer function, which is indicative of system response to output disturbances, is shown in Figure 4.8. Output disturbances presented in the 0-8 rad/sec frequency range will be attenuated.

4.4.2 Linear Simulations

The linear system response to a unit step command on power turbine speed is shown in Figure 4.9. The settling time (~1.5 secs) and the maximum overshoot (~.2) of the power turbine speed output is consistent with the underdamped characteristics displayed by the closed-loop transfer function presented in the previous section. The response of the system to a unit step output disturbance on power turbine speed is shown in Figure 4.10. The step disturbance is rejected.

The behavior of the fuel flow control variable during the transients depicted in Figures 4.9 and 4.10 is oscillatory. Fuel flow is oscillatory at the frequency (~1 Hz) at which the compensator provided an underdamped pole

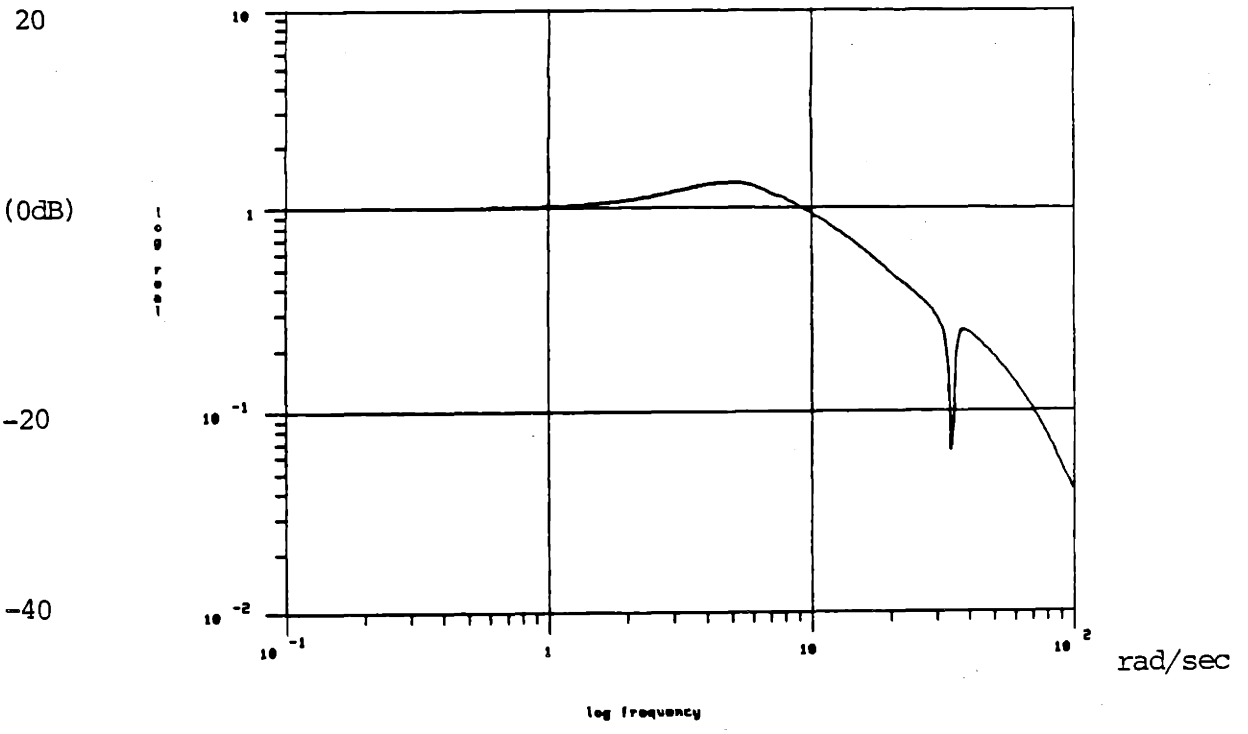

FIGURE 4.7: CLOSED-LOOP TRANSFER FUNCTION

MAGNITUDE vs. FREQUENCY

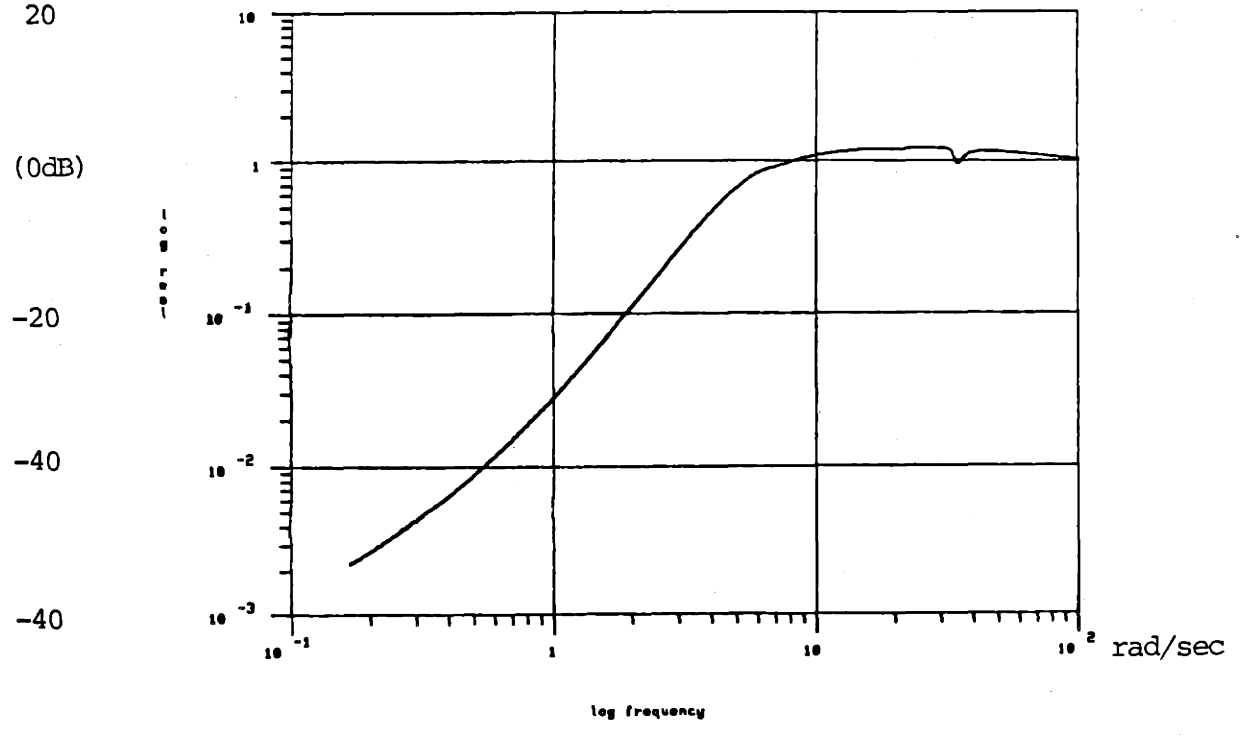

FIGURE 4.8: SENSITIVITY TRANSFER FUNCTION

MAGNITUDE vs. FREQUENCY

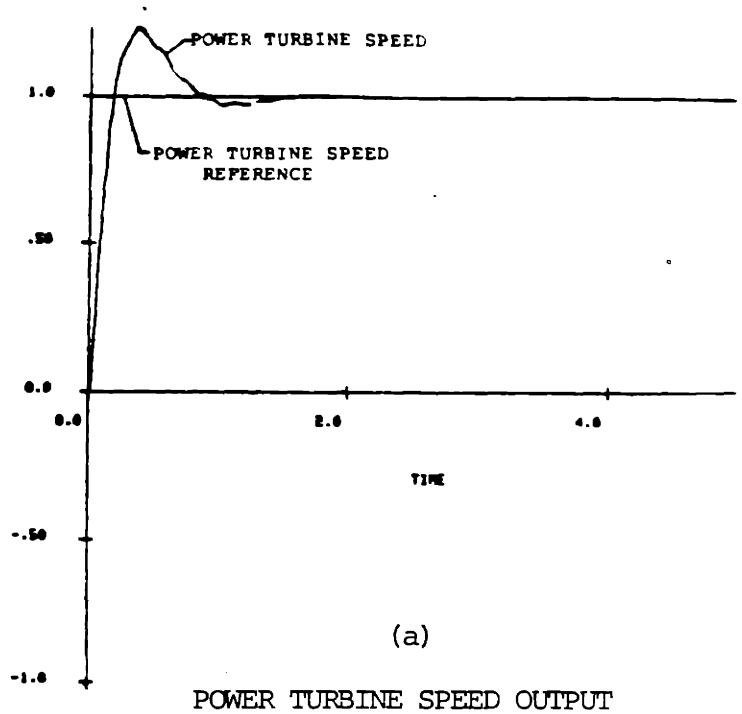

(a)

POWER TURBINE SPEED OUTPUT

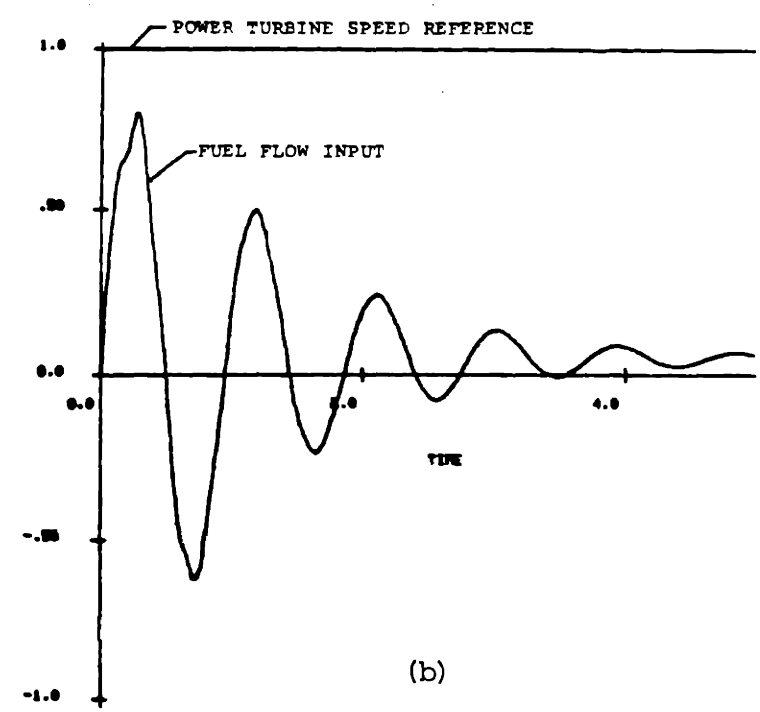

(b)

FUEL FLOW INPUT

FIGURE 4.9: LINEAR SIMULATION OF STEP RESPONSE OF COMPENSATED SYSTEM TO POWER TURBINE SPEED DEMAND

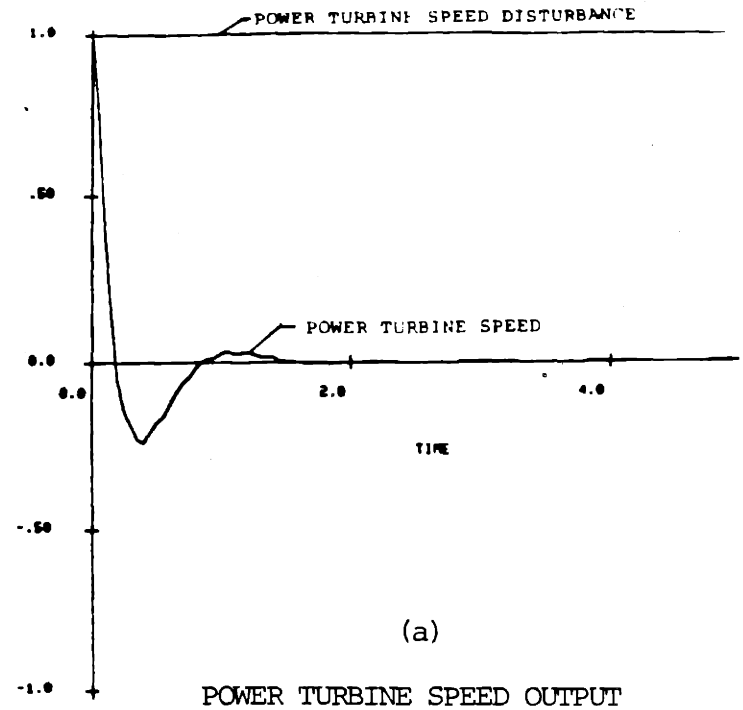

(a)

POWER TURBINE SPEED OUTPUT

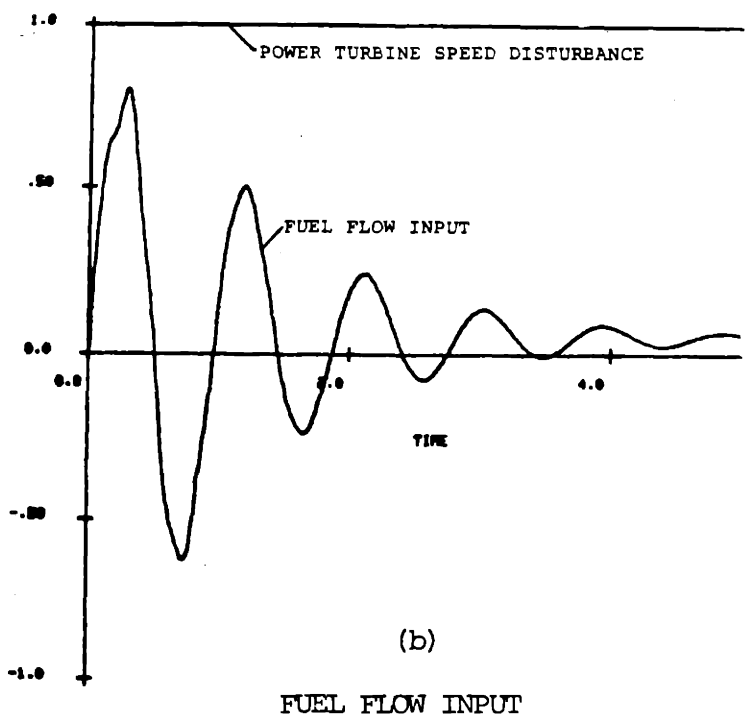

(b)

FUEL FLOW INPUT

FIGURE 4.10: LINEAR SIMULATION OF STEP RESPONSE OF COMPENSATED SYSTEM TO POWER TURBINE SPEED OUTPUT DISTURBANCE

pair to cancel the first rotor system anti-resonance. So that while the input-output behavior is given by Figure 4.7, the internal variables, including the fuel-flow control, will clearly be influenced by the compensator dynamics. The oscillatory characteristic shown in Figures 4.9 and 4.10 will be evaluated for a typical system transient on the non-linear simulation, to be presented in the next section.

4.4.2 Non-Linear Simulation

A typical system transient is displayed in Figure 4.11. The transient is a 1 sec load demand by the helicopter rotor systems that represents ~30% of total helicopter power capability. The transient is performed about the 90% N_g design point. Negligible power turbine speed deviation from referenced value (i.e. 100%) is displayed.

Note that the fuel flow control variable is not as oscillatory as was demonstrated in the linear simulation. This is because the realizeable ramp load disturbance exercised on the non-linear simulation has a lower frequency content than the step disturbance utilized in the linear simulation. Further evaluation is required to determine if the compensator performance is acceptable for all realizeable transients.

The identical load disturbance as performed on a non-linear simulation of the current controller is shown in Figure 4.12. Power turbine speed deviation of 2-1/2% from the 100% referenced value is noted. An approximate inverse of the sensitivity transfer function of the current controller as compared to that of the LQG/LTR controller is shown in Figure 4.13. The smaller frequency

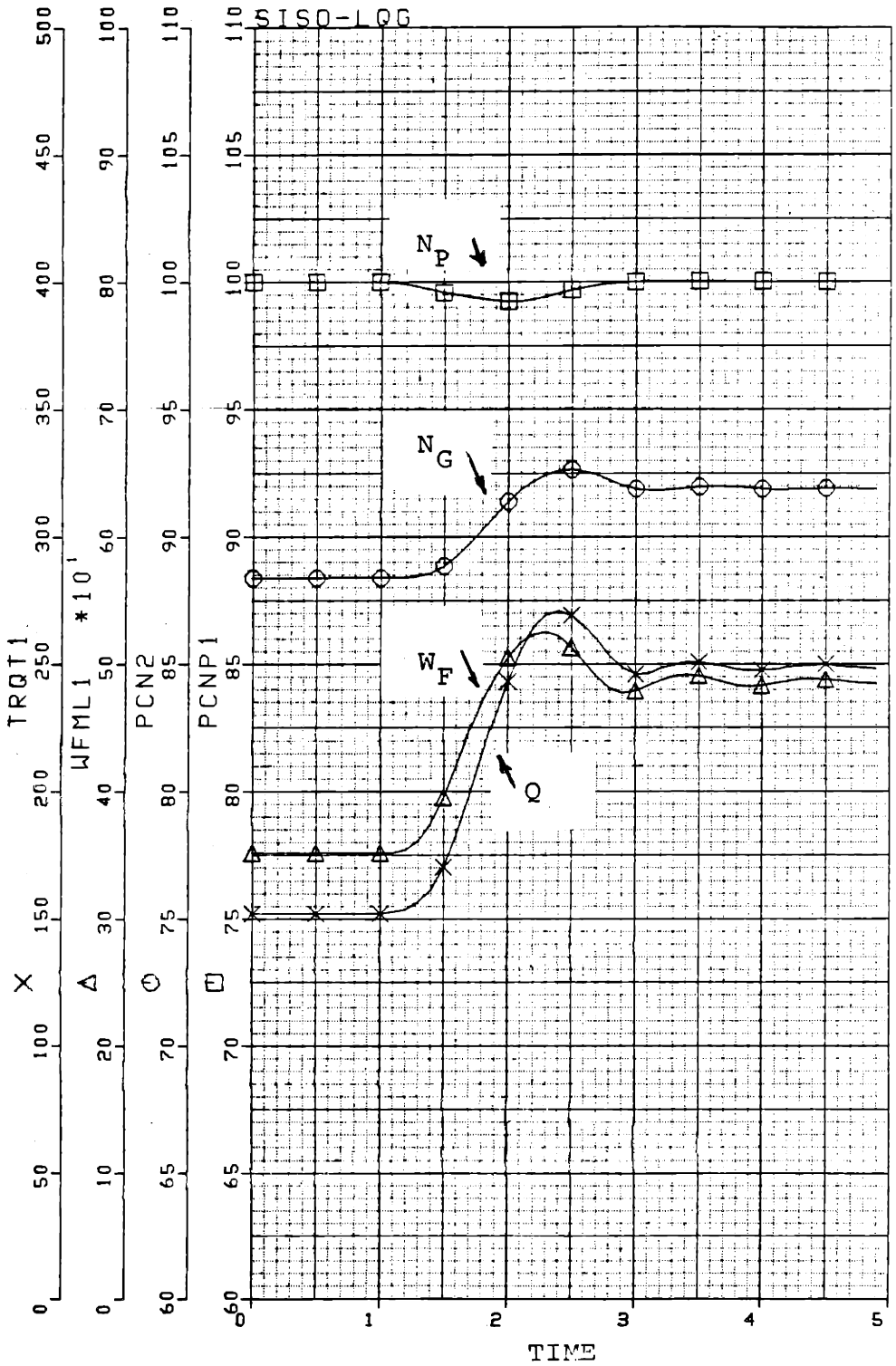

FIGURE 4.11: NON-LINEAR SIMULATION OF SISO LQG/LTR COMPENSATED SYSTEM RESPONSE TO 30% LOAD DEMAND IN 1 sec

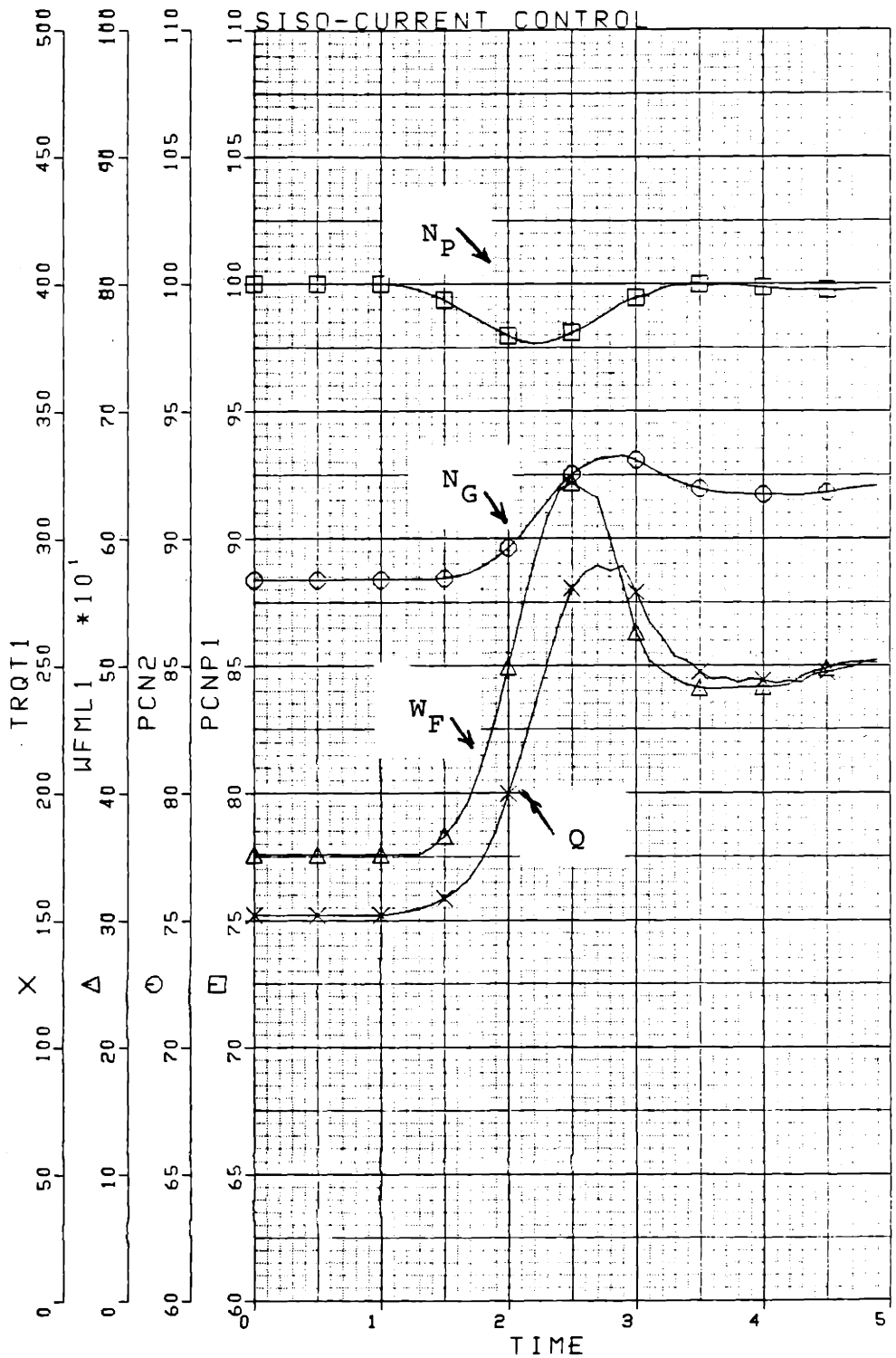

FIGURE 4.12: NON-LINEAR SIMULATION OF CURRENT CONTROLLER COMPENSATED SYSTEM RESPONSE TO 30% LOAD DEMAND IN 1 sec

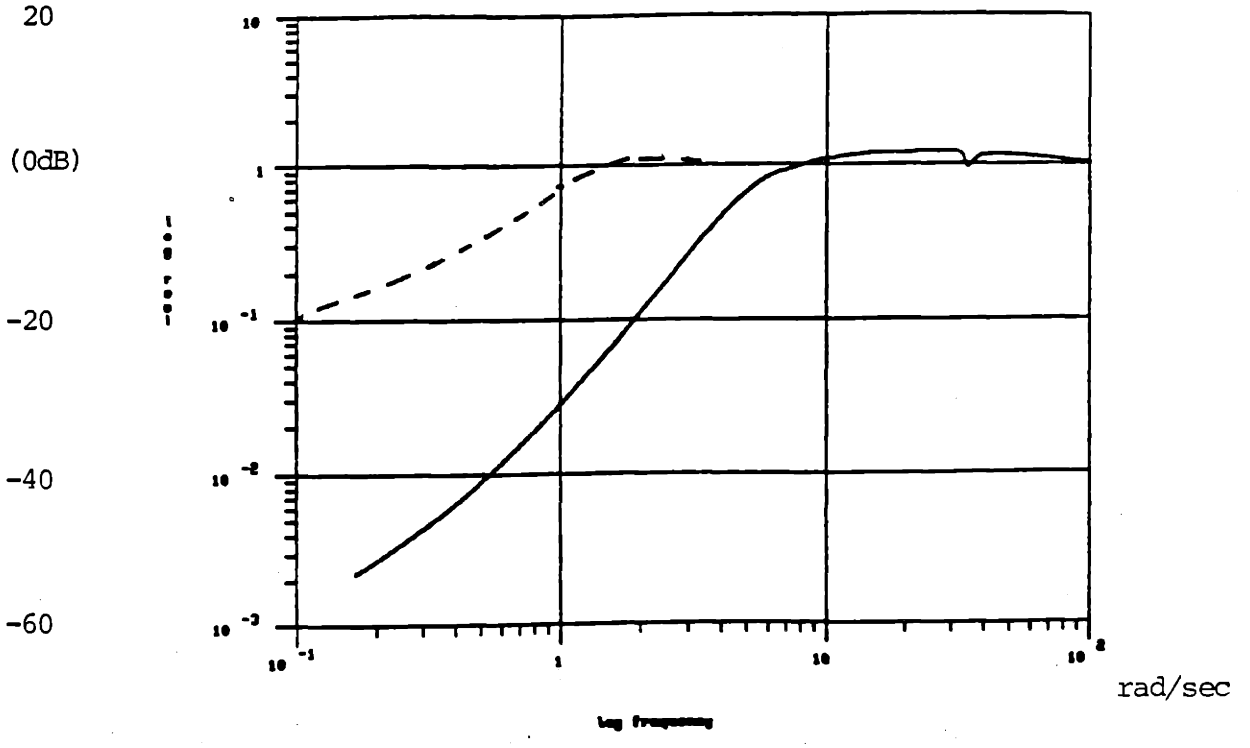

LEGEND

----CURRENT CONTROL SYSTEM
——LQG/LTR CONTROL SYSTEM

FIGURE 4.13: COMPARISON OF THE SENSITIVITY TRANSFER FUNCTIONS OF THE CURRENT AND LQG/LTR CONTROL SYSTEM DESIGN

range, as compared to the LQG/LTR controller, for which the current controller can reject or attenuate output disturbances is the cause for the larger power turbine speed deviation displayed in Figure 4.12.

4.4.4 Design Summary

The performance and robustness goals, as evaluated in the frequency domain, were achieved for the SISO system definition. Linear simulations of the compensated system displayed fast response times consistent with the characteristics of the frequency dependent plots of the system transfer functions. A non-linear simulation comparison of the LQG/LTR SISO controller with the current controller for a realizeable helicopter transient displayed the potential for an increase in performance attainable with an LQG/LTR controller. The increase in system performance was quantified by noting that the sensitivity transfer function of the LQG/LTR controller provided load disturbance rejection over a wider range of frequencies than did the current SISO controller.

4.5 Scaling

Scaling is necessary in MIMO system controller design in order to non-dimensionalize the gain relations represented by the singular value plots. Scaling provides an absolute basis for numerical comparison. Scaling is a linear transformation of the nominal linear state description

accomplished by redefining the state, $\underline{x}$, output, $\underline{y}$, and control variables $\underline{u}$ such that

$$\underline{x} = \underline{N}_x \underline{x}_n \ , \tag{4.16a}$$

$$\underline{y} = \underline{N}_y \underline{y}_n \ , \tag{4.16b}$$

and

$$\underline{u} = \underline{N}_u \underline{u}_n \ . \tag{4.16c}$$

Where $\underline{N}_x$, $\underline{N}_y$ and $\underline{N}_u$ are square, diagonal matrices. The above scaling definition results in the following transformation of the system matrices.

$$\underline{A}_n = \underline{N}_x^{-1} \underline{A} \underline{N}_x \tag{4.17a}$$

$$\underline{B}_n = \underline{N}_x^{-1} \underline{B} \underline{N}_u \tag{4.17b}$$

$$\underline{C}_n = \underline{N}_y^{-1} \underline{C} \underline{N}_x \tag{4.17c}$$

$$\underline{D}_n = \underline{N}_y^{-1} \underline{D} \underline{N}_u \tag{4.17d}$$

The choice of an appropriate scaling transformation is problem dependent. The scaling transformation matrices utilized for this research are given in Appendix F, along with the scaled system matrices for each MIMO design model.

The singular value plots of the open-loop, scaled MIMO system definitions are shown in Figures 4.14-4.16. Note that the singular values are less skewed, or closer together than in the unscaled depictions of Figures 3.2-3.4.

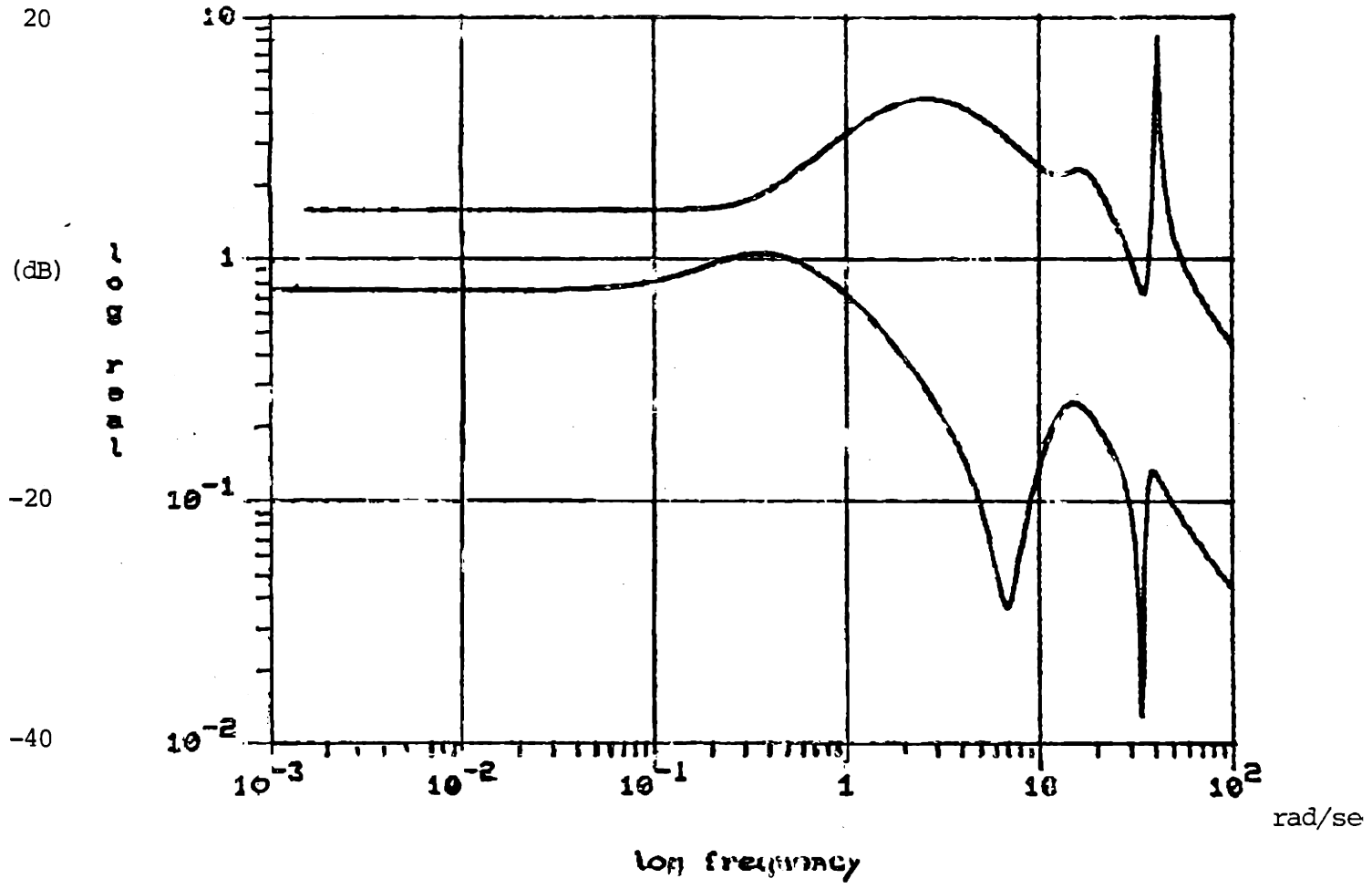

FIGURE 4.14: SINGULAR VALUE PLOT OF SCALED OPEN-LOOP

TRANSFER FUNCTION

MIMO SYSTEM I - 83% N_g DESIGN MODEL (MIMO)

SINGULAR VALUES vs. FREQUENCY

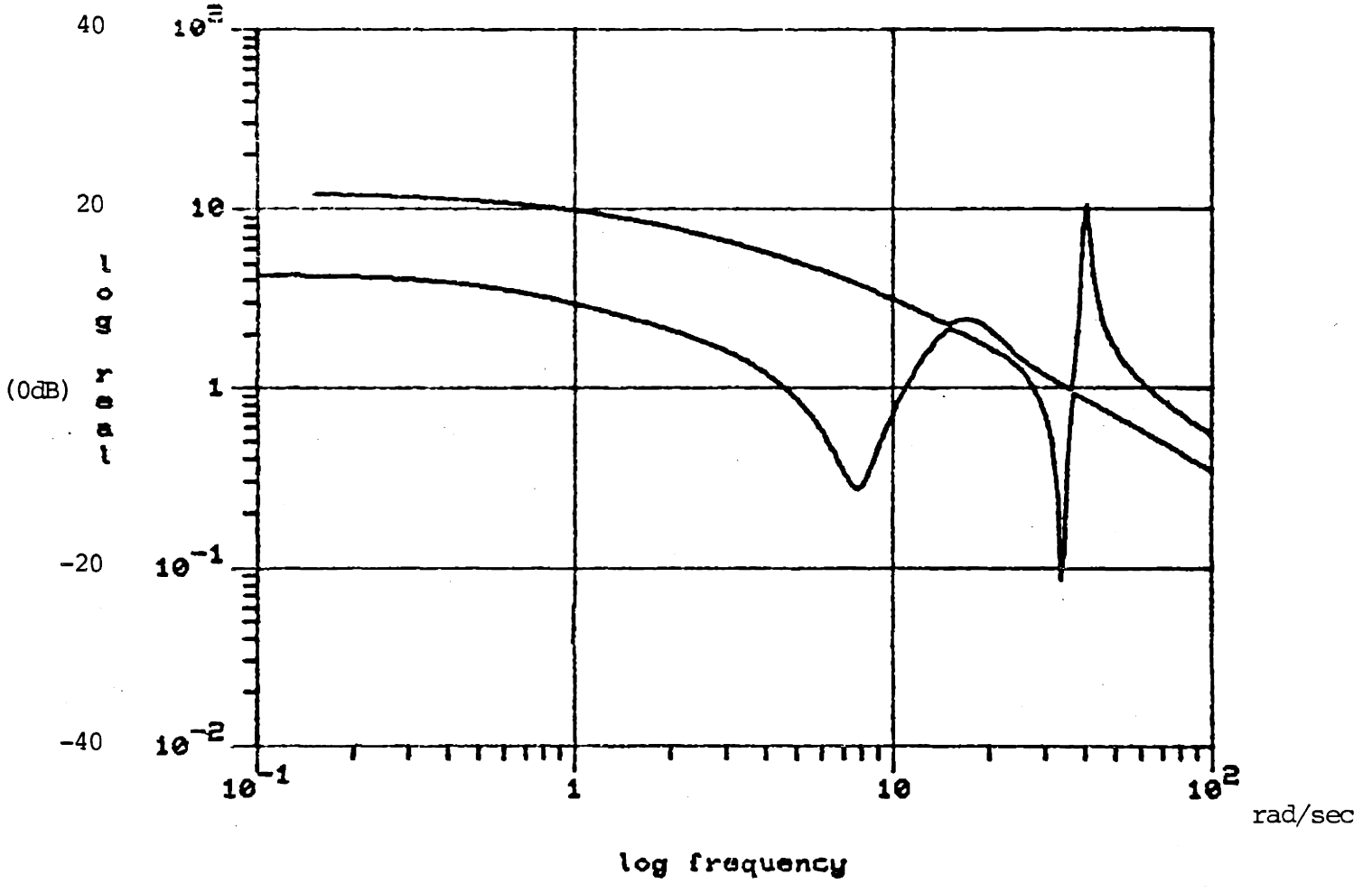

FIGURE 4.15: SINGULAR VALUE PLOT OF SCALED OPEN-LOOP

TRANSFER FUNCTION

MIMO SYSTEM II-90% N_g DESIGN MODEL (MIMO)

SINGULAR VALUES vs. FREQUENCY

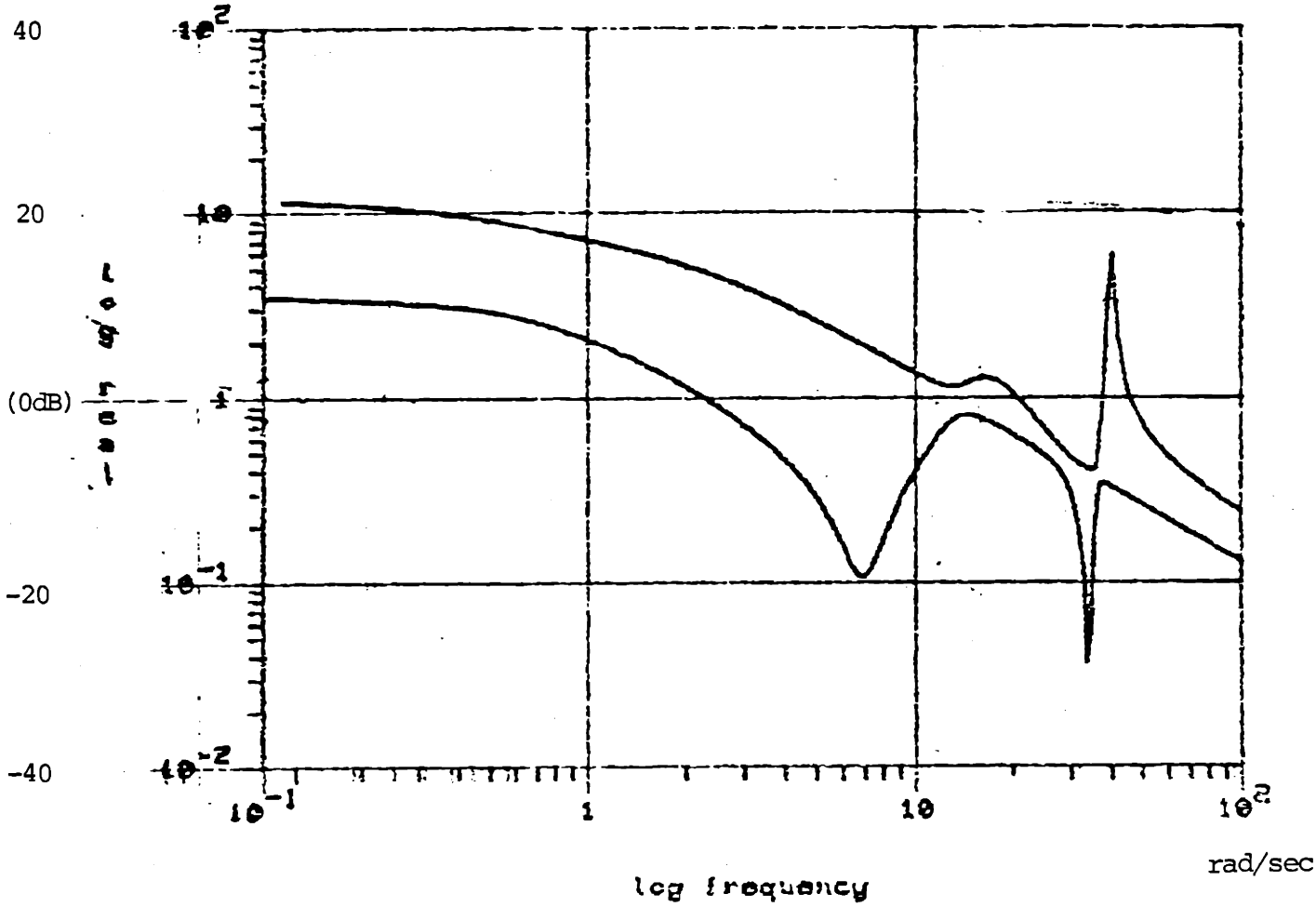

FIGURE 4.16: SINGULAR VALUE PLOT OF SCALED OPEN-LOOP TRANSFER FUNCTION

MIMO SYSTEM II-95% N_g DESIGN MODEL (MIMO)

SINGULAR VALUES vs. FREQUENCY

4.6 MIMO System I

The system definition presented by MIMO System I is formulated to provide multivariable control using the fuel flow and variable geometry control variables to regulate both the power turbine speed and gas generator speed. The ability to have the gas generator follow step command inputs while maintaining constant power turbine speed will be evaluated on a linear simulation. The use of this control system definition for input and output disturbance rejection as compared to a SISO controller will also be evaluated on a linear simulation. Non-linear simulations were not at all successful due to numerical constraints of the non-linear simulation.

Integral augmentation on both input channels was performed. The design was carried out at one operating point using the 83% N_g design model (MIMO). A desireable or "good" loop shape will be attained at the plant output in order to provide for good command following and output disturbance rejection as specified in Chapter 3.

4.6.1 Loop Shaping

A singular value plot of the integral augmented, scaled, open-loop plant is shown in Figure 4.17. The design $\underline{G}_{KF}(j\omega)$ representing the loop shape to be recovered at the plant output is shown in Figure 4.18 with the applicable design parameters and performance specifications. The loop shape recovered at the output is shown in Figure 4.19. Performance specifications, in terms of low frequency gain, are achieved. A singular value plot of the Closed-Loop Transfer Function Matrix (CLTFM) is shown in Figure 4.20. The system band-

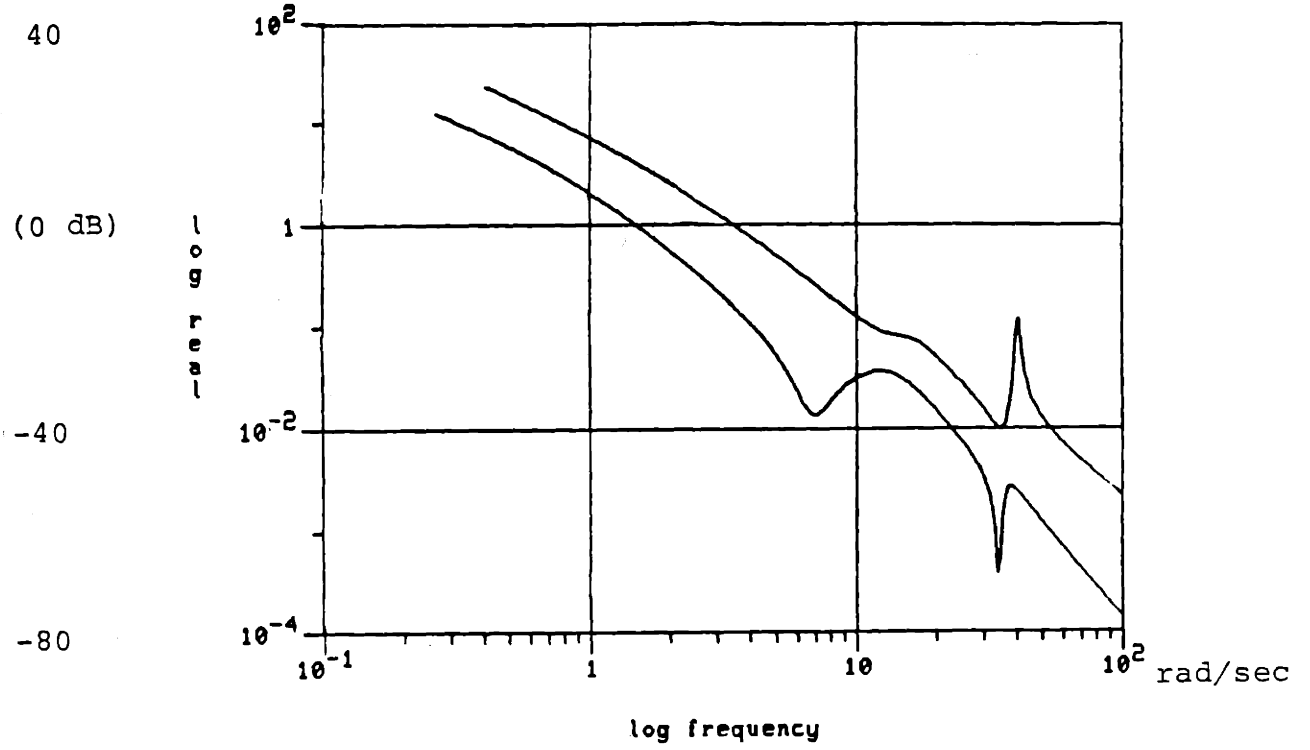

FIGURE 4.17: MIMO SYSTEM I - 83% N_g DESIGN MODEL
INTEGRAL AUGMENTED OPEN-LOOP PLANT
SINGULAR VALUES vs. FREQUENCY

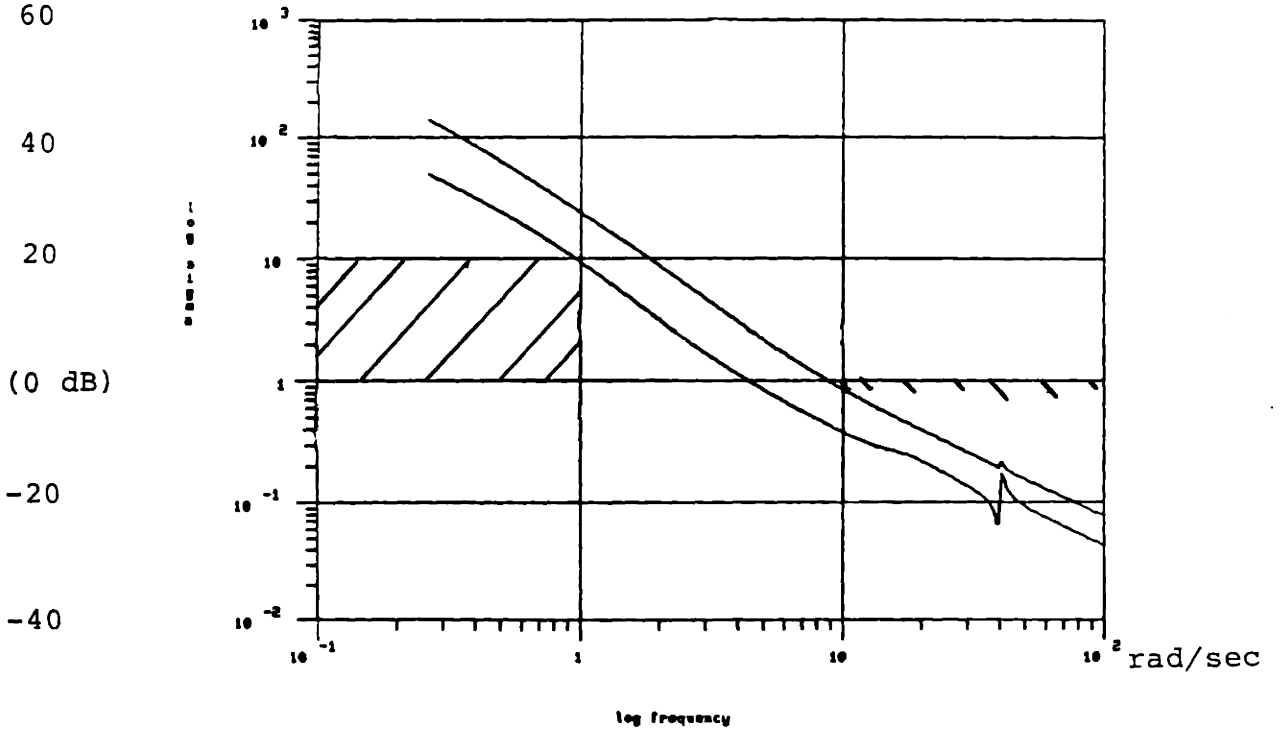

FIGURE 4.18: $\underline{G}_{KF}(j\omega)$ FOR $\underline{L}=\underline{B}$, $\underline{\Theta}=\begin{bmatrix} .05 & 0 \\ 0 & .1 \end{bmatrix}$
SINGULAR VALUES vs. FREQUENCY

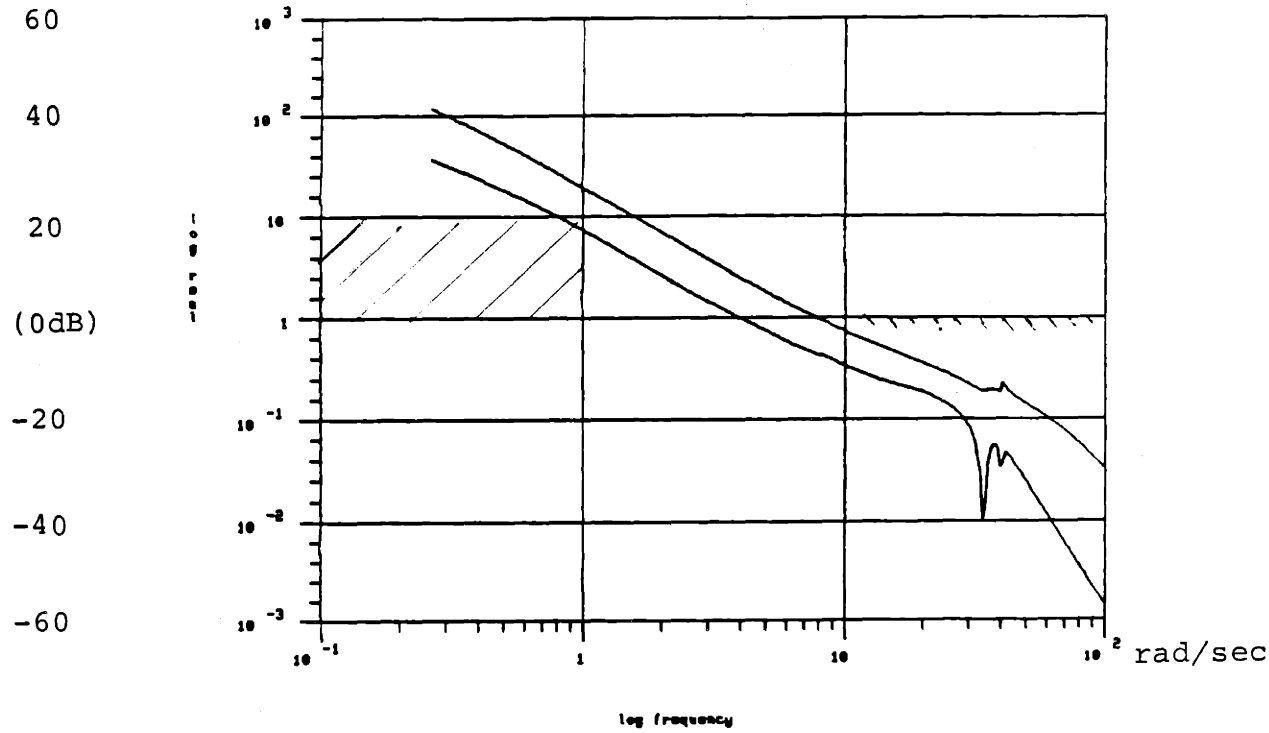

FIGURE 4.19: LOOP TRANSFER RECOVERY: q=100

SINGULAR VALUES vs. FREQUENCY

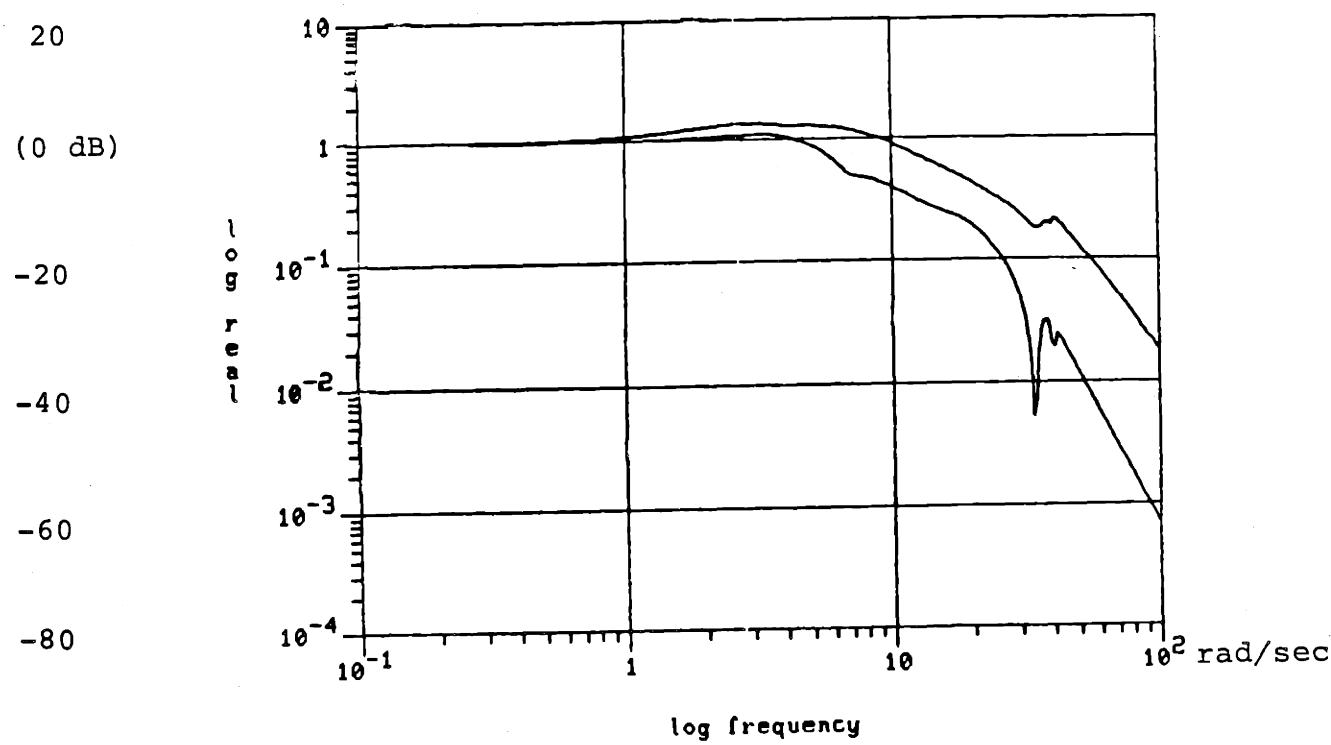

FIGURE 4.20: CLOSED-LOOP TRANSFER FUNCTION

SINGULAR VALUES vs. FREQUENCY

width is in the approximate range of 6-10 rad/sec. The specific bandwidth realized will depend upon the specific input direction. It is readily seen that by keeping the singular values of the system together, the system response can be made independent of command input direction. Since the bandwidth of this system is high and the singular values are relatively close together, little variation in system response due to command input direction is expected.

A singular value plot of the Sensitivity Transfer Function Matrix (STFM) is shown in Figure 4.21. Since the singular values of the STFM are relatively close together, the system will reject output disturbances uniformly, or independent of output disturbance direction.

Robustness, for the modeling errors defined in Chapter 3, is achieved as shown in Figure 4.22.

A singular value plot of the LQG/LTR compensator, $\underline{K}_D(s)$ is shown in Figure 4.23. Note that the compensator provides underdamped poles and zeros to cancel helicopter rotor system dynamics, as did the SISO controller. The state space description of $\underline{K}_D(s)$ is given in Appendix G1.

4.6.2 Linear Simulation

The response of the system to a step command on gas generator speed is shown in Figure 4.24. The setting time (~1 sec) is consistent with the system bandwidth presented in the previous section and with the fact that $\underline{T}(j\omega)$ is made "large" over a wide range of frequencies. The response of the system to a step disturbance on power turbine speed output is shown in Figure 4.25. The step disturbance is rejected.

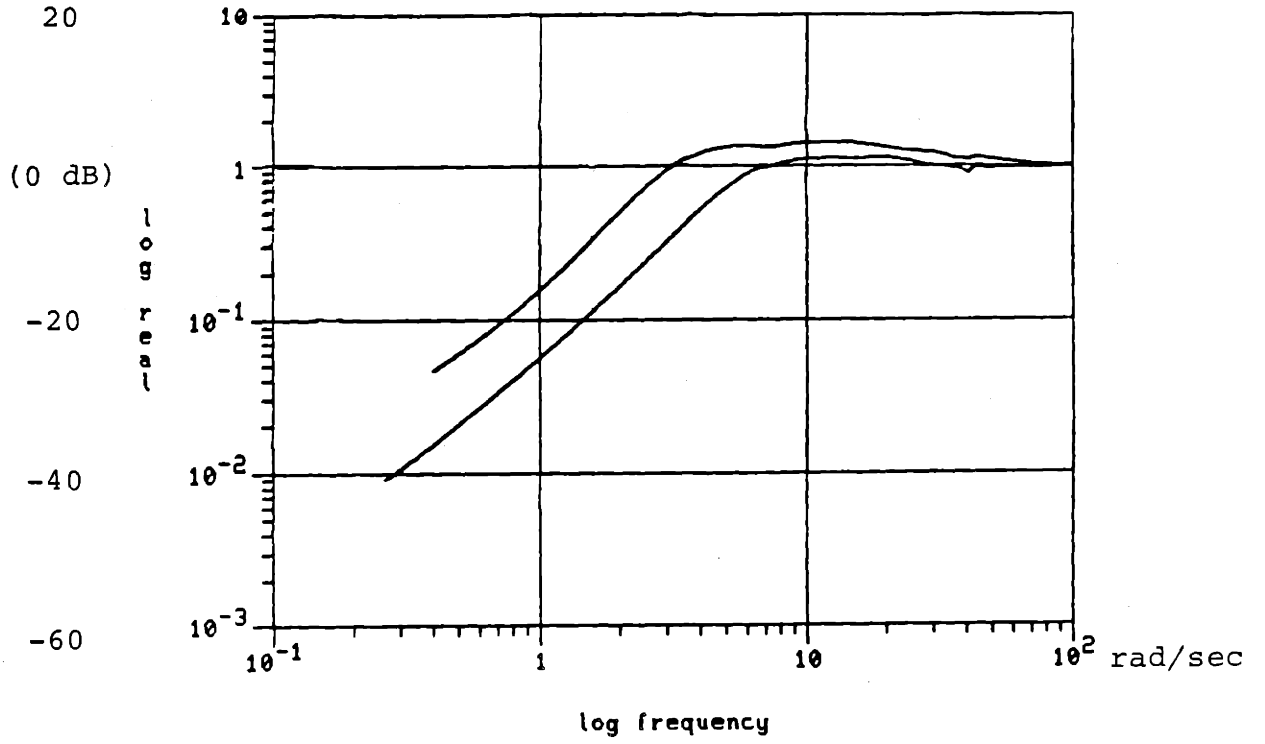

FIGURE 4.21: SENSITIVITY TRANSFER FUNCTION

SINGULAR VALUES vs. FREQUENCY

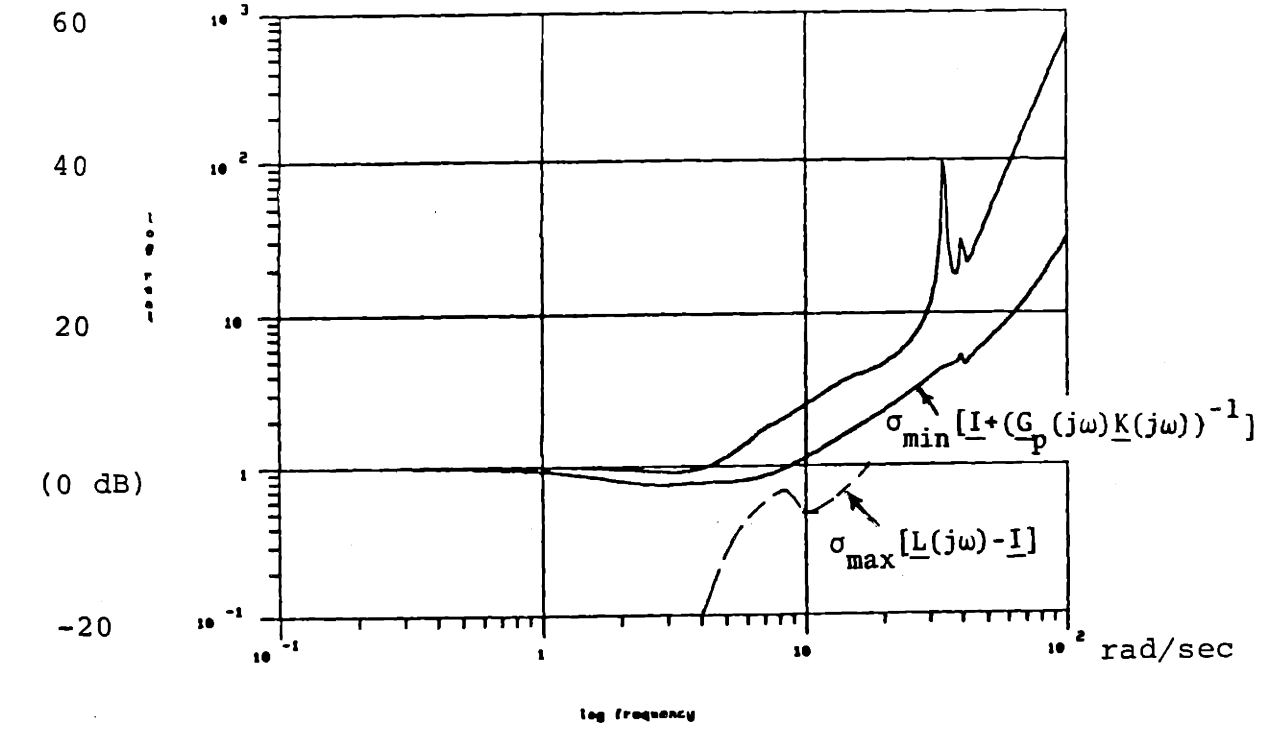

FIGURE 4.22: ROBUSTNESS REQUIREMENT PLOT

SINGULAR VALUES vs. FREQUENCY

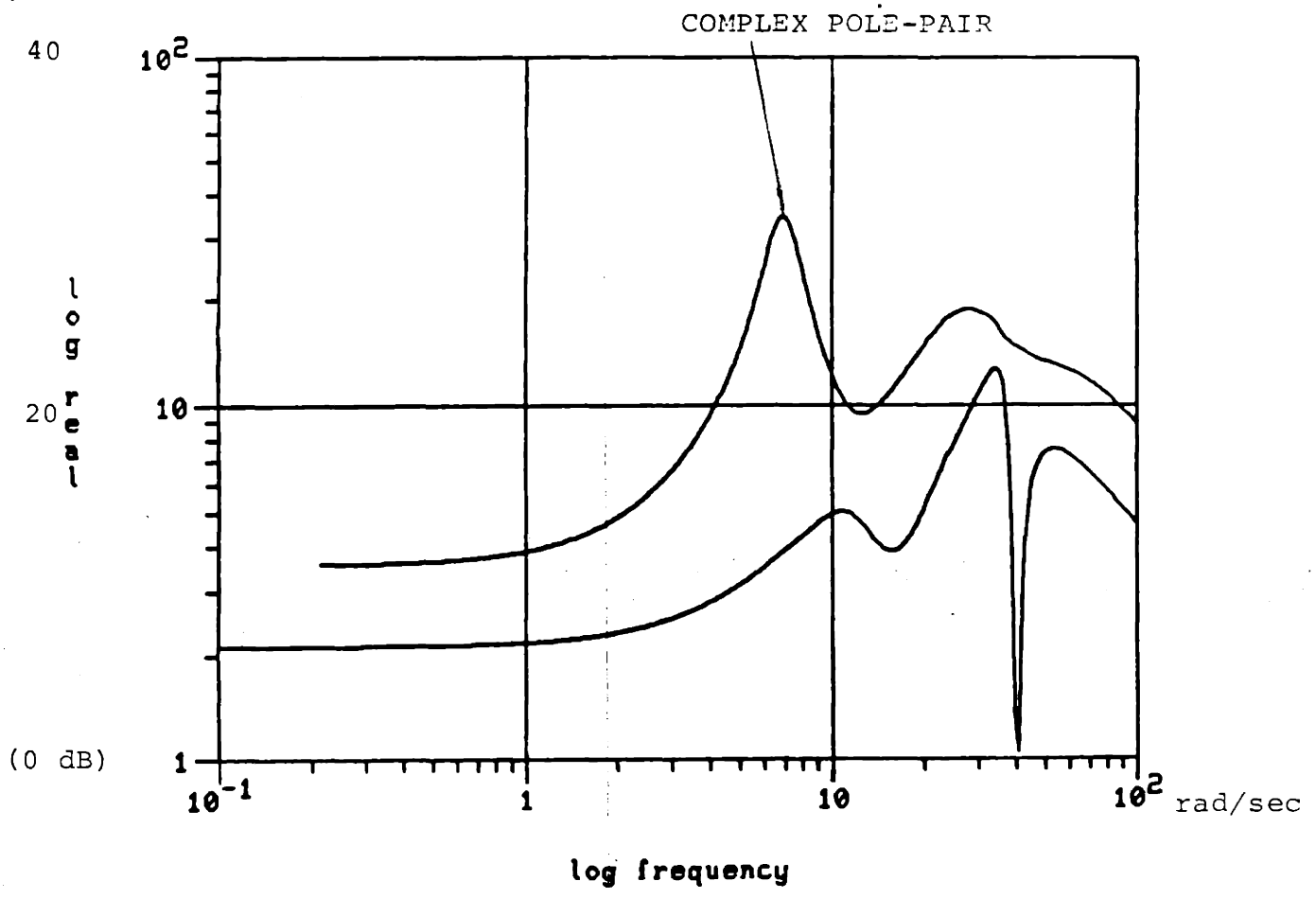

FIGURE 4.23: LQG/LTR COMPENSATOR $\underline{K}_D(j\omega)$

SINGULAR VALUES vs. FREQUENCY

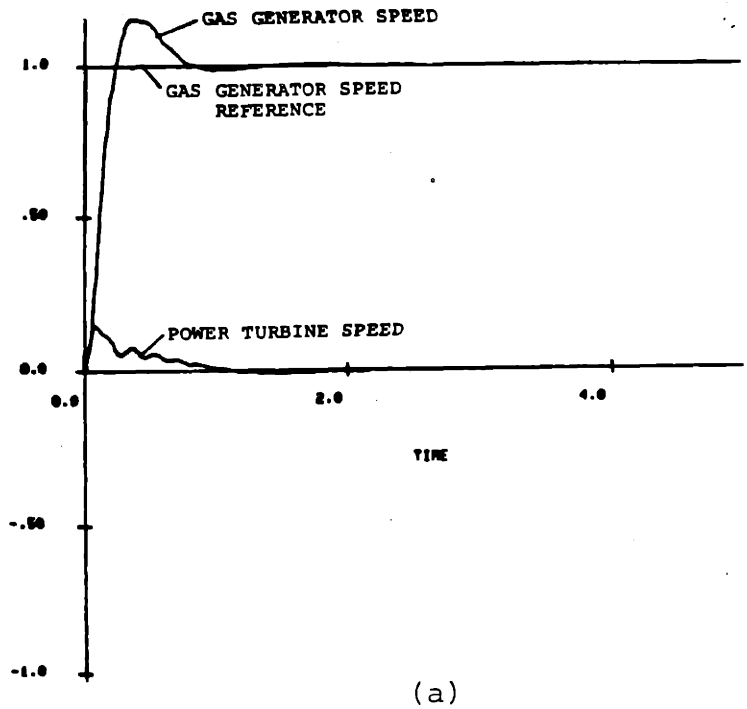

(a)

POWER TURBINE AND GAS GENERATOR SPEED OUTPUTS

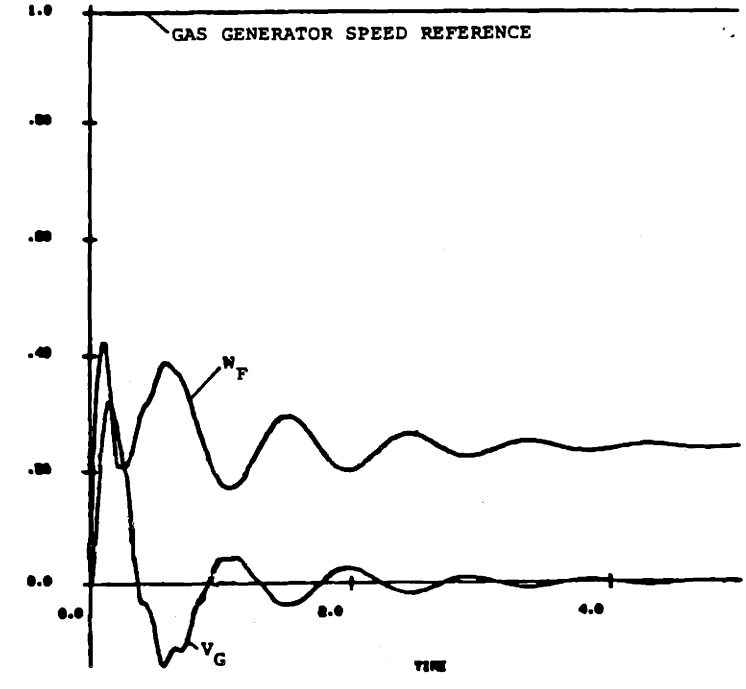

(b)

W_F AND V_G INPUT VARIABLES

FIGURE 4.24: LINEAR SIMULATION OF STEP RESPONSE OF COMPENSATED SYSTEM TO GAS GENERATOR SPEED DEMAND

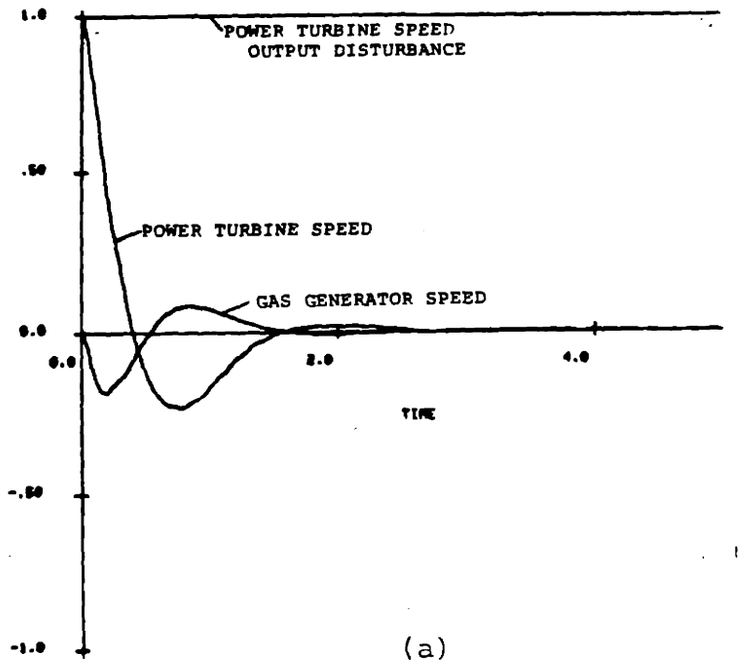

(a)

POWER TURBINE AND GAS GENERATOR SPEED OUTPUTS

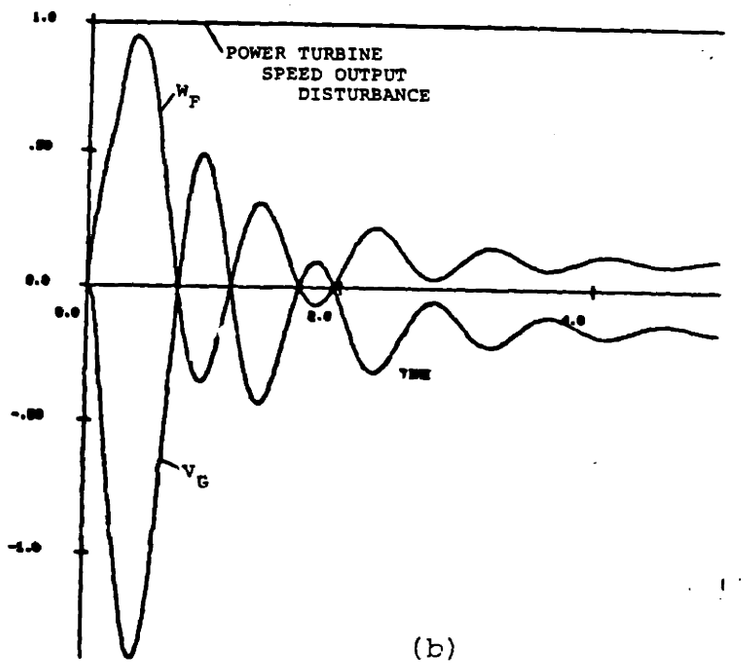

(b)

W_F AND V_G INPUT VARIABLES

FIGURE 4.25: LINEAR SIMULATION OF STEP RESPONSE OF COMPENSATED SYSTEM TO POWER TURBINE SPEED OUTPUT DISTURBANCE

Note that the control variables for both the command input and disturbance rejection transients are oscillatory at the frequency of the underdamped compensator poles. A meaningful way to quantify this behavior in a MIMO sense is to plot the frequency dependent singular values of the command input-to-plant input transfer function matrix. The output disturbance-to-plant input transfer function matrix is identical but with a sign change. The transfer function matrix description is given by

$$\underline{u} = [\underline{I}+\underline{K}_D(s)\underline{G}_D(s)]^{-1}\ \underline{K}_D(s)\underline{G}_a(s)\underline{r} \qquad (4.18)$$

where the variables are as defined in Section 4.3.

A singular value plot of the transfer function matrix for this system and defined by Eq(4.18) is shown in Figure 4.26. Note that at the frequency that the inputs are shown to oscillate (~1 Hz), an underdamped complex pole pair is apparant. This pole pair is attributable to cancelling rotor system dynamics.

4.6.3 MIMO vs SISO Comparison

It is instructive at this point to perform a comparison between this MIMO system definition and the SISO system definition presented in Section 4.4. in terms of the ability of these systems to reject disturbances. The basis for comparison will be to determine if it is possible, by using the coordinated control of several variables, to provide a system that exhibits disturbance rejection capabilities without the use of excessive control energy. If we consider that the variable geometry input variable is available at no cost to

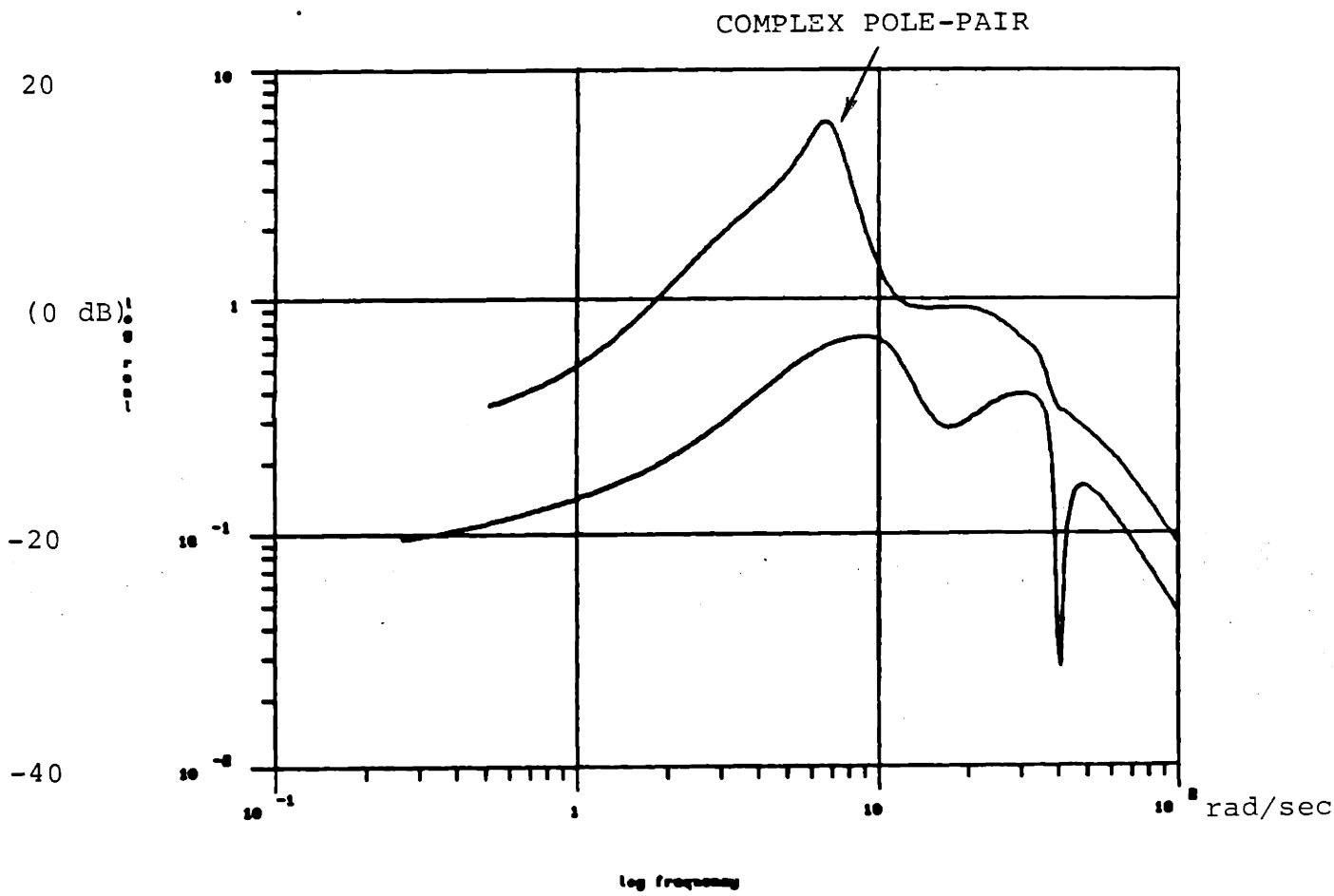

FIGURE 4.26: COMMAND INPUT-TO-PLANT INPUT
TRANSFER FUNCTION MATRIX
SINGULAR VALUES vs. FREQUENCY

the user, then any use of the variable geometry input can be considered a savings of fuel.

A comparison of MIMO System I to the SISO system design in rejecting a power turbine speed output disturbance can be quantified by examining Figures 4.10 and 4.25. Note that while the fuel flow input is oscillatory in both Figures 4.10 and 4.25, the utilization of the variable geometry input in the MIMO system definition appears to dampen the fuel flow input more rapidly than in the SISO system definition.

It is possible to incur disturbances in the gas generator speed due to power extraction or engine inlet distortion. The response of MIMO System I to a step disturbance on gas generator speed is shown in Figure 4.27. A step disturbance on gas generator speed for the SISO system definition is shown in Figure 4.28. Note that while both the MIMO and SISO system definitions reject the gas generator speed disturbance, the MIMO system rejects the disturbance rapidly and at no steady-state fuel offset which is incurred in the SISO system definition.

Figure 4.29 displays the ability of the MIMO system to reject a step disturbance on the fuel flow input variable. Even though the disturbance is rejected, the power turbine speed output oscillates at the tail rotor resonant frequency (~40 rad/sec). The cause of the oscillation can be determined by examining the singular value plot of the input disturbance-to-plant output transfer function matrix, shown in Figure 4.30 and given by

$$\underline{y} = [\underline{I}+\underline{G}_D(s)\underline{K}_D(s)]^{-1}\underline{G}_p(s)\underline{d}_i \qquad (4.19)$$

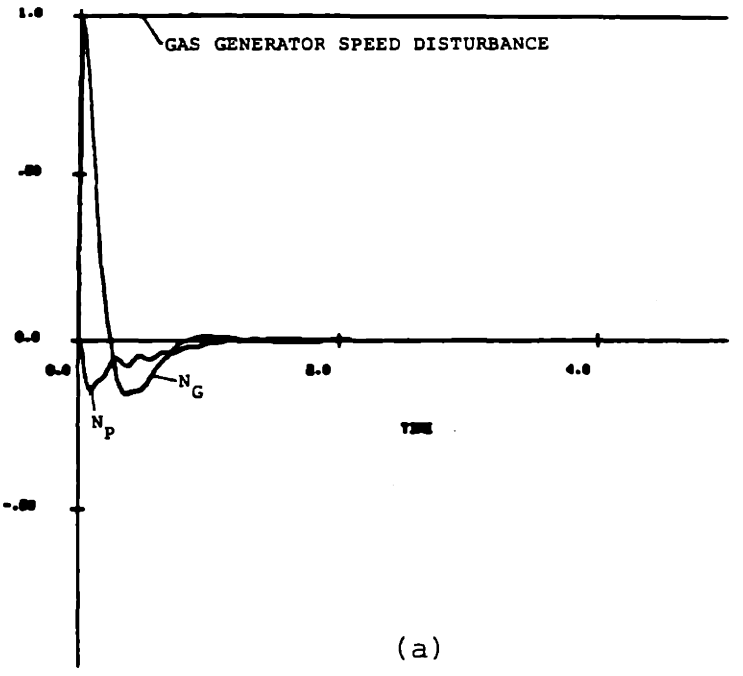

(a)

POWER TURBINE AND GAS GENERATOR SPEED OUTPUTS

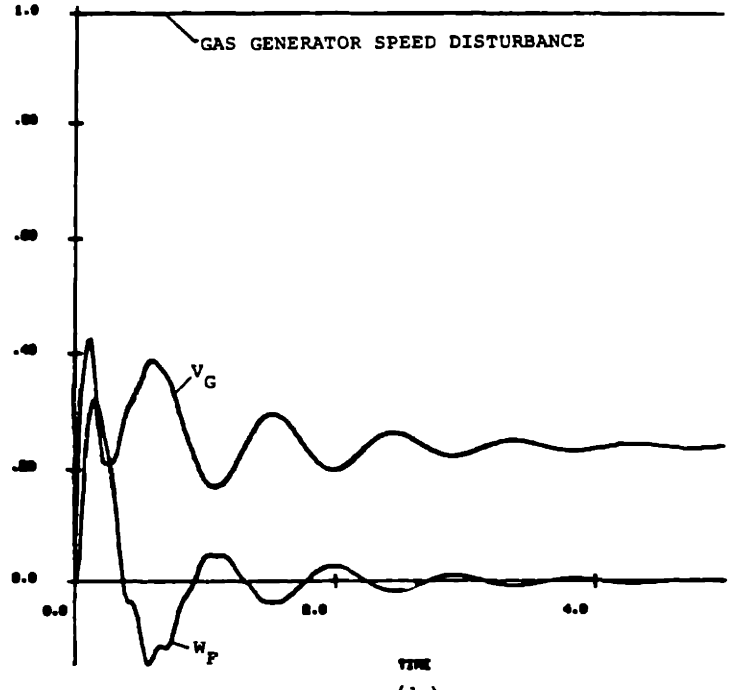

(b)

W_F AND V_G INPUT VARIABLES

FIGURE 4.27: LINEAR SIMULATION OF STEP RESPONSE OF MIMO SYSTEM I TO A GAS GENERATOR SPEED DISTURBANCE

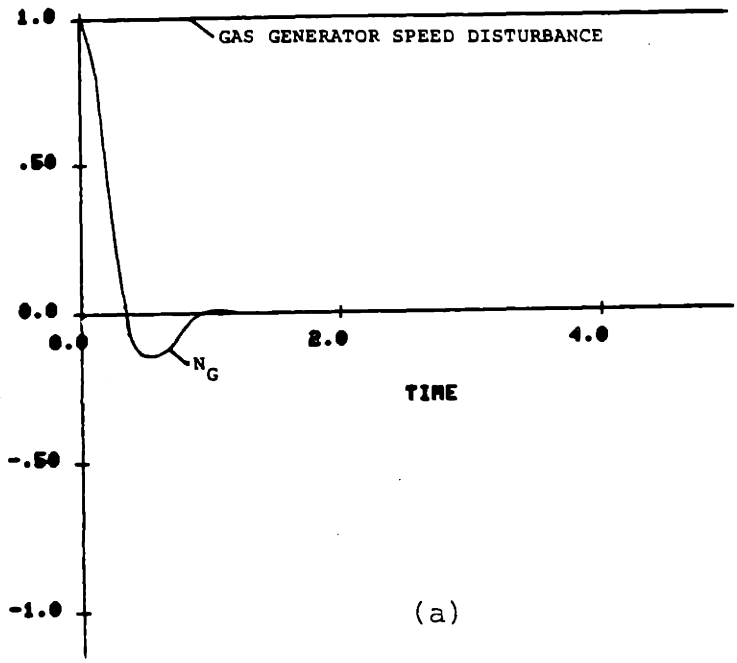

(a)

GAS GENERATOR SPEED

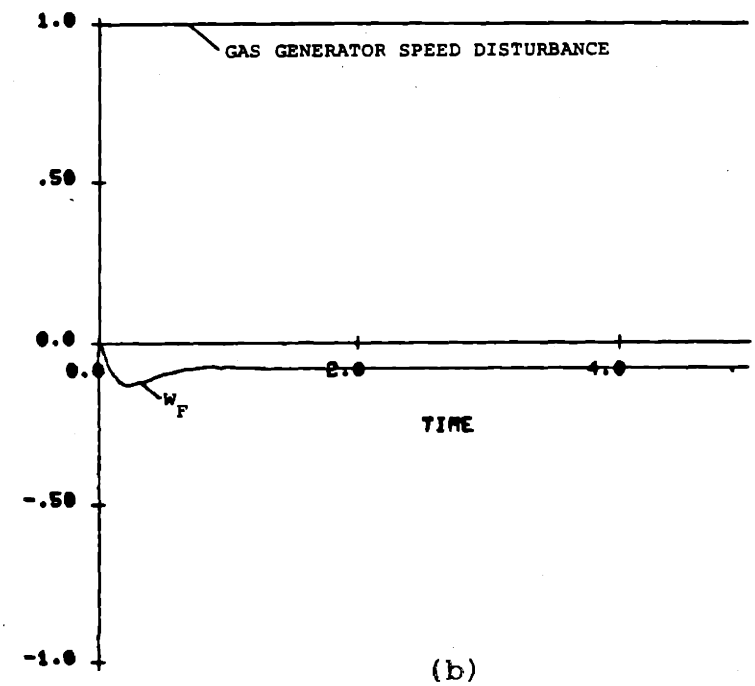

(b)

W_F INPUT

FIGURE 4.28: LINEAR SIMULATION OF STEP RESPONSE OF SISO SYSTEM TO A GAS GENERATOR SPEED DISTURBANCE

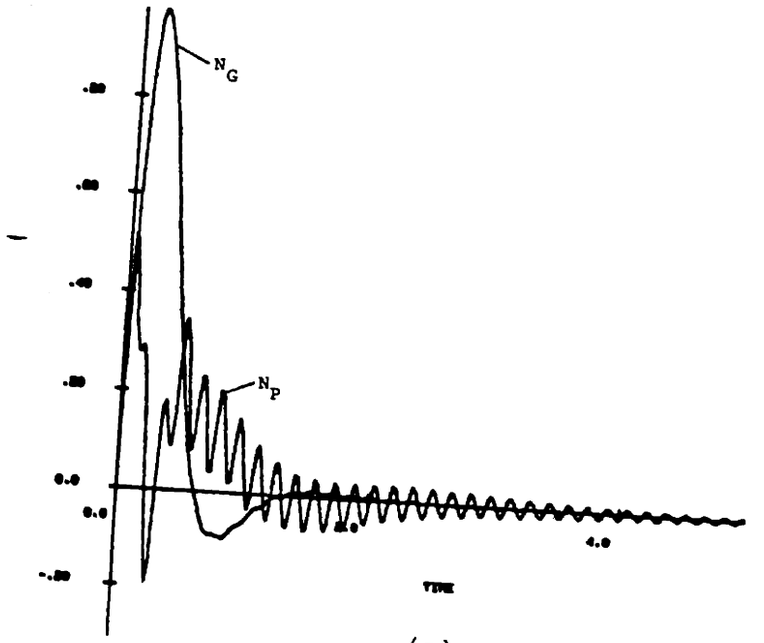

(a)

POWER TURBINE AND GAS GENERATOR SPEED OUTPUTS

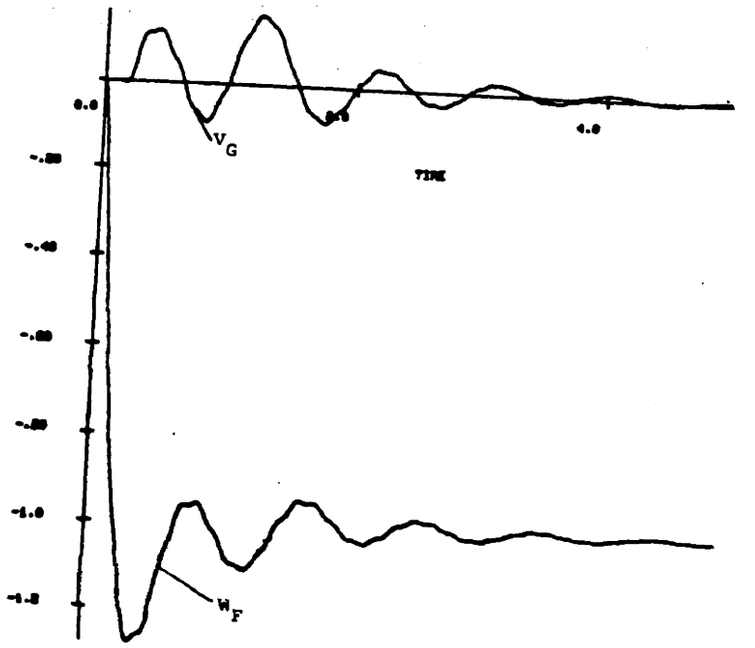

(b)

W_F AND V_G INPUT VARIABLES

FIGURE 4.29: LINEAR SIMULATION OF STEP RESPONSE OF MIMO SYSTEM I TO A W_F INPUT DISTURBANCE

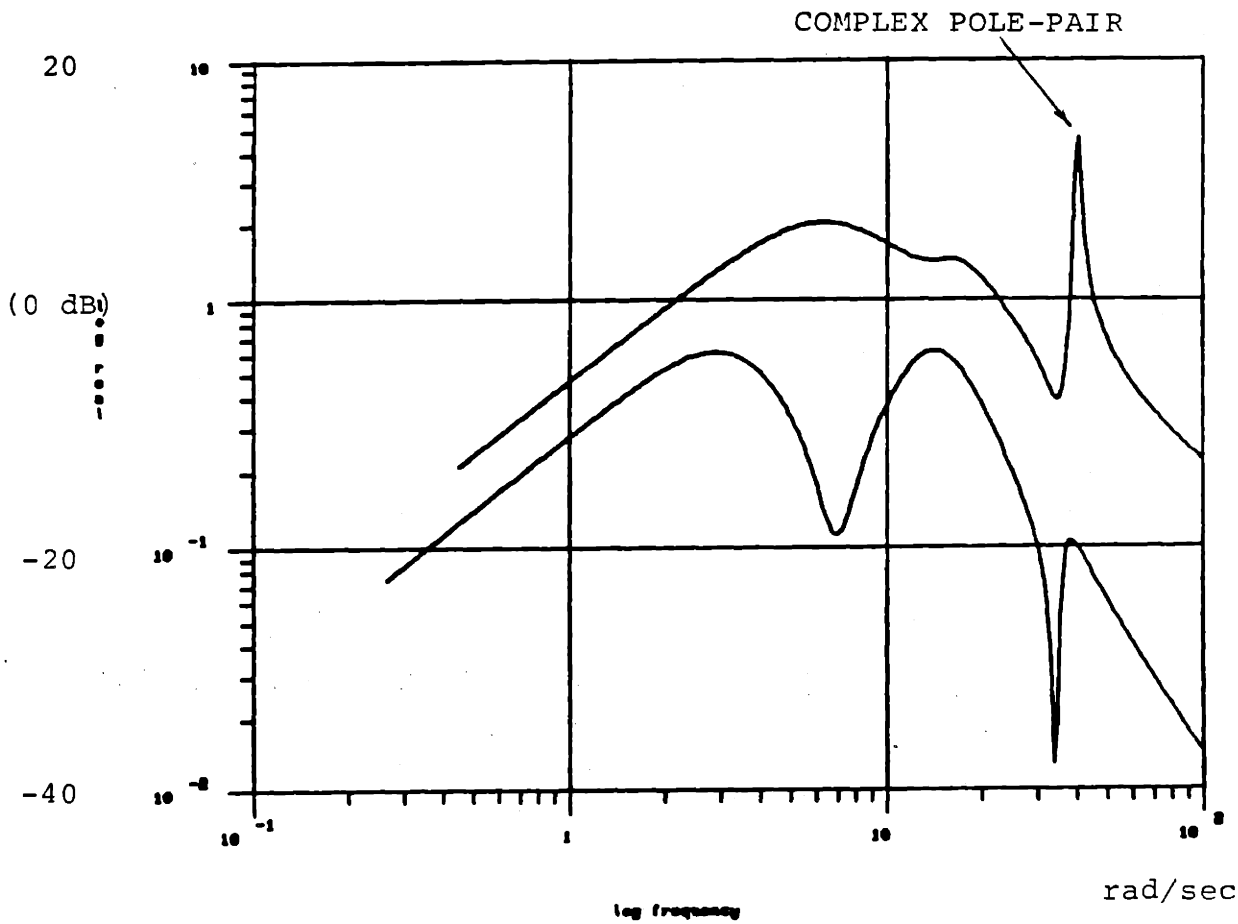

FIGURE 4.30: INPUT DISTURBANCE-TO-PLANT OUTPUT

TRANSFER FUNCTION MATRIX

SINGULAR VALUES vs. FREQUENCY

where the variables are as defined in Section 4.3.

The cause of the oscillation, as noted in Figure 4.30, is an underdamped complex pole pair occuring at the tail rotor resonant frequency. Remember that a desireable loop shape for this MIMO System was obtained at the plant output to provide good command following and to reject output disturbances. Obtaining a desireable loop shape simultaneously at the plant input is still of current research interest and will not be explored further in this research. For this reason, no further comparisons with the SISO system design are attempted.

4.6.4 Design Summary

The performance and robustness goals, as evaluated in the frequency domain, were achieved for MIMO System I which provides isochronous power turbine and isochronous gas generator speed governing. The desired performance was obtained at the plant output to provide "good" command following and output disturbance rejection. Linear simulations of the controlled system displayed fast response times consistent with the interpretations provided by the frequency-dependent singular value plots of the system transfer function matrices.

A comparison of this MIMO system definition to the SISO system definition presented in the previous section in terms of the ability of these two system definitions to reject load disturbances was performed. The ability of the MIMO system definition, through the coordinated control of both control variables, to reject output load disturbances faster than the SISO system

definition and without incurring a steady-state offset in fuel consumption, as did the SISO system, was displayed. The disturbance rejection capabilities of the MIMO system to an input disturbance was judged not to be satisfactory. This observation was useful in pointing out the fact that desireable MIMO system performance, at the present state-of-the-art, is attainable at the input or at the output of the plant, but not both.

4.7 MIMO System II Controller Design

The system definition presented by MIMO System I is formulated to provide multivariable control using the fuel flow and variable geometry inputs over power turbine speed and inter-turbine gas temperature. The ability to trim the inter-turbine gas temperature while maintaining constant power turbine speed will be evaluated. Integral augmentation on both input channels was performed to insure zero steady-state error to constant reference inputs. The design for this system definition was performed at two operating points using the 90% N_g (MIMO) and the 95% N_g (MIMO) Design Models. The design for each operating condition, and the respective linear and non-linear simulations will be presented separately. In both cases, it will be desired to obtain a "good" loop shape at the plant output to obtain the specified command following and output disturbance rejection performance specified in Chapter 3.

4.7.1 90% Ng (MIMO) Design Loop Shaping

A singular value plot of the integral augmented, scaled, open-loop plant is shown in Figure 4.31. The design $\underline{G}_{KF}(j\omega)$, representing the loop shape to

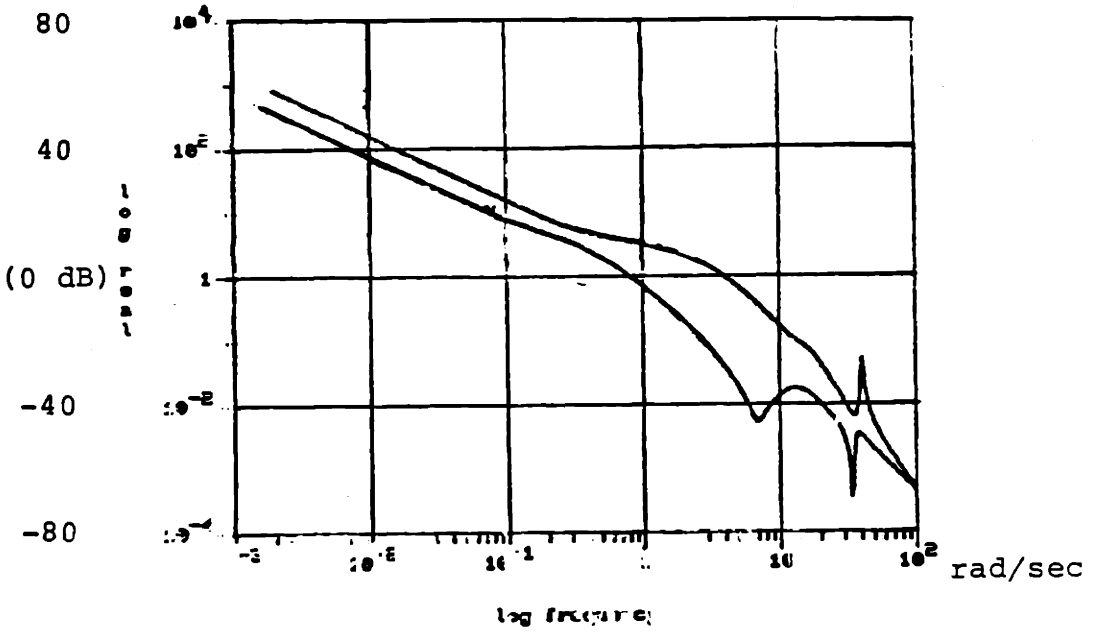

FIGURE 4.31: MIMO SYSTEM II-90% N_g DESIGN MODEL
INTEGRAL AUGMENTED OPEN-LOOP PLANT
SINGULAR VALUES vs. FREQUENCY

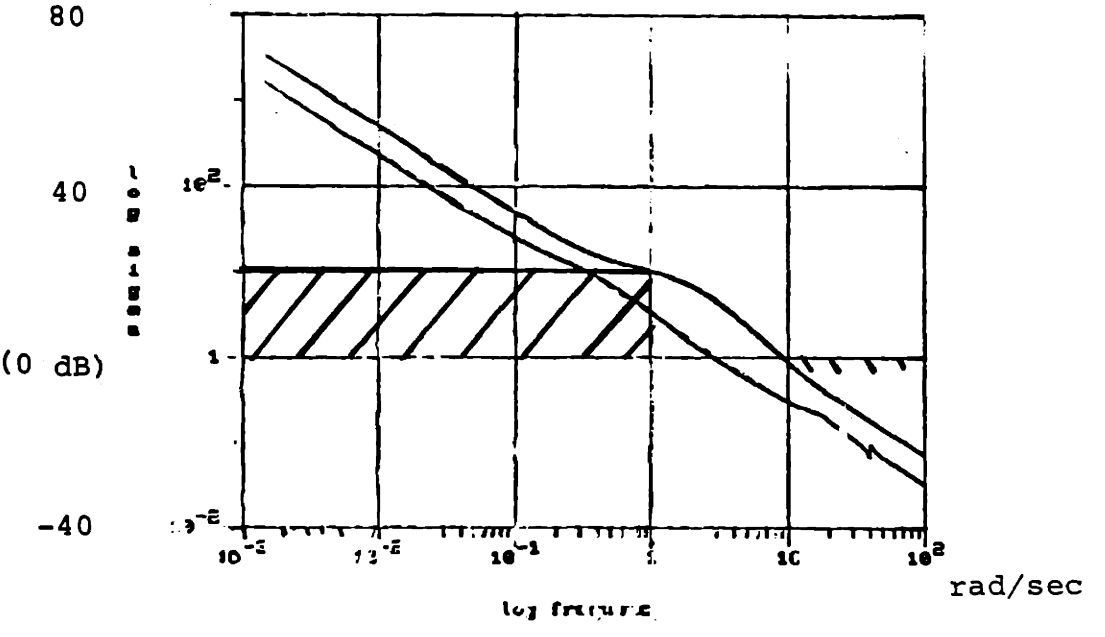

FIGURE 4.32: $\underline{G}_{KF}(j\omega)$ FOR $\underline{L}=\underline{B}$, $\underline{\Theta}=.1*\underline{I}$
SINGULAR VALUES vs. FREQUENCY

be recovered, is shown in Figure 4.32 with the applicable design parameters and the performance specifications. The recovered loop shape is shown in Figure 4.33. Performance specifications are not met because of the expected (Ref. Section 4.2) poor recovery of the minimum singular value in the frequency range (.2 rad/sec) of the non-minimum phase zero. Degraded performance, from what was desired, can be expected for this system definition at this particular design point. Degraded performance is expected because of the small frequency range over which $\sigma_{min}\ \underline{T}(j\omega)$ is "large". Singular value plots of the Closed-Loop Transfer Function Matrix (CLTFM) and the Sensitivity Transfer Function Matrix (STFM) are shown in Figures 4.34 and 4.35, respectively. Figure 4.34 displays that the system bandwidth is in the approximate frequency range of .1-10 rad/sec. The specific bandwidth realized will depend on the specific command input direction. The same general characteristics, the large spread of singular values, is shown in the singular value plot of the STFM shown in Figure 4.35. The response of the system to output disturbances will depend upon the specific direction of the output disturbance vector imposed on the system.

The system is robust, however, for the modeling errors defined in Chapter 3, as shown in Figure 4.36.

A singular value plot of the MIMO compensator $\underline{K}_D(s)$ is shown in Figure 4.37. Note again that the compensator provides underdamped poles and zeros to cancel rotor system dynamics, as did the SISO and the MIMO System I controller. The state-space description of $\underline{K}_D(s)$ is given in Appendix G2.

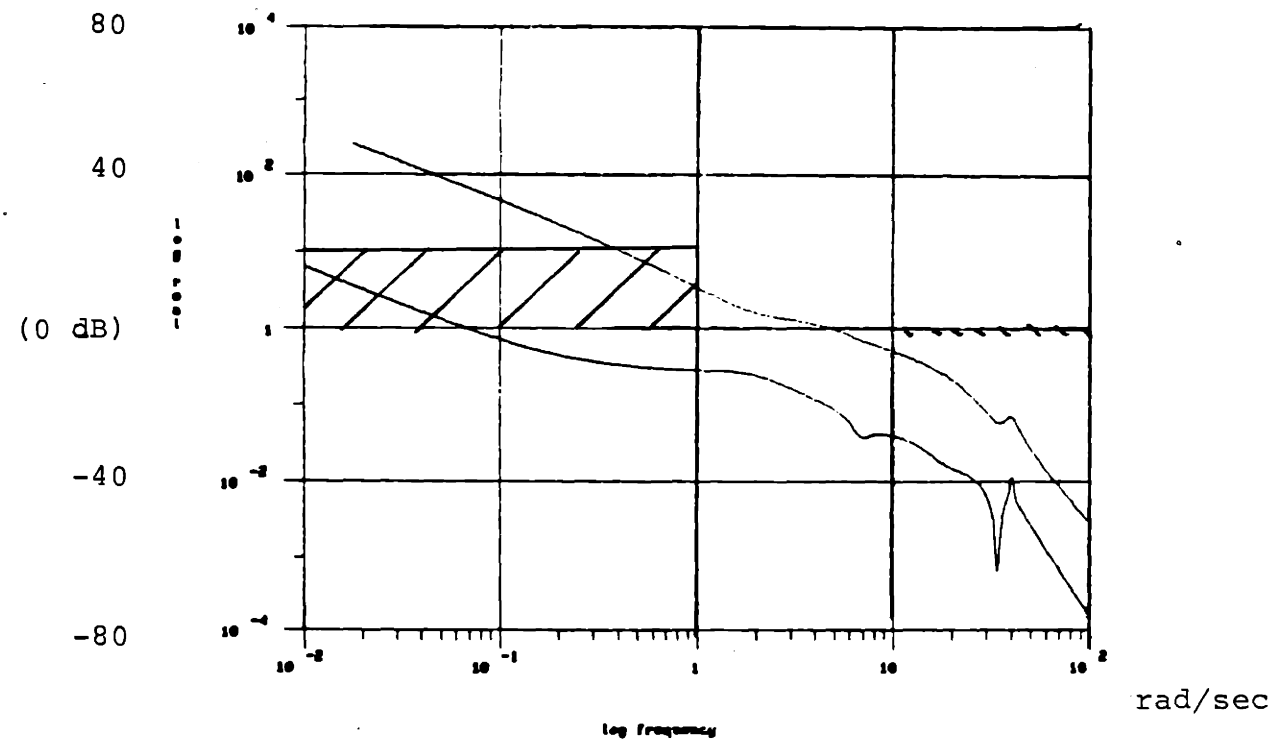

FIGURE 4.33: LOOP TRANSFER RECOVERY: q=100

SINGULAR VALUES vs. FREQUENCY

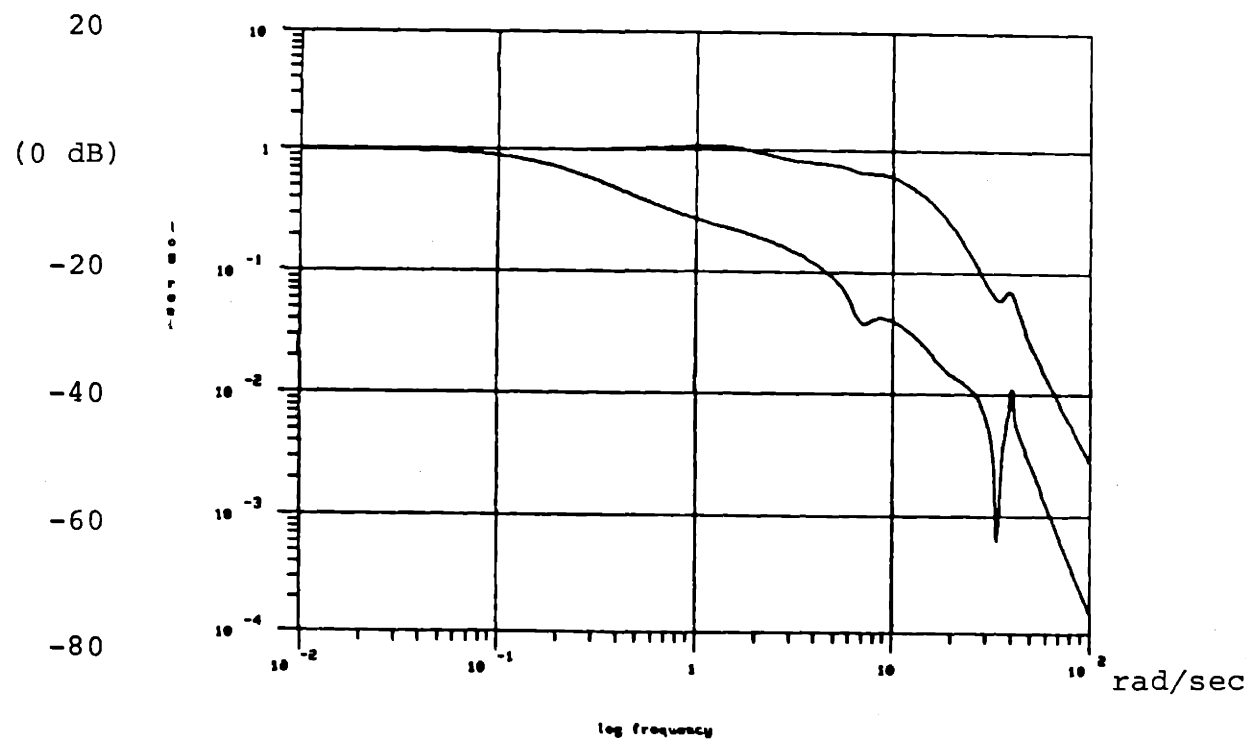

FIGURE 4.34: CLOSED-LOOP TRANSFER FUNCTION MATRIX

SINGULAR VALUES vs. FREQUENCY

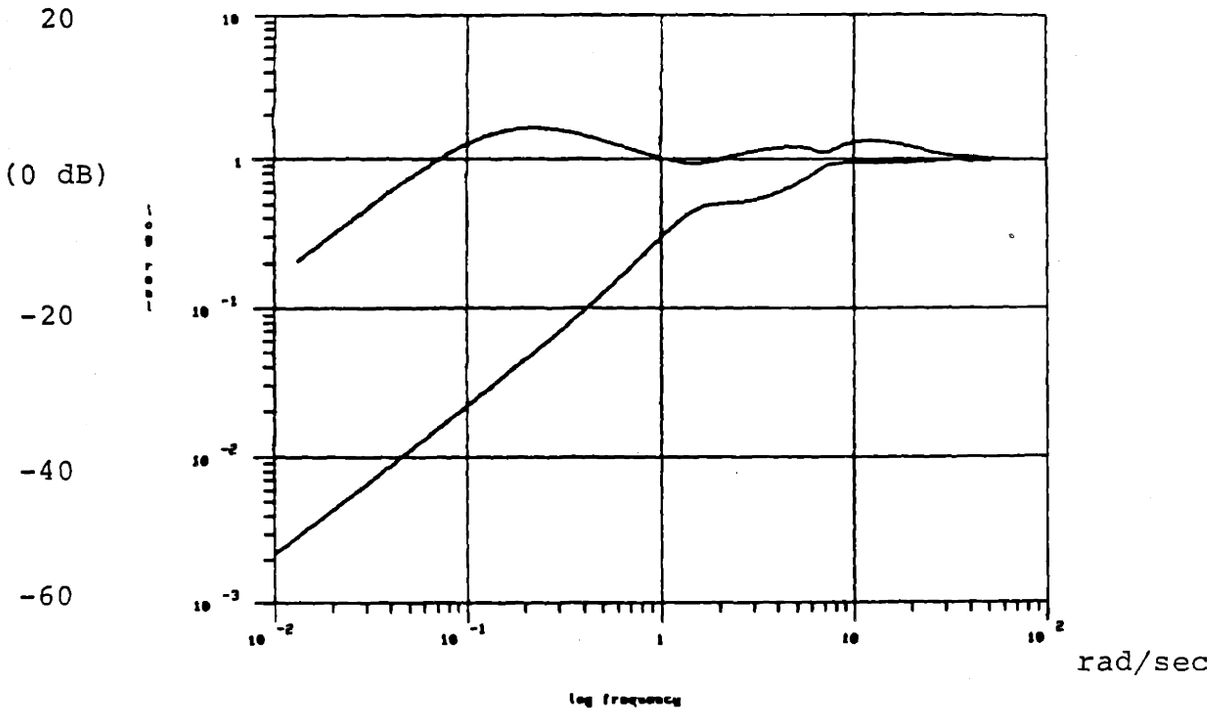

FIGURE 4.35: SENSITIVITY TRANSFER FUNCTION MATRIX

SINGULAR VALUES vs. FREQUENCY

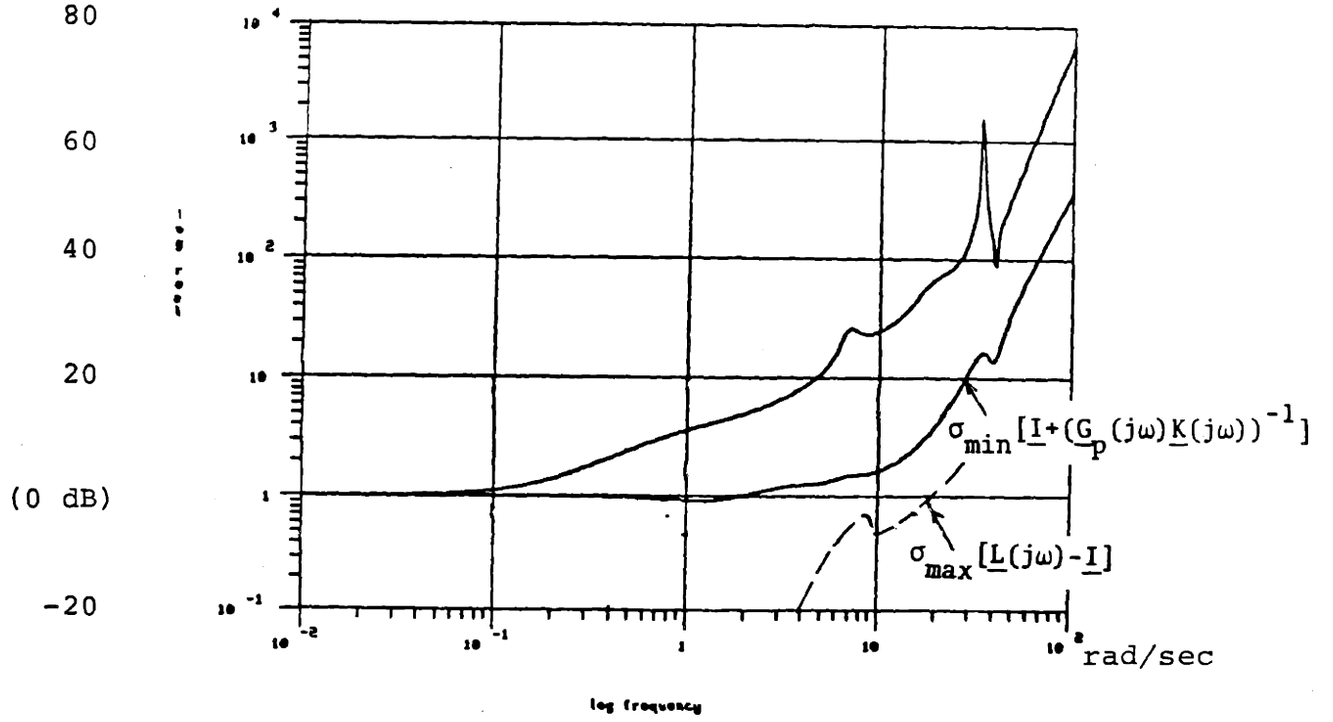

FIGURE 4.36: ROBUSTNESS REQUIREMENT PLOT

SINGULAR VALUES vs. FREQUENCY

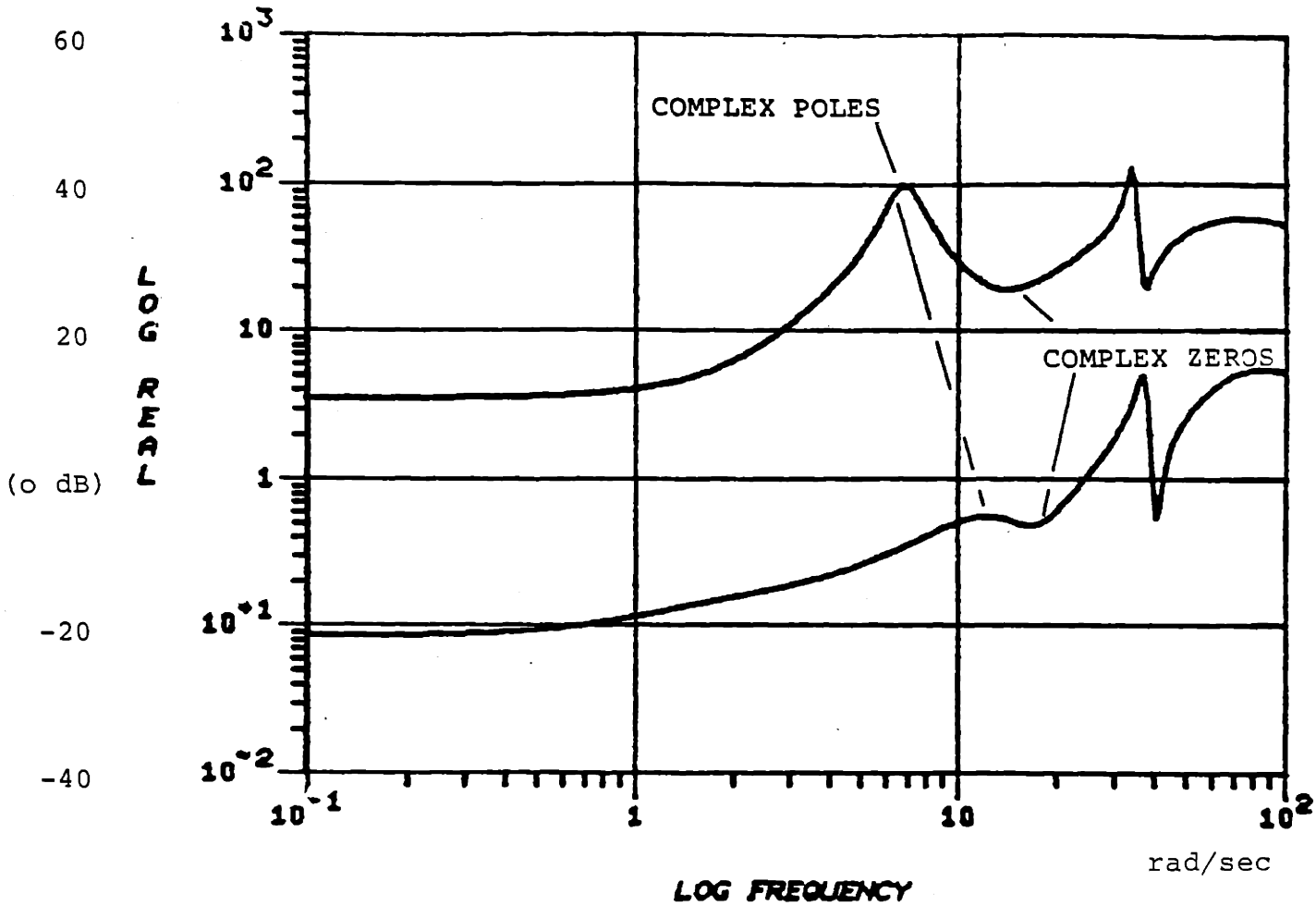

FIGURE 4.37: LQG/LTR COMPENSATOR $\underline{K}_D(j\omega)$ TRANSFER FUNCTION MATRIX SINGULAR VALUES vs. FREQUENCY

Linear Simulation

The response of the system to a step command on sensed inter-turbine gas temperature is shown in Figure 4.38. The settling time of the transient is about 30 secs., which is consistent with the system bandwidth (.1-10 rad/sec) presented in Figure 4.34. The response of the system to a step disturbance on power turbine speed output is shown in Figure 4.39. The poor disturbance response characteristics of this design make it unacceptable for flight conditions, such as manuevering flight, where large load disturbances are expected. A cruise condition, where engine efficiency is a prime objective and load disturbances are not expected is a possible application. Note, as in the SISO case, that the input variables for both the command input and output disturbance transients are oscillatory at the frequency of the underdamped compensator poles. A singular value plot of the command, input-to-plant output transfer function matrix for this system and defined by Eq(4.18) is shown in Figure 4.40. Note that at the frequency at which the inputs are shown to oscillate in the linear simulation (~1 Hz), an underdamped complex pole pair is apparent. The pole pair underdamped is attributable to the effect of cancelling rotor system dynamics.

Non-Linear Simulation

A trim signal on the inter-turbine gas temperature reference, a 10 sec ramp of $20^{o}F$, was performed on the non-linear simulation as shown in Figure 4.41. The transient does not depict the final steady-state condition because of the excessive computer time required. The error magnitude between the

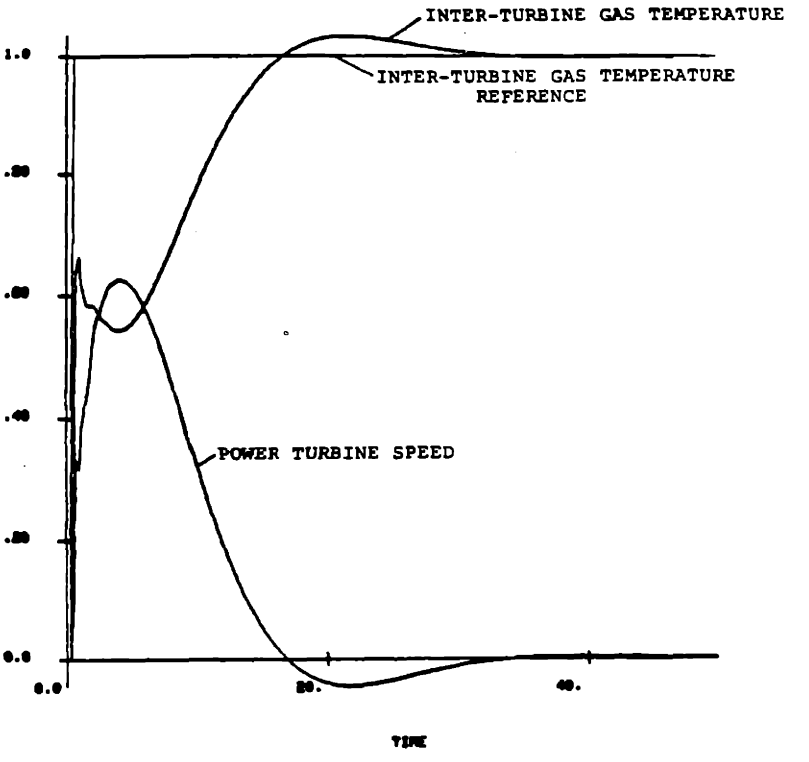

(a)

POWER TURBINE SPEED AND INTER-TURBINE GAS TEMPERATURE OUTPUTS

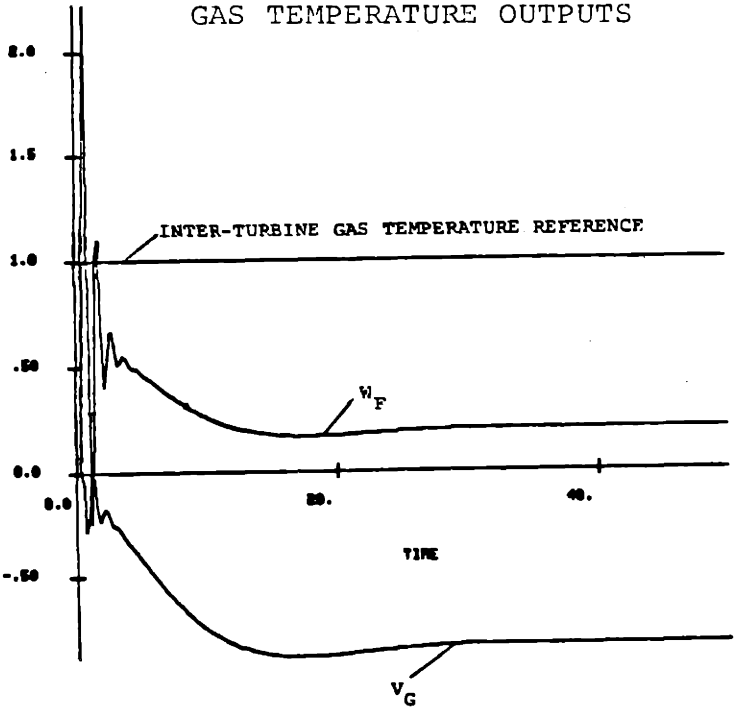

(b)

W_F AND V_G INPUT VARIABLES

FIGURE 4.38A: LINEAR SIMULATION OF STEP RESPONSE OF COMPENSATED SYSTEM TO INTER-TURBINE GAS TEMPERATURE DEMAND

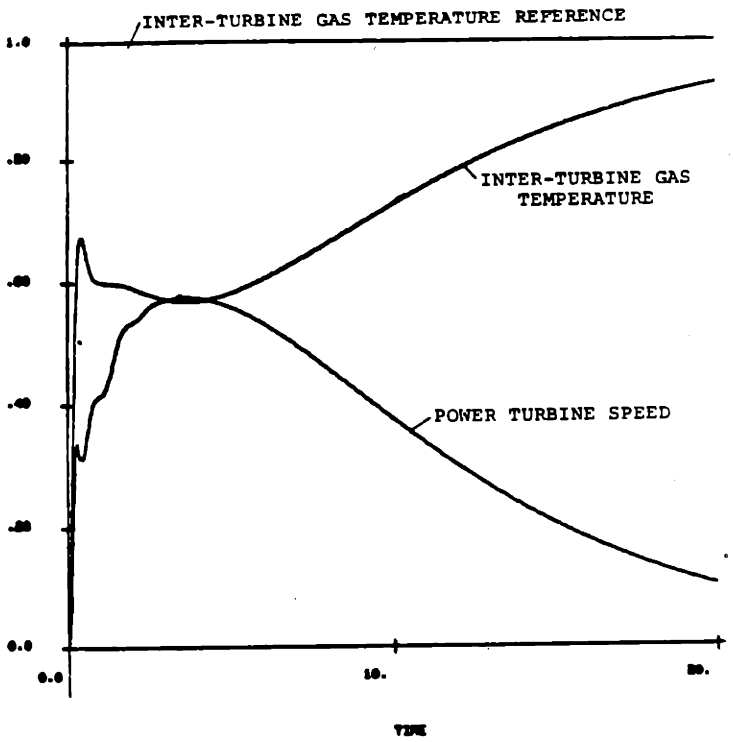

(a)

POWER TURBINE SPEED AND INTER-TURBINE GAS TEMPERATURE OUTPUTS

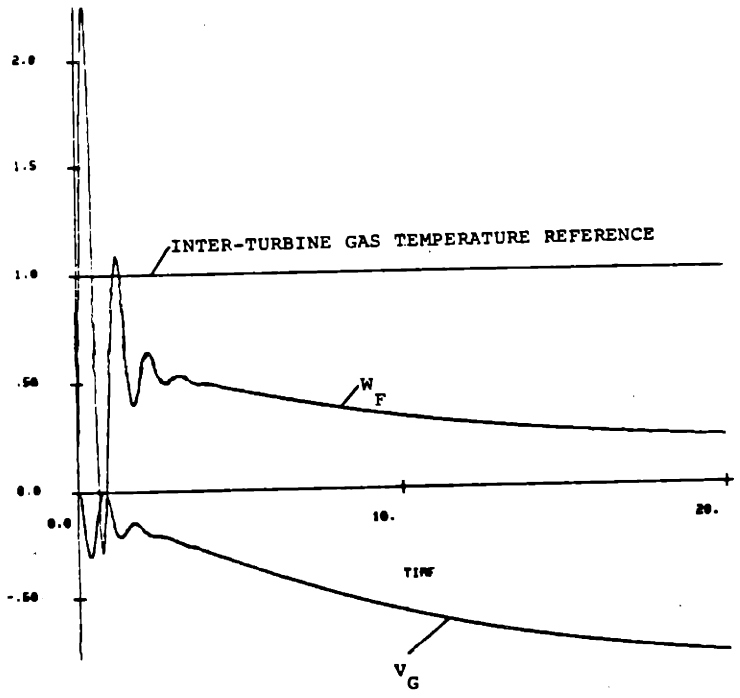

(b)

W_F AND V_G INPUT VARIABLES

FIGURE 4.38B: EXPANDED TIME SCALE OF FIGURE 4.38A

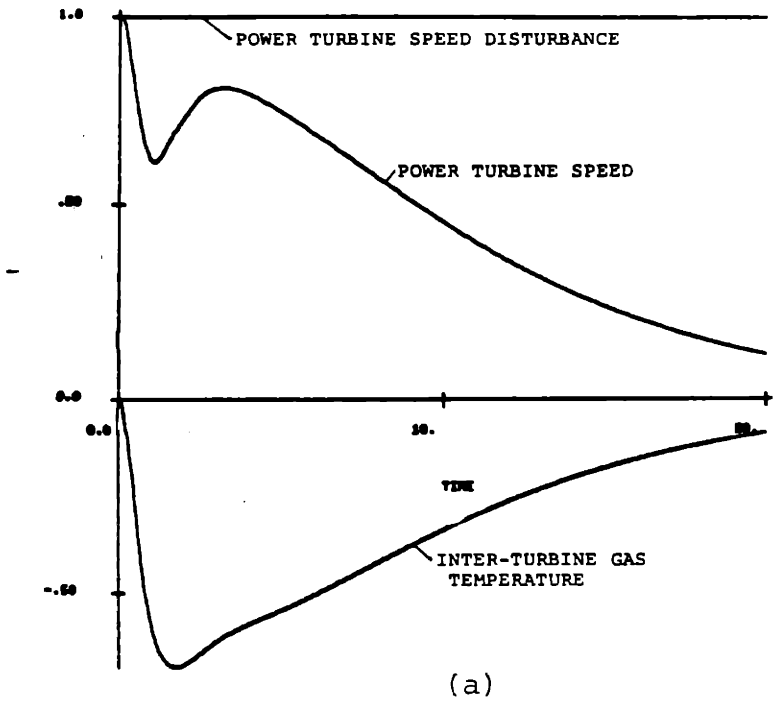

(a)

POWER TURBINE SPEED AND INTER-TURBINE GAS TEMPERATURE OUTPUTS

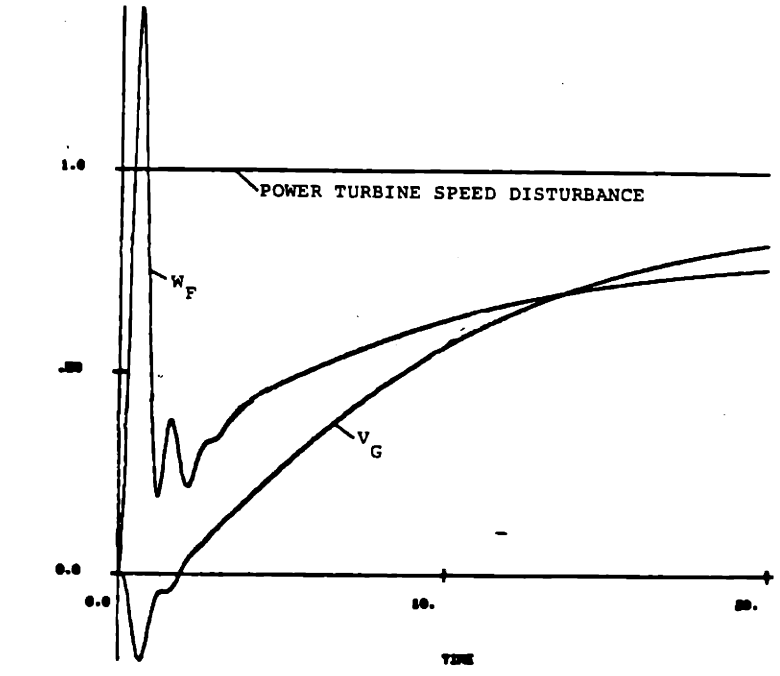

(b)

W_F AND V_G INPUT VARIABLES

FIGURE 4.39: LINEAR SIMULATION OF STEP RESPONSE OF COMPENSATED SYSTEM TO POWER TURBINE SPEED OUTPUT DISTURBANCE

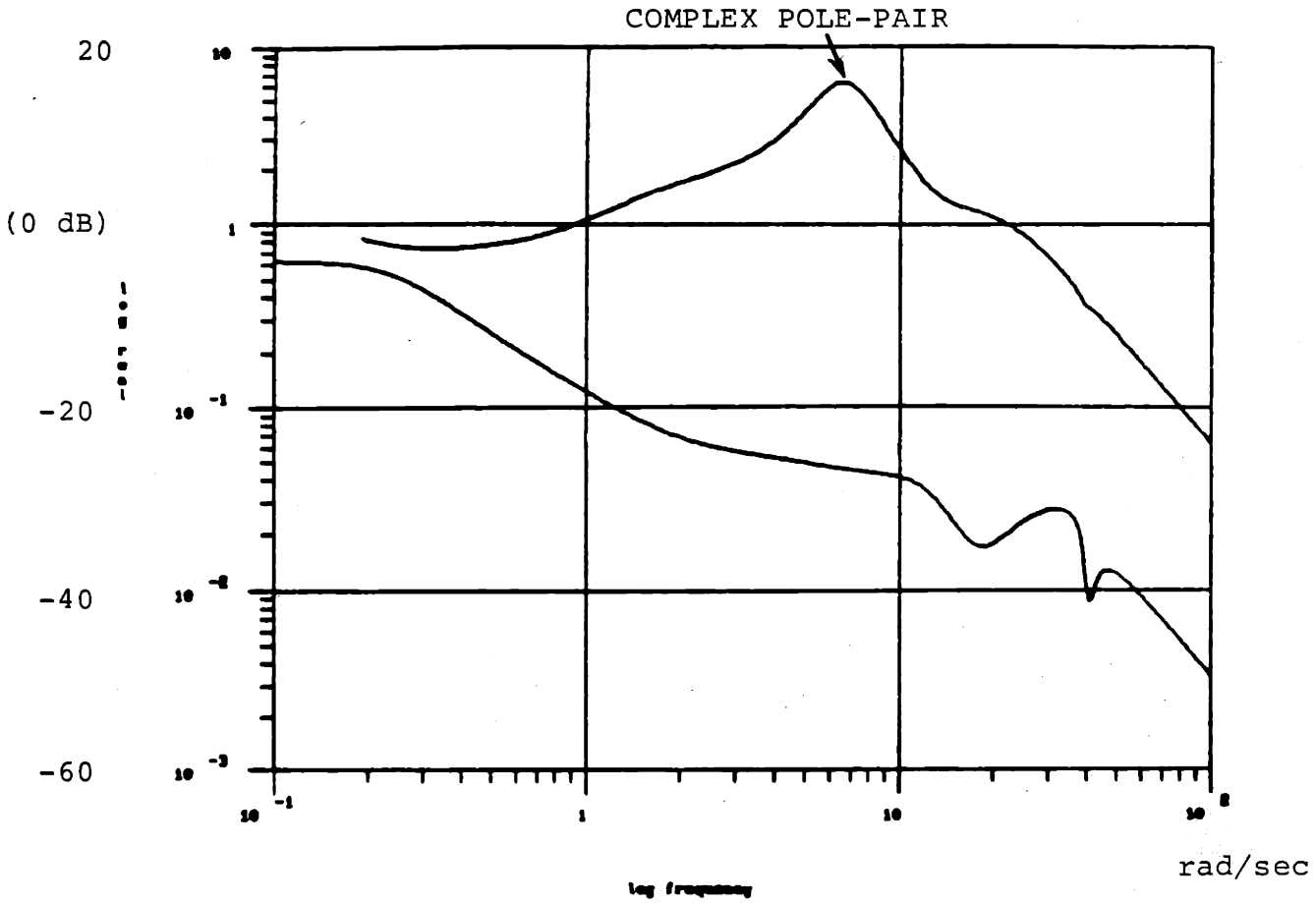

FIGURE 4.40: COMMAND INPUT-TO-PLANT INPUT
TRANSFER FUNCTION MATRIX
SINGULAR VALUES vs. FREQUENCY

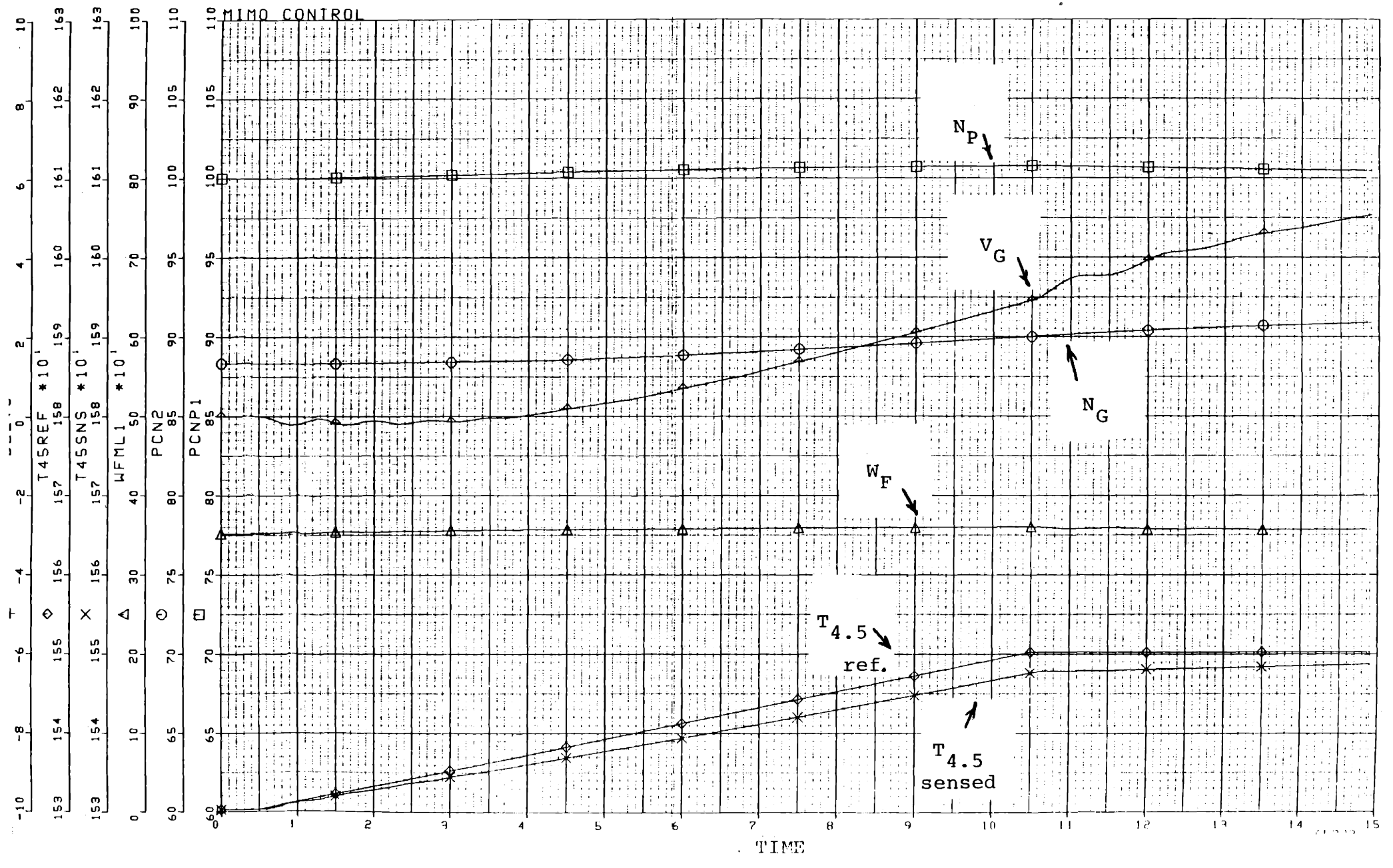

FIGURE 4.41: NON-LINEAR SIMULATION OF MIMO SYSTEM II-90% N_g DESIGN MODEL

temperature reference and sensed temperature is determined by $\sigma_{min}\underline{T}(j\omega)$. The 10 sec ramp trim signal was chosen to represent the fact that the command error magnitude could be maintained at a relatively small level if the trim command is in the frequency range for which $\sigma_{min}\underline{T}(j\omega)$ is "large". Note also that the other controlled variable, power turbine speed, also reacts to the trim signal. The extent to which this behavior is detrimental requires further evaluation.

Design Summary

The performance goals, as evaluated in the frequency domain, were not met for MIMO System II (90% N_g(MIMO) Design Model), which provides isochronous power turbine speed governing and inter-turbine gas temperature control. Performance specifications were not achieved due to the generic system performance limitations presented by the non-minimum zero in the 90% N_g (MIMO) design model at .199 rad/sec. The performance was evaluated at the plant output. Robustness specifications were attained, however. Linear simulations of the controlled system displayed very slow response times consistent with the interpretations provided by the frequency singular value plots of the system transfer function matrices.

A non-linear simulation of the reponse of this controller to a low frequency command input (10 sec ramp) on the inter-turbine gas temperature was presented. The non-linear simulation displayed that the error between sensed and referenced gas temperature could be made small if the command input was in the frequency range where $\sigma_{min}\underline{T}(j\omega)$ for this system was "large".

4.7.2 95% Ng (MIMO) Design Loop Shaping

A singular value plot of the integral augmented, scaled open-loop plant is shown in Figure 4.42. The design $\underline{G}_{KF}(j\omega)$, representing the loop shape to be recovered is shown in Figure 4.43 with the applicable design parameters and performance specifications. The recovered loop shape is shown in Figure 4.44. Performance specifications are met. There are no non-minimum phase zeros within the desired bandwidth, thus insuring a desireable recovery proceedure. Singular value plots of the CLTFM and STFM are shown in Figures 4.45 and 4.46, respectively. In both of these figures, the singular values are not widely skewed. Thus equitable command input and output disturbance rejection irregardless of command input or output disturbance direction is expected. Robustness, for the modeling errors defined in Chapter 3, is achieved as shown in Figure 4.47. The MIMO compensator, $\underline{K}_D(s)$, for the system is shown in Figure 4.48. Rotor system dynamics are again cancelled using underdamped complex pole-zero pairs. The state-space description of $\underline{K}_D(s)$ is given in Appendix G3.

Linear Simulation

The response of the system to a step command on sensed inter-turbine gas temperature is shown in Figure 4.49. The improved response, as compared to the previous design, is attributable to the larger frequency range over which $\sigma_{min}\underline{T}(j\omega)$ is "large". The response of the system to a step disturbance on power turbine speed output is shown in Figure 4.50. Improved response, as compared to the previous design, is also demonstrated in disturbance rejection.

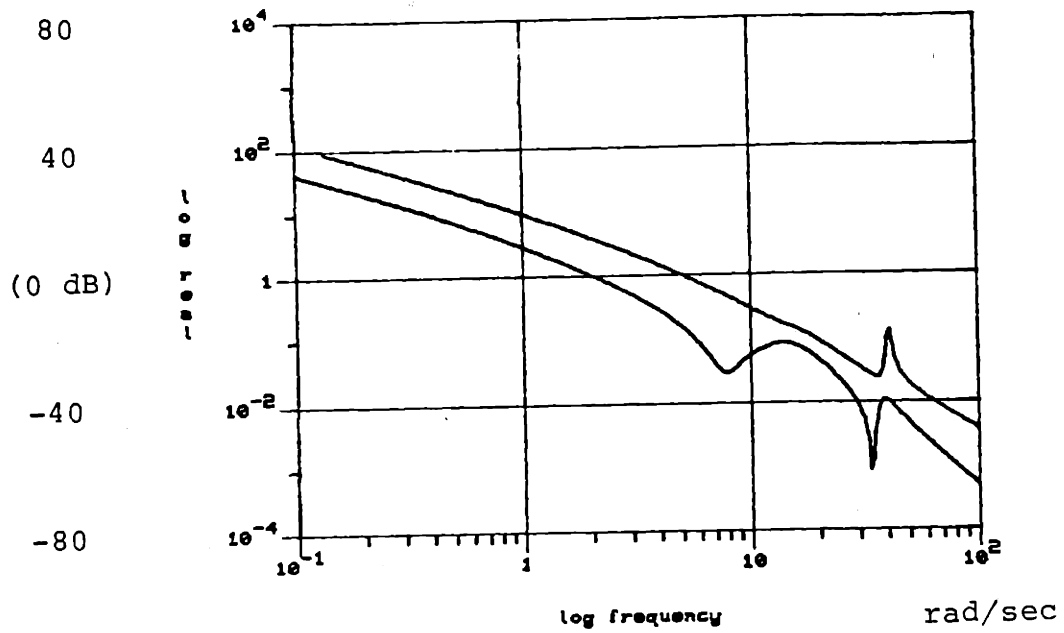

FIGURE 4.42: MIMO SYSTEM II-95% N_g DESIGN MODEL
INTEGRAL AUGMENTED OPEN-LOOP PLANT
SINGULAR VALUES vs. FREQUENCY

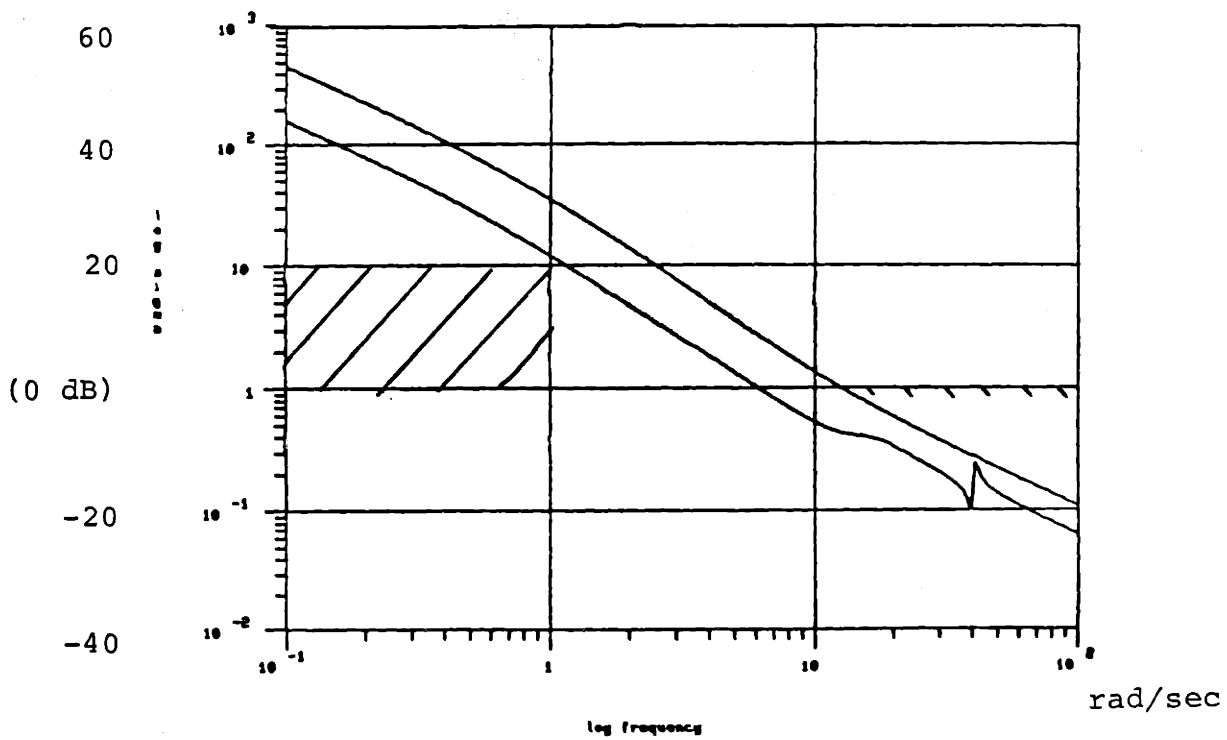

FIGURE 4.43: $\underline{G}_{KF}(j\omega)$ FOR $\underline{L}=\underline{B}$, $\underline{\Theta} = \begin{bmatrix} .05 & 0 \\ 0 & .1 \end{bmatrix}$
SINGULAR VALUES vs. FREQUENCY

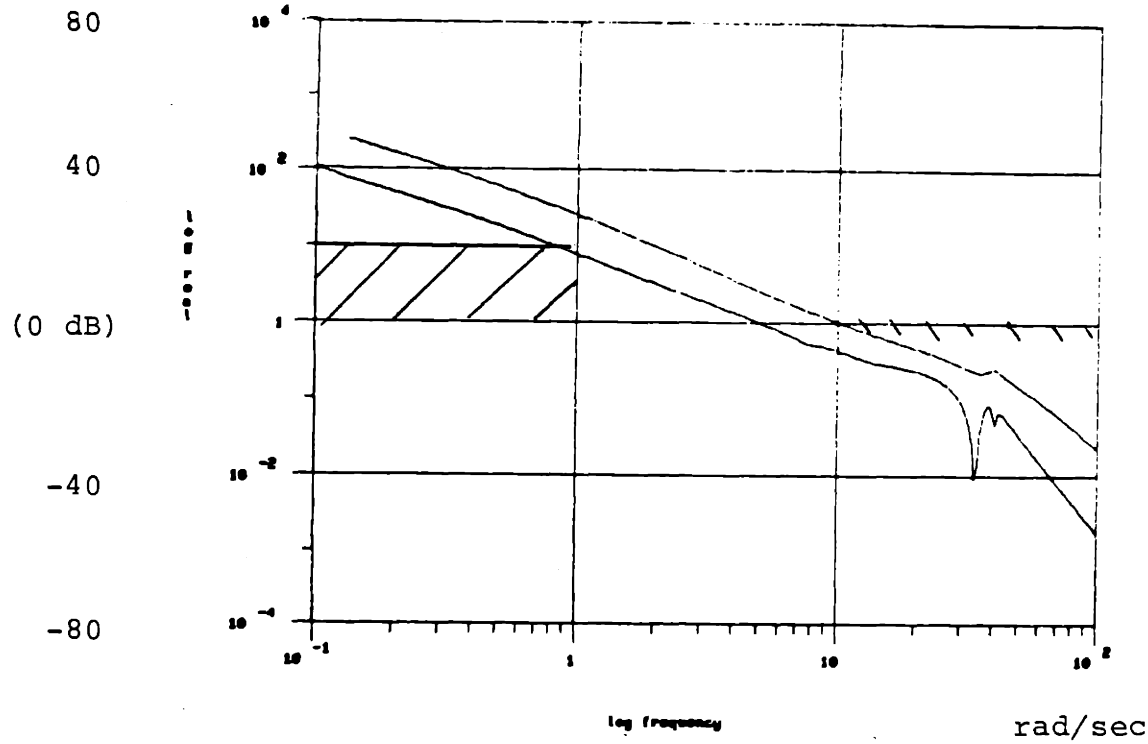

FIGURE 4.44: LOOP TRANSFER RECOVERY: q=50

SINGULAR VALUES vs. FREQUENCY

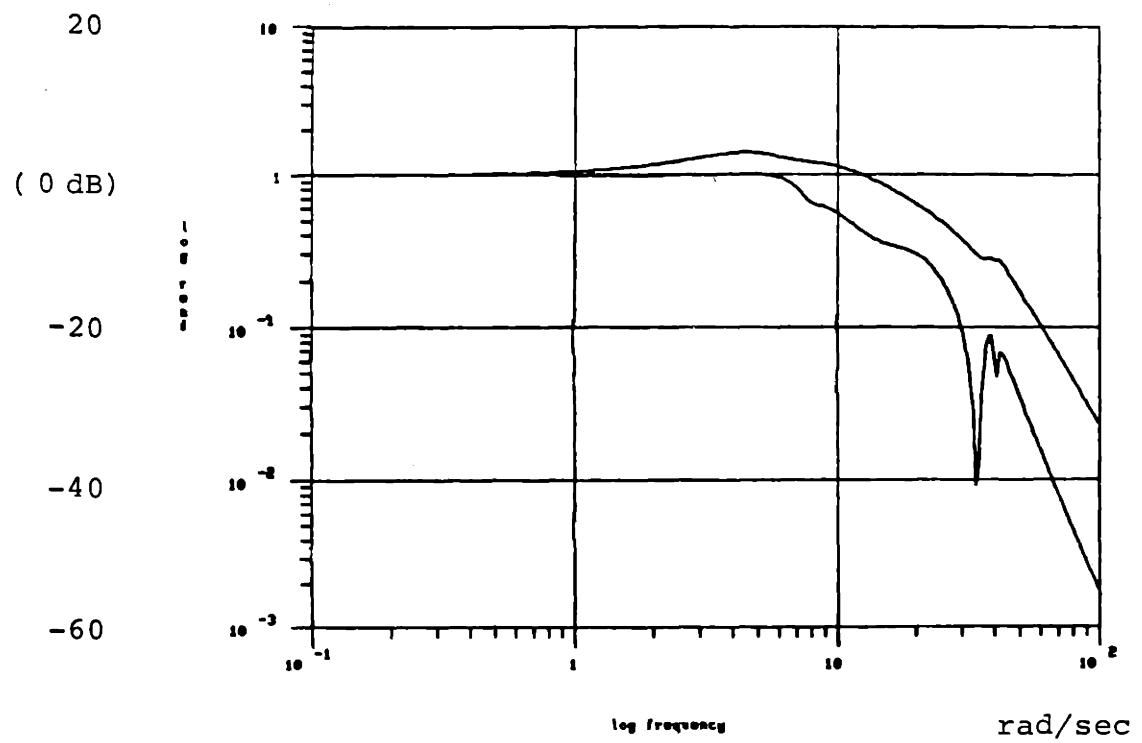

FIGURE 4.45: CLOSED-LOOP TRANSFER FUNCTION MATRIX

SINGULAR VALUES vs. FREQUENCY

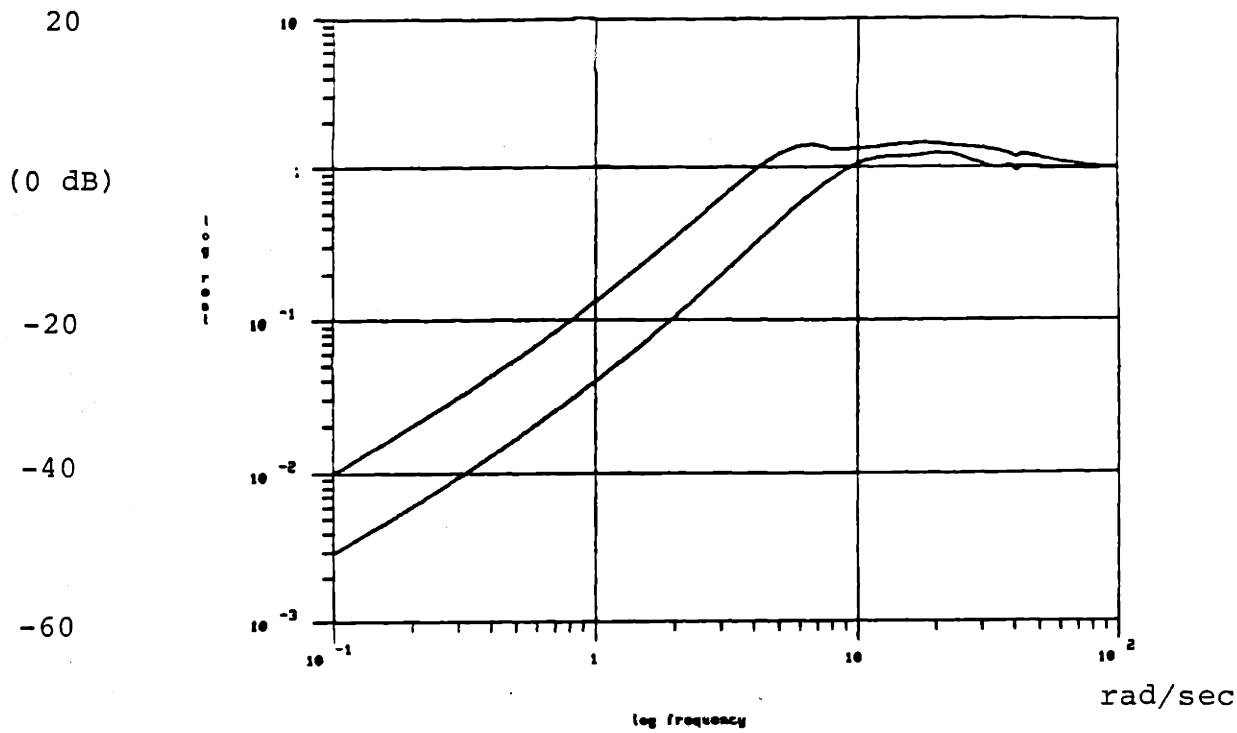

FIGURE 4.46: SENSITIVITY TRANSFER FUNCTION MATRIX

SINGULAR VALUES vs. FREQUENCY

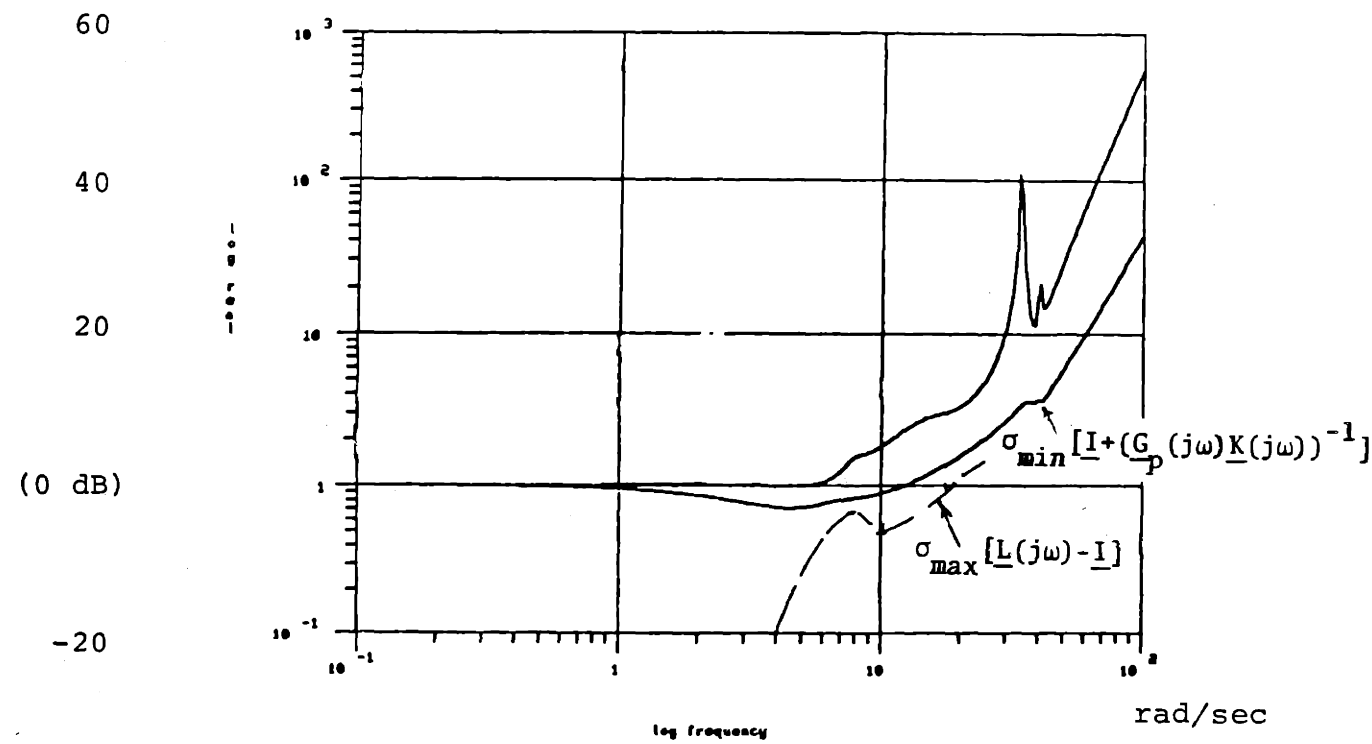

FIGURE 4.47: ROBUSTNESS REQUIREMENT PLOT

SINGULAR VALUES vs. FREQUENCY

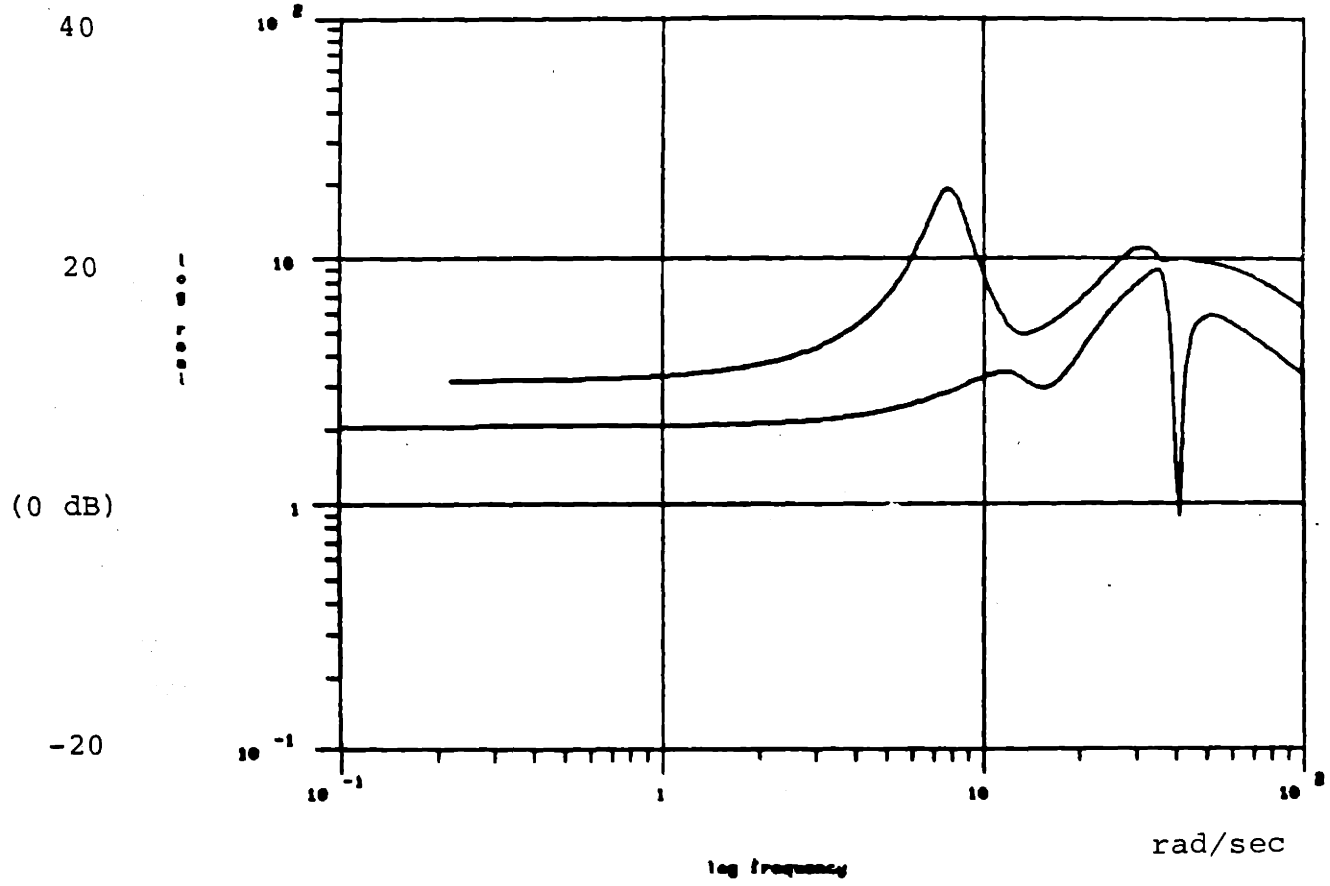

FIGURE 4.48: LQG/LTR COMPENSATOR $\underline{K}_D(j\omega)$

SINGULAR VALUES vs. FREQUENCY

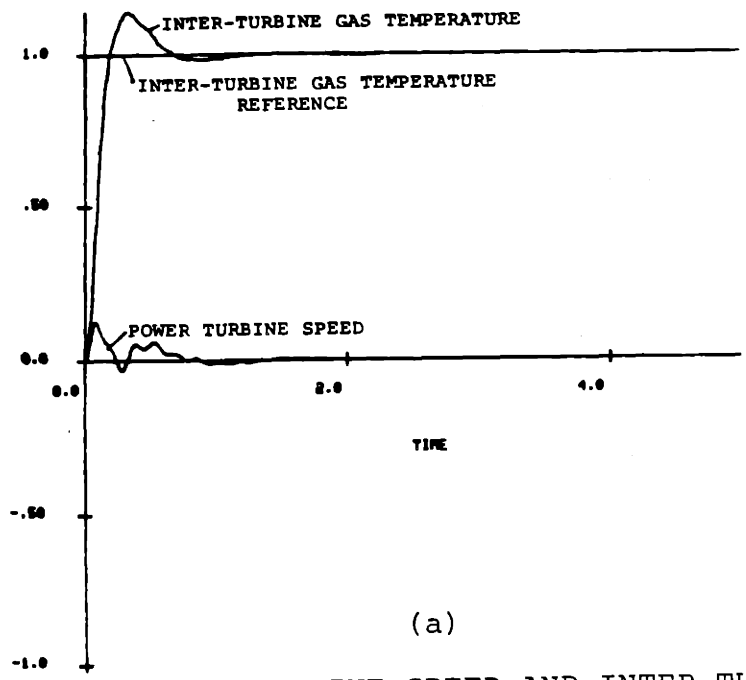

(a)

POWER TURBINE SPEED AND INTER-TURBINE GAS TEMPERATURE OUTPUTS

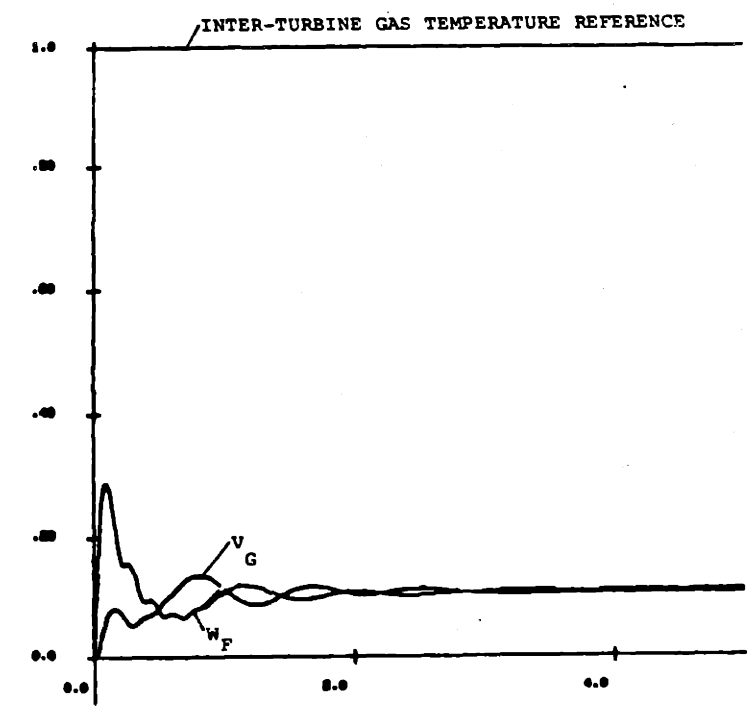

(b)

W_F AND V_G INPUT VARIABLES

FIGURE 4.49: LINEAR SIMULATION OF STEP RESPONSE OF COMPENSATED SYSTEM TO INTER-TURBINE GAS TEMPERATURE DEMAND

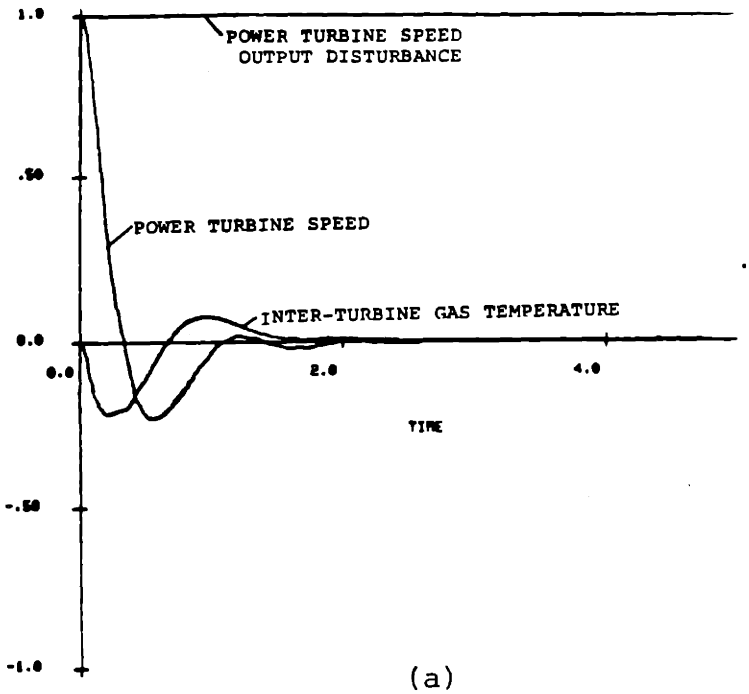

(a)

POWER TURBINE SPEED AND INTER-TURBINE GAS TEMPERATURE OUTPUTS

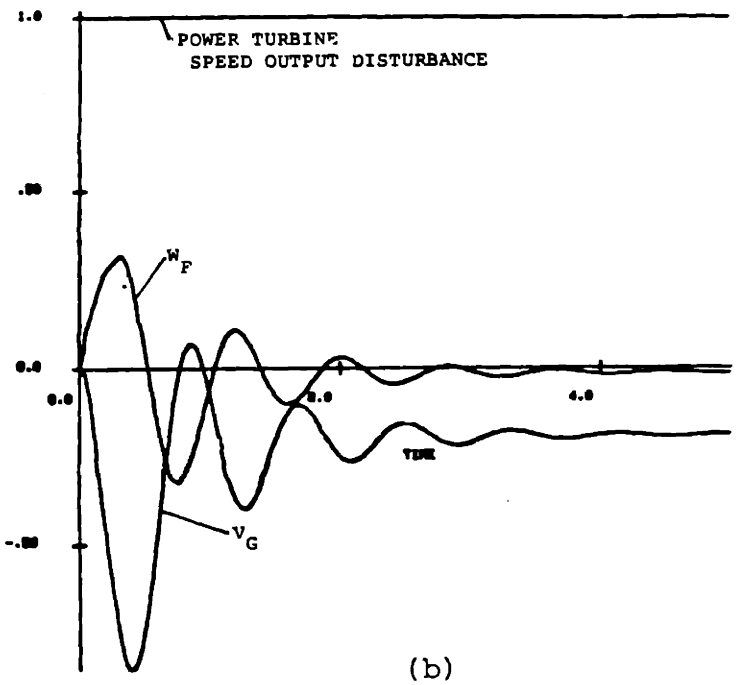

(b)

W_F AND V_G INPUT VARIABLES

FIGURE 4.50: LINEAR SIMULATION OF STEP RESPONSE OF COMPENSATED SYSTEM TO POWER TURBINE SPEED OUTPUT DISTURBANCE

Note that these simulations (i.e. Figures 4.49 and 4.50) are almost identical to those presented for MIMO System I shown in Figures 4.24 and 4.25. This is not surprising, due to the fact that the recovered loop shape $\underline{T}(j\omega)$ is almost identical for the two system definitions. The response behavior of the two systems to identical inputs will thus be similiar.

The input variables for the command following and disturbance rejection transients are oscillatory as was the case in the previous design. A singular value plot of the command input-to-plant-input transfer function matrix as defined by Eq(4.18) is shown in Figure 4.51. At the frequency at which the plant inputs oscillate (~1 Hz), an underdamped complex pole pair is apparant. These dynamics are attributable to the effect of canceling rotor system dynamics.

Non-Linear Simulation

Non-linear simulations of this design were not entirely successful. A step command to sensed temperature reference is shown in Figure 4.52. The numerical integration routines are suspect because of the short time step needed for successful execution. No interpretation other than the fact that an increase in system responsiveness over the previous design is evident is even attempted. The differential behavior of the system in different command directions is also suspect, and further investigation of this phenomenon is outside the scope of this research.

Design Summary

The performance and robustness goals, as evaluated in the frequency

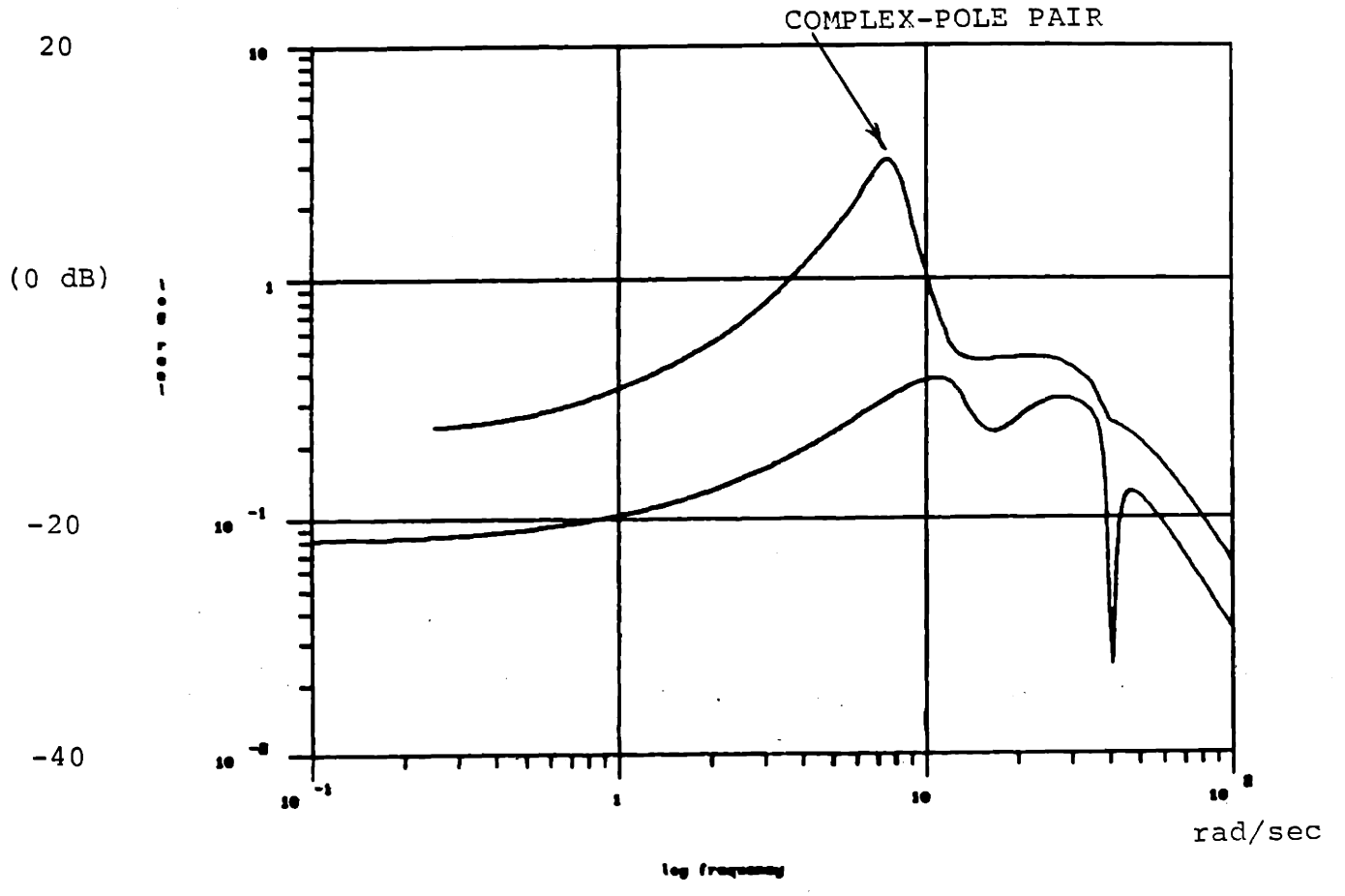

FIGURE 4.51: COMMAND INPUT-TO-PLANT INPUT TRANSFER FUNCTION MATRIX

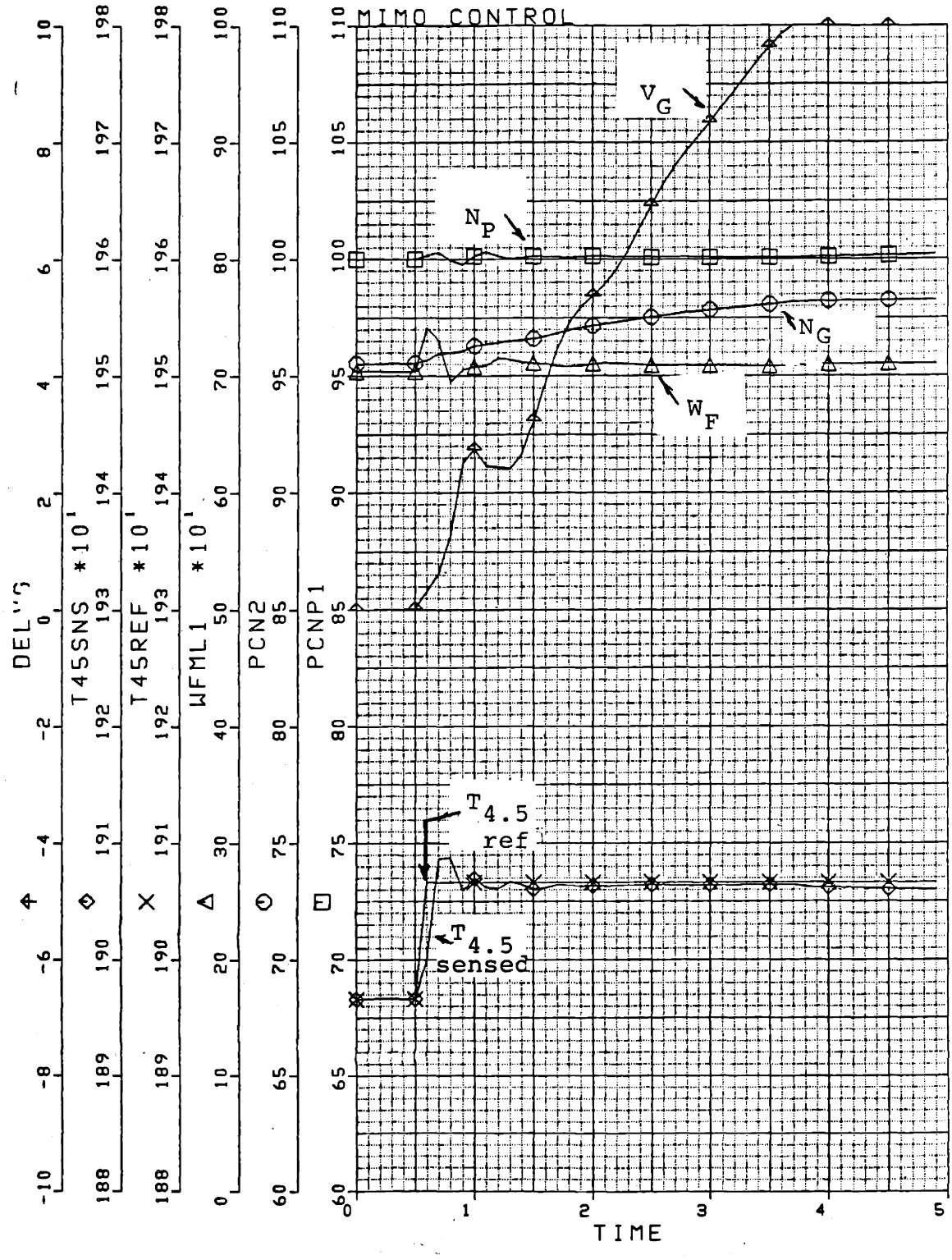

FIGURE 4.52: NON-LINEAR SIMULATION OF MIMO SYSTEM II- N_G=95% CONTROLLER DESIGN- STEP IN $T_{4.5}$ REFERENCE

domain, were achieved for MIMO System II (95% N_g (MIMO) Design Model). Since there were no non-minimum phase zeros within the desired control bandwidth for this particular design model, desireable performance was easily achieved. Performance was achieved at the plant output. Linear simulations of the controlled system displayed fast response times consistent with the interpretations provided by the frequency-dependent plots of the singular values of the system transfer function matrices.

A non-linear simulation of the controlled system was presented which displayed a fast response time consistent with the results provided by the linear simulations.

4.8 Summary

This Chapter represents the culmination of the design work of this research. The LQG/LTR design methodology and resulting control structure was presented in this Chapter and utilized to formulate robust controllers for several system definitions. The system definitions included one SISO system and two MIMO system definitions.

The single SISO system definition provides isochronous power turbine speed governing. The design was performed utilizing the 90% N_g (SISO) Design Model. The LQG/LTR controller for this system definition met the performance and robustness specifications posed in Chapter 3. The transient response of the linear system was demonstrated to be consistent with the frequency domain properties of the system transfer functions. Non-linear simulations comparing the LQG/LTR SISO controller to a current SISO controller

displayed the potential for an increase in performance attainable with an LQG/LTR controller. The increase in performance was quantified through examining the sensitivity transfer functions of both the LQG/LTR and the current SISO controller. The LQG/LTR controller displayed a significant increase in output load disturbance rejection capability as compared to the current SISO controller.

The first MIMO system definition, MIMO System I, provides isochronous speed governing for both the power turbine and gas generator. The design was carried out at one operating condition as represented by the 83% N_g (MIMO) Design Model. Performance and robustness specifications, posed in Chapter 3, were satisfied at the plant output. The evaluation of the frequency-dependent singular value plots of loop transfer function matrices were illustrative in unfolding why the linear simulations of this system definition depicted fast transient response. The comparison of this MIMO system definition to the SISO controller in rejecting disturbances defined the potential of a multivariable control law in providing fast output disturbance rejection with no steady-state fuel cost. Steady state fuel cost was incurred in the SISO design.

The final MIMO system definition, MIMO System II, was formulated to provide isochronous power turbine speed governing and inter-turbine gas temperature control. The design was performed at two separate operating conditions utilizing the 90% N_g (MIMO) and 95% N_g (MIMO) Design Models. A non-minimum zero within the desired control bandwidth in the 90% N_g (MIMO)

Design Model restricted the range for which $\sigma_{min}\underline{T}(j\omega)$ could be made "large" and performance specifications could not be met. Performance was evaluated at the plant output. Robustness was achieved however. The interpretations provided by frequency-dependent singular value plots of the system transfer function matrices explained the slow transient response of the system as displayed by linear and non-linear transient simulations. Performance and robustness goals were realized for the 95% N_g (MIMO) Design Model as evaluated at the plant output. There were no non-minimum phase zeros within the desired controller bandwidth for the 95% N_g (MIMO) Design Model. Linear and non-linear simulations showed fast transient response times as expected based on the interpretations provided by the frequency-dependent singular value plots of the system transfer function matrices.

In conclusion, this Chapter has provided several detailed examples of the LQG/LTR design methodology. The results, while not intended as final engineering designs, do demonstrate that the LQG/LTR design methodology is an invaluable tool in control system design. This conclusion is supported by the increase in system performance demonstrated by the SISO LQG/LTR design over a current design and in the results provided by the linear and non-linear simulations of the MIMO system designs. Specifically, the results of the MIMO system designs demonstrated that the coordinated control of several variables can provide an increase in system performance that is not attainable with conventional scalar control.

5. SUMMARY AND DIRECTIONS FOR FURTHER RESEARCH

5.1 Summary

This thesis has provided several detailed examples of the application of the LQG/LTR design methodology to the GE T700 engine. The design process was presented from the fundamental first steps of system description to controller evaluation. Although final engineering designs were not formulated, the LQG/LTR design methodology is shown to provide a systematic control design methodology that embodies the classical frequency domain approach to controller synthesis.

The turboshaft engine/helicopter system and its operational characteristics were described in detail in order to examine the physical requirements on system operation and to provide the motivation for the investigation of an LQG/LTR controller formulation for the turboshaft engine/helicopter system. A series of linear models were presented and several systems, one SISO and two MIMO, were defined. The linear models of the system definitions were examined utilizing eigenvalue/eigenvector analysis, modal decomposition and the singular value decomposition to provide physical insight into the open-loop system characteristics. The concept of frequency-dependent singular value plots of a system transfer function matrix as utilized to examine system dynamics was presented. The insight gained from linear model analysis coupled with the system operational presentation was utilized to pose frequency domain performance specifications. Robustness requirements were posed utilizing a novel method that characterizes the maximum system open-loop magnitude variations with frequency due to

realizeable helicopter rotor system parametric variations.

The controller designs and evaluations demonstrated that the LQG/LTR SISO controller, as compared to the current controller, shows the potential for system performance improvement. The MIMO controller evaluations demonstrated that the coordinated control of several variables can provide a system with performance capabilities outside of the realm of conventional scalar controllers. The performance restrictions associated with the presence of a non-minimum phase zero within the desired control bandwidth was poignantly displayed in one case. The utilization of frequency-dependent plots of the singular values of a system loop transfer function matrix was instrumental throughout the controller design process, especially in interpreting MIMO system transient behavior.

5.2 Conclusions and Directions for Further Research

It is obvious throughout this research that the LQG/LTR design methodology provides a systematic means to an end. The desired end is a high performance controller. The LQG/LTR methodology is particularly invaluable in MIMO linear system design.

It also became obvious in the course of this research that the transitioning of the linear control design into the non-linear environment is not a trivial task. A fundamental problem encountered by the author was the requirement for adequate software to handle non-linear transient evaluation of the controller. While the bandwidths of the systems examined in this research were only ~10 rad/sec, the internal control integrators were high gain and the

integration routines in the non-linear simulation program would not converge.

The subject of gain scheduling of a series of controllers designed at specific operating conditions is a common approach utilized to achieve a global design. The number of design points required for satisfactory system performance and the required characteristics of the scheduling parameter are still open issues.

The utilization of integrators in the primary control loops to achieve specified performance have associated windup and saturation concerns. Questions of stability and degraded performance in the presence of integrator windup/saturation or any inherent system non-linearity are still to be answered.

In most cases, the concerns associated with the transitioning of the linear controller design to a global non-linear controller are problem dependent and unique solutions may be available based on the insight of the individual designer.

While not expounded in this thesis, there are several explicit frequency domain [23] relations that relate the design parameters of the LQG/LTR design methodology to the singular value loop shapes. Further research is needed to expand the existing relations and to develop new ones.

The applicability of directionality, i.e. making one control loop purposely slower than the other as it can be achieved with the LQG/LTR design methodology, has still to be determined.

APPENDIX A

NUMERICAL RESULTS OF MODEL GENERATION

SECTION	CONTENTS
1	Engine Partial Derivatives
2	$T_{4.5}$ Sensor Time Constant
3	Helicopter Rotor System Parameters

SECTION 1: UNBALANCED TORQUE PARTIAL DERIVATIVES ($\delta A/\delta B$)

(NUMERICAL RESULTS OF MODEL GENERATION)

Case		1	2	3	4	5	6	
		F/I				IRP		Units
Ng *1		73.7	83.0	90.0	95	97.2	100.0	%
Np		20900	20900	20900	20900	20900	20900	RPM
Wf		156	219	420	687	772	831	PPH
Tt.5		1387	1439	1611	1827	1968	2054	°R
Ps3		69	96	165.7	224	241	255	PSIA
SHP		0	155	763	1454	1709	1822	SHP
$\frac{\delta A}{A}$ / $\frac{\delta B}{B}$								
Qg	Ng	-.0025	-.0090	-.017	-.029	-.011	-.0068	FT-LB/RPM
Qp	Ng	+.0022	+.012	+.029	+.042	+.011	+.0050	FT-LB/RPM
T4.5	Ng	-.034	-.063	-.066	-.070	+.0073	+.0070	°R/RPM
Ps3	Ng	+.0037	+.0093	+.016	+.020	+.0045	+.0020	PSI/RPM
Qg	NP	-.00035	+.0001	-.00070	-.001	-.0010	-.0009	/RPM
Qp	Np	-.0041	-.0060	-.0099	-.014	-.015	-.015	
T4.5	Np	+.0019	-	+.0019	+.002	+.002	+.0019	
Ps3	NP	-	-	-	-	-	-	
Qg	Wf	+.26	+.24	+.21	+.18	+.17	+.165	/PPH
Qp	Wf	+.25	+.29	+.35	+.35	+.36	+.35	
T4.5	Wf	+4.68	+3.27	+1.87	+1.45	+1.31	+1.29	
Ps3	Wf	+.070	+.070	+.082	+.076	+.077	+.076	
Qg	VG	+.335	+1.69	+3.51	+4.62	+1.66	+.375	/DEG
Qp	VG	-.23	-2.23	-5.66	-7.53	-1.35	-.24	
T4.5	VG	+3.1	+11.1	+12.35	+10.45	-1.35	-.55	
Ps3	VG	-.33	-1.66	-2.95	-3.275	-.46	-.075	

*1 POWER LEVEL IS DENOTED BY % N_g. SYSTEM MODEL IS AS DEFINED IN TABLE 2.2.

SECTION 2: THERMOCOUPLE TIME CONSTANT

N_G (%)	TTC (sec)
100	1.88
98	1.93
96	1.98
95	2.00
94	2.07
92	2.11
90	2.20

SECTION 3: Helicopter Rotor System Parameter Values

J_T=.01648 ft-lb-sec/RPM

K_{MR}=5.265 ft-lb/RPM-sec

D_{MR}=.1445 ft-lb/RPM

J_{MR}=.1103 ft-lb-sec/RPM

D_{AM}=.05 ft-lb/RPM

K_{TR}=6.296 ft-lb/RPM-sec

J_{TR}=.00538 ft-lb-sec/RPM

D_{AT}=.002 ft-lb/RPM

APPENDIX B

STATE-SPACE DESCRIPTIONS OF DESIGN MODELS UTILIZED FOR COMPENSATOR DESIGNS

SECTION	CONTENTS
1	90% N_g (SISO) Design Model
2	83% N_g (MIMO) Design Model MIMO System I
3	90% N_g (MIMO) Design Model MIMO System II
4	95% N_g (MIMO) Design Model MIMO System II

SECTION 1:90% N_G DESIGN MODEL(SISO)

A MATRIX

Number of rows = 6
Number of columns = 6

-3.6400E+00	0.0000E+00	0.0000E+00	0.0000E+00	0.0000E+00	0.0000E+00
3.5100E+00	-1.0900E+00	-6.0600E+01	0.0000E+00	-6.0600E+01	0.0000E+00
5.0800E-01	5.1800E+00	-1.0000E+01	-5.2000E+00	0.0000E+00	0.0000E+00
0.0000E+00	0.0000E+00	9.0600E+00	-4.5000E-01	0.0000E+00	0.0000E+00
0.0000E+00	6.2900E+00	0.0000E+00	0.0000E+00	0.0000E+00	-6.2900E+00
0.0000E+00	0.0000E+00	0.0000E+00	0.0000E+00	1.8600E+02	-3.7100E-01

B MATRIX

Number of rows = 6
Number of columns = 1

4.5200E+01
4.2700E+01
6.1400E+00
0.0000E+00
0.0000E+00
0.0000E+00

C MATRIX

Number of rows = 1
Number of columns = 6

0.0000E+00	1.0000E+00	0.0000E+00	0.0000E+00	0.0000E+00	0.0000E+00

SECTION 2 : 83% N_G DESIGN MODEL (MIMO)

A MATRIX

Number of rows = 7
Number of columns = 7

-1.9200E+00	0.0000E+00	0.0000E+00	0.0000E+00	0.0000E+00	0.0000E+00
3.6200E+02					
1.4500E+00	-7.2700E-01	-6.0600E+01	0.0000E+00	-6.0600E+01	0.0000E+00
-2.7000E+02					
2.1000E-01	5.2000E+00	-1.0000E+01	-5.2000E+00	0.0000E+00	0.0000E+00
-3.9000E+01					
0.0000E+00	0.0000E+00	9.0600E+00	-4.5000E-01	0.0000E+00	0.0000E+00
0.0000E+00					
0.0000E+00	6.2900E+00	0.0000E+00	0.0000E+00	0.0000E+00	-6.2900E+00
0.0000E+00					
0.0000E+00	0.0000E+00	0.0000E+00	0.0000E+00	1.8600E+02	-3.7100E-01
0.0000E+00					
0.0000E+00	0.0000E+00	0.0000E+00	0.0000E+00	0.0000E+00	0.0000E+00
-1.0000E+01					

B MATRIX

Number of rows = 7
Number of columns = 2

5.1300E+01	0.0000E+00
3.5100E+01	0.0000E+00
5.0700E+00	0.0000E+00
0.0000E+00	0.0000E+00
0.0000E+00	0.0000E+00
0.0000E+00	0.0000E+00
0.0000E+00	1.0000E+01

C MATRIX

Number of rows = 2
Number of columns = 7

0.0000E+00	1.0000E+00	0.0000E+00	0.0000E+00	0.0000E+00	0.0000E+00	
0.0000E+00						
1.0000E+00	0.0000E+00	0.0000E+00	0.0000E+00	0.0000E+00	0.0000E+00	
0.0000E+00						

SECTION 3 :90% N_G DESIGN MODEL (MIMO)

A MATRIX

Number of rows = 8
Number of columns = 8

-3.6400E+00	0.0000E+00	0.0000E+00	0.0000E+00	0.0000E+00	0.0000E+00	0.0000E+00	
7.3280E+02	0.0000E+00						
3.5100E+00	-1.0900E+00	-6.0600E+01	0.0000E+00	-6.0600E+01	0.0000E+00		
-6.8750E+02	0.0000E+00						
5.0800E-01	5.1800E+00	-1.0000E+01	-5.2000E+00	0.0000E+00	0.0000E+00		
-9.9300E+01	0.0000E+00						
0.0000E+00	0.0000E+00	9.0600E+00	-4.5000E-01	0.0000E+00	0.0000E+00		
0.0000E+00	0.0000E+00						
0.0000E+00	6.2900E+00	0.0000E+00	0.0000E+00	0.0000E+00	-6.2000E+00		
0.0000E+00	0.0000E+00						
0.0000E+00	0.0000E+00	0.0000E+00	0.0000E+00	1.8600E+02	-3.7100E-01		
0.0000E+00	0.0000E+00						
0.0000E+00	0.0000E+00	0.0000E+00	0.0000E+00	0.0000E+00	0.0000E+00		
-1.0000E+01	0.0000E+00						
-6.6000E-02	0.0000E+00	0.0000E+00	0.0000E+00	0.0000E+00	0.0000E+00		
1.2360E+01	-2.2000E+00						

B MATRIX

Number of rows = 8
Number of columns = 2

4.5200E+01	0.0000E+00
4.2700E+01	0.0000E+00
6.1400E+00	0.0000E+00
0.0000E+00	0.0000E+00
0.0000E+00	0.0000E+00
0.0000E+00	0.0000E+00
0.0000E+00	1.0000E+01
1.8700E+00	0.0000E+00

C MATRIX

Number of rows = 2
Number of columns = 8

0.0000E+00	1.0000E+00	0.0000E+00	0.0000E+00	0.0000E+00	0.0000E+00		
0.0000E+00	0.0000E+00						
0.0000E+00	0.0000E+00	0.0000E+00	0.0000E+00	0.0000E+00	0.0000E+00		
0.0000E+00	1.0000E+00						

SECTION 4 : 95% N_G DESIGN MODEL (MIMO)

A MATRIX

Number of rows = 8
Number of columns = 8

-6.2300E+00	0.0000E+00	0.0000E+00	0.0000E+00	0.0000E+00	0.0000E+00	0.0000E+00	0.0000E+00
9.9100E+02	0.0000E+00						
2.5400E+00	-1.6900E+00	-6.0600E+01	0.0000E+00	-6.0600E+01	0.0000E+00	0.0000E+00	0.0000E+00
-9.1400E+02	0.0000E+00						
7.3600E-01	5.0200E+00	-1.0000E+01	-5.2000E+00	0.0000E+00	0.0000E+00	0.0000E+00	0.0000E+00
-1.3200E+02	0.0000E+00						
0.0000E+00	0.0000E+00	9.0600E+00	-4.5000E-01	0.0000E+00	0.0000E+00	0.0000E+00	0.0000E+00
0.0000E+00	0.0000E+00						
0.0000E+00	6.2900E+00	0.0000E+00	0.0000E+00	0.0000E+00	-6.2900E+00	0.0000E+00	0.0000E+00
0.0000E+00	0.0000E+00						
0.0000E+00	0.0000E+00	0.0000E+00	0.0000E+00	1.8600E+02	-3.7100E-01	0.0000E+00	0.0000E+00
0.0000E+00	0.0000E+00						
0.0000E+00	0.0000E+00	0.0000E+00	0.0000E+00	0.0000E+00	0.0000E+00	0.0000E+00	0.0000E+00
-1.0000E+01	0.0000E+00						
-7.0000E-02	0.0000E+00	0.0000E+00	0.0000E+00	0.0000E+00	0.0000E+00	0.0000E+00	0.0000E+00
1.0450E+01	-2.0000E+00						

B MATRIX

Number of rows = 8
Number of columns = 2

3.8600E+01	0.0000E+00
4.2400E+01	0.0000E+00
6.1400E+00	0.0000E+00
0.0000E+00	0.0000E+00
0.0000E+00	0.0000E+00
0.0000E+00	0.0000E+00
0.0000E+00	1.0000E+01
1.4500E+00	0.0000E+00

C MATRIX

Number of rows = 2
Number of columns = 8

0.0000E+00	1.0000E+00	0.0000E+00	0.0000E+00	0.0000E+00	0.0000E+00	0.0000E+00	0.0000E+00
0.0000E+00	0.0000E+00						
0.0000E+00	0.0000E+00	0.0000E+00	0.0000E+00	0.0000E+00	0.0000E+00	0.0000E+00	0.0000E+00
0.0000E+00	1.0000E+00						

APPENDIX C

STEADY-STATE GAIN AND SCALING MATRICES UTILIZED FOR SVD ANALYSIS

SECTION	CONTENTS
1	83% N_g Design Model - MIMO System
2	90% N_g Design Model - MIMO System
3	95% N_g Design Model - MIMO System

SECTION 1 : 83% N_G DESIGN MODEL

MIMO SYSTEM I

$\underline{G}_s(0)$ (2, 2) REAL

	COL 1	COL 2
1.	0.94500E-01	0.42700E-03
2.	0.59600E-01	0.41900E-01

$\underline{N}_{uu}$ (2, 2) REAL

	COL 1	COL 2
1.	1.0000	0.00000E+00
2.	0.00000E+00	0.10000

$\underline{N}_y$ (2, 2) REAL

	COL 1	COL 2
1.	200.00	0.00000E+00
2.	0.00000E+00	447.00

$\underline{G}(0)$ (2, 2) REAL

	COL 1	COL 2
1.	18.900	0.85400
2.	26.700	188.00

$\underline{G}_s(0)$=SCALED STEADY-STATE GAINS

$\underline{N}_u$=INPUT SCALING

$\underline{N}_y$=OUTPUT SCALING

$\underline{G}(0)$=STEADY-STATE GAINS

SECTION 2: 90% N_G DESIGN MODEL

MIMO SYSTEM II

$\underline{G}_s(0)$ (2, 2) REAL

	COL 1	COL 2
1.	0.10096	0.22200E-02
2.	0.65100E-01	-0.58000E-02

$\underline{N}_u$ (2, 2) REAL

	COL 1	COL 2
1.	1.0000	0.00000E+00
2.	0.00000E+00	0.10000

$\underline{N}_y$ (2, 2) REAL

	COL 1	COL 2
1.	200.00	0.00000E+00
2.	0.00000E+00	16.100

$\underline{G}(0)$ (2, 2) REAL

	COL 1	COL 2
1.	20.191	4.4470
2.	1.0500	-0.93600

$\underline{G}_s(0)$=SCALED STEADY-STATE GAINS

$\underline{N}_u$=INPUT SCALING

$\underline{N}_y$=OUTPUT SCALING

$\underline{G}(0)$=STEADY-STATE GAINS

SECTION 3 : 95% N_G DESIGN MODEL

MIMO SYSTEM II

$G_s(0)$ (2, 2) REAL

	COL 1	COL 2
1.	0.58800E-01	-0.56000E-01
2.	0.53800E-01	-0.35600E-02

N_u (2, 2) REAL

	COL 1	COL 2
1.	1.0000	0.00000E+00
2.	0.00000E+00	0.10000

N_y (2, 2) REAL

	COL 1	COL 2
1.	200.00	0.00000E+00
2.	0.00000E+00	18.870

$G(0)$ (2, 2) REAL

	COL 1	COL 2
1.	11.760	-112.00
2.	1.0160	-0.68400

$G_s(0)$=SCALED STEADY-STATE GAINS

N_u=INPUT SCALING

N_y=OUTPUT SCALING

$G(0)$=STEADY-STATE GAINS

APPENDIX D

DERIVATION OF HELICOPTER

LOAD DISTURBANCE DYNAMICS

DISTURBANCE DYNAMICS

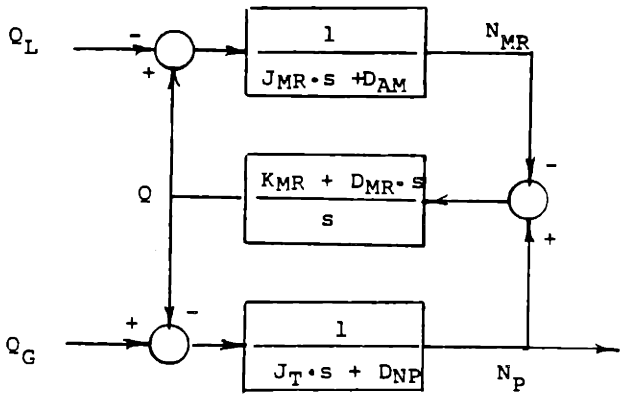

$$\dot{\underline{x}} = \frac{d}{dt}\begin{bmatrix} N_{MR} \\ Q \\ N_P \end{bmatrix} \begin{bmatrix} -D_{AM}/J_{MR} & 1/J_{MR} & 0 \\ K_{MR} + \frac{D_{MR} D_{AM}}{J_{MR}} & -D_{MR}/J_T - D_{MR}/J_{MR} & K_{MR} - D_{MR}/J_T \\ 0 & -1/J_T & -D_{NP}/J_T \end{bmatrix} \begin{bmatrix} N_{MR} \\ Q \\ N_P \end{bmatrix}$$

$$+ \begin{bmatrix} -1/J_{MR} & 0 \\ D_{MR}/J_{MR} & D_{MR}/J_T \\ 0 & 1/J_T \end{bmatrix} \begin{bmatrix} Q_L \\ Q_G \end{bmatrix}$$

LOAD DISTURBANCE TO N_P OUTPUT

$$\underline{y} = \begin{bmatrix} 0 & 0 & 1 \end{bmatrix} \underline{x}$$

$$u = Q_L$$

APPENDIX E

STATE-SPACE DESCRIPTION OF

SISO LQG/LTR COMPENSATOR

90% N_G (SISO) LQG/LTR COMPENSATOR

A MATRIX

Number of rows = 7
Number of columns = 7

-3.6400E+00	-1.0136E+02	0.0000E+00	0.0000E+00	0.0000E+00	0.0000E+00
4.5200E+01					
3.5100E+00	-8.2274E+01	-6.0600E+01	0.0000E+00	-6.0600E+01	0.0000E+00
4.2700E+01					
5.0800E-01	-1.2707E+01	-1.0000E+01	-5.2000E+00	0.0000E+00	0.0000E+00
6.1400E+00					
0.0000E+00	-2.4645E+00	9.0600E+00	-4.5000E-01	0.0000E+00	0.0000E+00
0.0000E+00					
0.0000E+00	3.6842E+00	0.0000E+00	0.0000E+00	0.0000E+00	-6.2900E+00
0.0000E+00					
0.0000E+00	-2.2896E+01	0.0000E+00	0.0000E+00	1.8600E+02	-3.7100E-01
0.0000E+00					
-7.2885E-02	-1.0010E+02	-3.4960E-02	-6.8024E-01	4.2463E-03	-3.1620E-02
-4.0356E+00					

B MATRIX

Number of rows = 7
Number of columns = 1

1.0136E+02
8.1184E+01
1.7887E+01
2.4645E+00
2.6058E+00
2.2896E+01
1.0000E+02

C MATRIX

Number of rows = 1
Number of columns = 7

7.2885E-02	9.6813E-02	3.4960E-02	6.8024E-01	-4.2463E-03	3.1620E-02
4.0356E+00					

APPENDIX F

SCALING MATRICES AND SCALED DESIGN MODELS UTILIZED FOR THE MIMO SYSTEM CONTROLLER DESIGNS

SECTION	CONTENTS
1	83% N_g (MIMO) Design Model - MIMO System I
2	90% N_g (MIMO) Design Model - MIMO System II
3	95% N_g (MIMO) Design Model - MIMO System II

83% N_q DESIGN MODEL (MIMO)-SCALED SYSTEM MATRICES

A

	COL 1	COL 2	COL 3	COL 4	COL 5
1.	-1.9200	0.00000E+00	0.00000E+00	0.00000E+00	0.00000E+00
2.	3.2400	-0.72700	-0.12120	0.00000E+00	-0.12120E-01
3.	234.00	2600.0	-10.000	-2600.0	0.00000E+00
4.	0.00000E+00	0.00000E+00	0.18120E-01	-0.45000	0.00000E+00
5.	0.00000E+00	31450.	0.00000E+00	0.00000E+00	0.00000E+00
6.	0.00000E+00	0.00000E+00	0.00000E+00	0.00000E+00	0.37200E-01
7.	0.00000E+00	0.00000E+00	0.00000E+00	0.00000E+00	0.00000E+00

	COL 6	COL 7
1.	0.00000E+00	8.0884
2.	0.00000E+00	-13.500
3.	0.00000E+00	-975.00
4.	0.00000E+00	0.00000E+00
5.	-31450.	0.00000E+00
6.	-0.37100	0.00000E+00
7.	0.00000E+00	-10.000

B

	COL 1	COL 2
1.	11.477	0.00000E+00
2.	17.550	0.00000E+00
3.	1267.0	0.00000E+00
4.	0.00000E+00	0.00000E+00
5.	0.00000E+00	0.00000E+00
6.	0.00000E+00	0.00000E+00
7.	0.00000E+00	10.000

C

	COL 1	COL 2	COL 3	COL 4	COL 5
1.	0.00000E+00	1.0000	0.00000E+00	0.00000E+00	0.00000E+00
2.	1.0000	0.00000E+00	0.00000E+00	0.00000E+00	0.00000E+00

	COL 6	COL 7
1.	0.00000E+00	0.00000E+00
2.	0.00000E+00	0.00000E+00

SCALING MATRICES

$\underline{N}_x$

	COL 1	COL 2	COL 3	COL 4	COL 5
1.	447.00	0.00000E+00	0.00000E+00	0.00000E+00	0.00000E+00
2.	0.00000E+00	200.00	0.00000E+00	0.00000E+00	0.00000E+00
3.	0.00000E+00	0.00000E+00	0.40000	0.00000E+00	0.00000E+00
4.	0.00000E+00	0.00000E+00	0.00000E+00	200.00	0.00000E+00
5.	0.00000E+00	0.00000E+00	0.00000E+00	0.00000E+00	0.40000E-01
6.	0.00000E+00	0.00000E+00	0.00000E+00	0.00000E+00	0.00000E+00
7.	0.00000E+00	0.00000E+00	0.00000E+00	0.00000E+00	0.00000E+00
8.	0.00000E+00	0.00000E+00	0.00000E+00	0.00000E+00	0.00000E+00

	COL 6	COL 7	COL 8
1.	0.00000E+00	0.00000E+00	0.00000E+00
2.	0.00000E+00	0.00000E+00	0.00000E+00
3.	0.00000E+00	0.00000E+00	0.00000E+00
4.	0.00000E+00	0.00000E+00	0.00000E+00
5.	0.00000E+00	0.00000E+00	0.00000E+00
6.	200.00	0.00000E+00	0.00000E+00
7.	0.00000E+00	5.0000	0.00000E+00
8.	0.00000E+00	0.00000E+00	10.000

$\underline{N}_u$

	COL 1	COL 2
1.	100.00	0.00000E+00
2.	0.00000E+00	10.000

$\underline{N}_y$

	COL 1	COL 2
1.	200.00	0.00000E+00
2.	0.00000E+00	447.00

90% N_q DESIGN MODEL (MIMO)-SCALED SYSTEM MATRICES

A

	COL 1	COL 2	COL 3	COL 4	COL 5
1.	-3.6480	0.00000E+00	0.00000E+00	0.00000E+00	0.00000E+00
2.	7.8400	-1.0900	-1.2120	0.00000E+00	-0.15000
3.	56.760	259.00	-10.000	-260.00	0.00000E+00
4.	0.00000E+00	0.00000E+00	0.18120	-0.45000	0.00000E+00
5.	0.00000E+00	2516.0	0.00000E+00	0.00000E+00	0.00000E+00
6.	0.00000E+00	0.00000E+00	0.00000E+00	0.00000E+00	0.46500
7.	-5.9000	0.00000E+00	0.00000E+00	0.00000E+00	0.00000E+00
8.	0.00000E+00	0.00000E+00	0.00000E+00	0.00000E+00	0.00000E+00

	COL 6	COL 7	COL 8
1.	0.00000E+00	0.00000E+00	16.390
2.	0.00000E+00	0.00000E+00	-34.380
3.	0.00000E+00	0.00000E+00	-248.00
4.	0.00000E+00	0.00000E+00	0.00000E+00
5.	-2516.0	0.00000E+00	0.00000E+00
6.	-0.37100	0.00000E+00	0.00000E+00
7.	0.00000E+00	-22.000E+00	24.700
8.	0.00000E+00	66.000	-10.000

B

	COL 1	COL 2
1.	1.0110	0.00000E+00
2.	2.1350	0.00000E+00
3.	5.3500	0.00000E+00
4.	0.00000E+00	0.00000E+00
5.	0.00000E+00	0.00000E+00
6.	0.00000E+00	0.00000E+00
7.	3.7400	0.00000E+00
8.	0.00000E+00	10.000

C

	COL 1	COL 2	COL 3	COL 4	COL 5
1.	0.00000E+00	1.0000	0.00000E+00	0.00000E+00	0.00000E+00
2.	0.00000E+00	0.00000E+00	0.00000E+00	0.00000E+00	0.00000E+00

	COL 6	COL 7	COL 8
1.	0.00000E+00	0.00000E+00	0.00000E+00
2.	0.00000E+00	1.0000	0.00000E+00

SCALING MATRICES

$\underline{N}_x$

	COL 1	COL 2	COL 3	COL 4	COL 5
1.	447.00	0.00000E+00	0.00000E+00	0.00000E+00	0.00000E+00
2.	0.00000E+00	200.00	0.00000E+00	0.00000E+00	0.00000E+00
3.	0.00000E+00	0.00000E+00	4.0000	0.00000E+00	0.00000E+00
4.	0.00000E+00	0.00000E+00	0.00000E+00	200.00	0.00000E+00
5.	0.00000E+00	0.00000E+00	0.00000E+00	0.00000E+00	0.50000
6.	0.00000E+00	0.00000E+00	0.00000E+00	0.00000E+00	0.00000E+00
7.	0.00000E+00	0.00000E+00	0.00000E+00	0.00000E+00	0.00000E+00
8.	0.00000E+00	0.00000E+00	0.00000E+00	0.00000E+00	0.00000E+00

	COL 6	COL 7	COL 8
1.	0.00000E+00	0.00000E+00	0.00000E+00
2.	0.00000E+00	0.00000E+00	0.00000E+00
3.	0.00000E+00	0.00000E+00	0.00000E+00
4.	0.00000E+00	0.00000E+00	0.00000E+00
5.	0.00000E+00	0.00000E+00	0.00000E+00
6.	200.00	0.00000E+00	0.00000E+00
7.	0.00000E+00	5.0000	0.00000E+00
8.	0.00000E+00	0.00000E+00	10.000

$\underline{N}_u$

	COL 1	COL 2
1.	10.000	0.00000E+00
2.	0.00000E+00	10.000

$\underline{N}_y$

	COL 1	COL 2
1.	200.00	0.00000E+00
2.	0.00000E+00	5.0000

95% N_g DESIGN MODEL (MIMO)-SCALED SYSTEM MATRICES

A

	COL 1	COL 2	COL 3	COL 4	COL 5
1.	-6.2300	0.00000E+00	0.00000E+00	0.00000E+00	0.00000E+00
2.	5.6760	-1.6900	-1.2120	0.00000E+00	-0.15000
3.	82.248	251.00	-10.000	-260.00	0.00000E+00
4.	0.00000E+00	0.00000E+00	0.18120	-0.45000	0.00000E+00
5.	0.00000E+00	2516.0	0.00000E+00	0.00000E+00	0.00000E+00
6.	0.00000E+00	0.00000E+00	0.00000E+00	0.00000E+00	0.46500
7.	-6.2580	0.00000E+00	0.00000E+00	0.00000E+00	0.00000E+00
8.	0.00000E+00	0.00000E+00	0.00000E+00	0.00000E+00	0.00000E+00

	COL 6	COL 7	COL 8
1.	0.00000E+00	0.00000E+00	22.170
2.	0.00000E+00	0.00000E+00	-45.700
3.	0.00000E+00	0.00000E+00	-330.00
4.	0.00000E+00	0.00000E+00	0.00000E+00
5.	-2516.0	0.00000E+00	0.00000E+00
6.	-0.37100	0.00000E+00	0.00000E+00
7.	0.00000E+00	-2.0000	20.900
8.	0.00000E+00	0.00000E+00	-10.000

B

	COL 1	COL 2
1.	8.6400	0.00000E+00
2.	21.200	0.00000E+00
3.	153.50	0.00000E+00
4.	0.00000E+00	0.00000E+00
5.	0.00000E+00	0.00000E+00
6.	0.00000E+00	0.00000E+00
7.	29.000	0.00000E+00
8.	0.00000E+00	10.000

C

	COL 1	COL 2	COL 3	COL 4	COL 5
1.	0.00000E+00	1.0000	0.00000E+00	0.00000E+00	0.00000E+00
2.	0.00000E+00	0.00000E+00	0.00000E+00	0.00000E+00	0.00000E+00

	COL 6	COL 7	COL 8
1.	0.00000E+00	0.00000E+00	0.00000E+00
2.	0.00000E+00	1.0000	0.00000E+00

SCALING MATRICES

$\underline{N}_x$

	COL 1	COL 2	COL 3	COL 4	COL 5
1.	447.00	0.00000E+00	0.00000E+00	0.00000E+00	0.00000E+00
2.	0.00000E+00	200.00	0.00000E+00	0.00000E+00	0.00000E+00
3.	0.00000E+00	0.00000E+00	4.0000	0.00000E+00	0.00000E+00
4.	0.00000E+00	0.00000E+00	0.00000E+00	200.00	0.00000E+00
5.	0.00000E+00	0.00000E+00	0.00000E+00	0.00000E+00	0.50000
6.	0.00000E+00	0.00000E+00	0.00000E+00	0.00000E+00	0.00000E+00
7.	0.00000E+00	0.00000E+00	0.00000E+00	0.00000E+00	0.00000E+00
8.	0.00000E+00	0.00000E+00	0.00000E+00	0.00000E+00	0.00000E+00

	COL 6	COL 7	COL 8
1.	0.00000E+00	0.00000E+00	0.00000E+00
2.	0.00000E+00	0.00000E+00	0.00000E+00
3.	0.00000E+00	0.00000E+00	0.00000E+00
4.	0.00000E+00	0.00000E+00	0.00000E+00
5.	0.00000E+00	0.00000E+00	0.00000E+00
6.	200.00	0.00000E+00	0.00000E+00
7.	0.00000E+00	5.0000	0.00000E+00
8.	0.00000E+00	0.00000E+00	10.000

$\underline{N}_u$

	COL 1	COL 2
1.	100.00	0.00000E+00
2.	0.00000E+00	10.000

$\underline{N}_y$

	COL 1	COL 2
1.	200.00	0.00000E+00
2.	0.00000E+00	5.0000

APPENDIX G

STATE-SPACE DESCRIPTION OF MIMO LQG/LTR CONTROLLERS

SECTION 1: 83% N_G (MIMO) LQG/LTR COMPENSATOR

```
-1.5921E+01 -2.8341E+00  0.0000E+00  0.0000E+00  0.0000E+00  0.0000E+00
 1.1480E+01  8.0900E+00  0.0000E+00

 1.8229E+00 -1.1158E+01 -1.8120E-01  0.0000E+00 -1.2120E-02  0.0000E+00
 1.7600E+01 -1.3500E+01  0.0000E+00

-2.3820E+02  7.3161E+00 -1.0000E+01 -8.6000E+03  0.0000E+00  0.0000E+00
 1.2680E+03 -9.7500E+02  0.0000E+00

 3.3401E-01 -5.4873E+00  1.8120E-02 -4.5000E-01  0.0000E+00  0.0000E+00
 0.0000E+00  0.0000E+00  0.0000E+00

-2.8187E+02  3.0468E+04  0.0000E+00  0.0000E+00  0.0000E+00 -3.1450E+04
 0.0000E+00  0.0000E+00  0.0000E+00

-1.6424E+00 -7.2544E+00  0.0000E+00  0.0000E+00  3.7200E-02 -3.7100E-01
 0.0000E+00  0.0000E+00  0.0000E+00

-3.9191E+01 -2.8978E+01  5.9378E-02 -1.9194E+00  8.8353E-03  1.3430E+00
-3.5029E+01 -5.4307E+00 -4.0645E+00

-6.3336E+00  7.8503E+00  0.0000E+00  0.0000E+00  0.0000E+00  0.0000E+00
 0.0000E+00 -1.0000E+01  1.0000E+01

-1.9867E+01  1.4234E+01 -7.8450E-02  8.3322E+01 -8.6488E-04  4.1858E+00
-4.0645E+00 -1.4283E+01 -1.6405E+01
```

B MATRIX

```
Number of rows =  8
Number of columns =  2

 2.8341E+00  1.4001E+01

 1.0431E+01  1.4171E+00

 1.8684E+03  6.2280E+02

 5.4873E+00 -3.3401E-01

 9.8245E+02  2.8187E+02

 7.2544E+00  1.6424E+00

 1.0[illegible]E+01  4.5[illegible]E+00
-.78503  6.336
-9.3208  7.5207
```

C MATRIX

```
Number of rows =  2
Number of columns =  8

 3.2601E+01  1.8342E+01 -5.9376E-02  1.9194E+00 -8.8353E-03 -1.3430E+00
 3.5029E+01  5.4307E+00  4.0645E+00

 1.2347E+01 -4.9129E+00  7.8450E-02 -8.3322E+01  8.6488E-04 -4.1858E+00
 4.0645E+00  1.4283E+01  1.6405E+01
```

SECTION 2 :90% N_G (MIMO) LQG/LTR COMPENSATOR

A MATRIX

-3.6400E+00	-6.4443E+00	0.0000E+00	0.0000E+00	0.0000E+00	0.0000E+00
2.0858E+01	1.0110E+00	1.6390E+01	0.0000E+00		
7.8400E+00	-3.1154E+00	-1.2120E+00	0.0000E+00	-1.5150E-01	0.0000E+00
7.1851E-01	2.1350E+00	-3.4380E+01	0.0000E+00		
5.6760E+01	2.3914E+02	-1.0000E+01	-2.6000E+02	0.0000E+00	0.0000E+00
3.2804E+01	1.5350E+01	-2.4800E+02	0.0000E+00		
0.0000E+00	-1.8741E+00	1.8120E-01	-4.5000E-01	0.0000E+00	0.0000E+00
6.3967E-01	0.0000E+00	0.0000E+00	0.0000E+00		
0.0000E+00	2.5093E+03	0.0000E+00	0.0000E+00	0.0000E+00	-2.5160E+03
3.0867E+00	0.0000E+00	0.0000E+00	0.0000E+00		
0.0000E+00	-1.9995E+00	0.0000E+00	0.0000E+00	4.6500E-01	-3.7100E-01
7.4041E-01	0.0000E+00	0.0000E+00	0.0000E+00		
-5.9000E+00	7.1851E-01	0.0000E+00	0.0000E+00	0.0000E+00	0.0000E+00
-9.0374E+00	3.7400E+00	2.4700E+01	0.0000E+00		
1.3028E+01	-2.3398E+01	1.8067E+00	-2.7186E+01	5.2300E-02	-9.6778E+00
-6.7872E+01	-2.1375E+01	-3.3755E+01	-7.1601E+00		
0.0000E+00	-8.0180E-01	0.0000E+00	0.0000E+00	0.0000E+00	0.0000E+00
3.4879E+00	0.0000E+00	-1.0000E+01	1.0000E+01		
1.0095E+01	2.4501E+01	-2.3792E+00	-8.2960E+00	-2.7744E-01	1.1939E+01
-4.5338E+01	-7.1601E+00	-1.1428E+02	-4.7269E+01		

B MATRIX

Number of rows = 10
Number of columns = 2

6.4443E+00	-2.0858E+01
2.0254E+00	-7.1851E-01
1.9857E+01	-3.2804E+01
1.8741E+00	-6.3967E-01
6.6066E+00	-3.0867E+00
1.9995E+00	-7.4041E-01
-7.1851E-01	7.0374E+00
3.1078E+00	5.8430E-01
8.0180E-01	-3.4879E+00
5.8430E-01	-3.1078E+00

C MATRIX

Number of rows = 2
Number of columns = 10

-1.3028E+01	2.0290E+01	-1.8067E+00	2.7186E+01	-5.2300E-02	9.6778E+00
6.7288E+01	2.1375E+01	3.3755E+01	7.1601E+00		
-1.0095E+01	-2.5086E+01	2.3792E+00	8.2960E+00	2.7744E-01	-1.1939E+01
4.8446E+01	7.1601E+00	1.1428E+02	4.7269E+01		

SECTION 3: 95% N_G(MIMO) LQG/LTR COMPENSATOR

A MATRIX

```
-6.2309E+00  7.4435E+00  0.0000E+00  0.0000E+00  0.0000E+00  0.0000E+00
-4.1186E+00  8.6400E+00  2.2170E+01  0.0000E+00

 5.6760E+00 -8.1100E+00 -1.2120E+00  0.0000E+00 -1.5150E-01  0.0000E+00
-5.3101E-01  2.1200E+01 -4.5700E+01  0.0000E+00

 8.2248E+01  1.5401E+02 -1.0000E+01 -2.6000E+02  0.0000E+00  0.0000E+00
-3.4039E+01  1.5350E+02 -3.3000E+02  0.0000E+00

 0.0000E+00 -4.0367E+00  1.8120E-01 -4.5000E-01  0.0000E+00  0.0000E+00
-5.9873E-01  0.0000E+00  0.0000E+00  0.0000E+00

 0.0000E+00  2.4718E+01  0.0000E+00  0.0000E+00  0.0000E+00 -2.5160E+01
-2.7580E+00  0.0000E+00  0.0000E+00  0.0000E+00

 0.0000E+00 -5.8287E+00  0.0000E+00  0.0000E+00  4.6500E-01 -3.7100E-01
-5.9745E-01  0.0000E+00  0.0000E+00  0.0000E+00

-6.2580E+00 -1.0620E+00  0.0000E+00  0.0000E+00  0.0000E+00  0.0000E+00
-1.2706E+01  2.9000E+01  2.0900E+01  0.0000E+00

 7.1107E+00 -2.2214E+01  4.6318E-01 -9.6675E-01  4.2267E-02  3.5134E+00
-4.5927E+01 -5.5474E+01 -7.3488E+00 -4.6996E+00

 0.0000E+00  3.5603E+00  0.0000E+00  0.0000E+00  0.0000E+00  0.0000E+00
-9.4519E-01  0.0000E+00 -1.0000E+01  1.0000E+01

 9.7422E+00  1.7814E+01 -1.4605E+00  8.0655E+01 -5.8621E-02  9.6329E+00
-1.7260E+01 -4.6996E+00 -4.9458E+01 -3.1098E+01
```

B MATRIX

```
Number of rows = 10
Number of columns =  2

-7.4435E+00  4.1186E+00
 6.4200E+00  5.3101E-01
 9.6993E+01  3.4039E+01
 4.0367E+00  5.9873E-01
 4.4225E+01  2.7580E+00
 5.8287E+00  5.9745E-01
 1.0620E+00  1.0706E+01
 1.6763E+00  2.9317E+00
-3.5603E+00  9.4519E-01
-4.1461E+00  1.1853E+00
```

C MATRIX

```
Number of rows =  2
Number of columns = 10

-7.1107E+00  2.2637E+01 -4.6318E-01  9.6675E-01 -4.2267E-02 -3.5134E+00
 4.2995E+01  5.5474E+01  7.3488E+00  4.6996E+00

-9.7422E+00 -1.2868E+01  1.4605E+00 -8.0655E+01  5.8621E-02 -9.6329E+00
 1.6074E+01  4.6996E+00  4.9458E+01  3.1098E+01
```

REFERENCES

1. R. C. DeHoff and W. E. Hall, "Optimal Control of Turbine Engines," Journal of Dynamic Systems, Measurements, and Control, Vol. 101, June 1979.

2. J. Zeller, Belehtinen and W. Merril, "The Role of Modern Control Theory in the Design of Controls for Aircraft Gas Turbine Engines," NASA TM-82815, January 1982.

3. M. S. Idelchick, "An Application of Modern Control Theory to a High-bypass Variable Compressor Geometry Jet Engine", S. M. Thesis, MIT, Cambridge, Mass., June 1984.

4. P. Kapasouris, "Gain-Scheduled Multivariable Control for the GE-21 Turbofan Engine Using the LQG and LQG/LTR Methodologies", S. M. Thesis, MIT, Cambridge, Mass, June 1984.

5. E. Kappos, "Robust Multivariable Control for the F100 Engine," S. M. Thesis, MIT, Cambridge, Mass., September 1983.

6. R. L. DeHoff, W. Hall, "F100 Multivariable Control Synthesis Program Volume I", AFAPL-TR-77-35, WPAFB, Ohio, 1976.

7. A. D. Pisano, "Control System for Gas Turbine Engine," U.S. Patent No. 4, 276,744, Filed September 19, 1979.

8. G. Stein, J. Doyle, "Multivariable Feedback Design: Concepts for a Classical/Modern Synthesis," IEEE Trans on Automatic Control, AC-26, February 1981.

9. G. Stein and M. Athans, "The LQG/LTR Proceedure for Multivariable Feedback Control Design", IEEE Trans. on Auto. Control, (submitted, May 1984).

10. N. A. Lehtomaki, "Practical Robustness Measures in Multivariable Control System Analysis," Ph.D Thesis, MIT, 1981.

11. W. A. Kucynski, et.al, "The Influence of Engine/Fuel Control Design on Helicopter Dynamics and Handling Qualities," Journal of the American Helicopter Society, Vol. 25, No. 2, April 1980.

12. L. D. Corliss, "A Helicopter Handling Qualities Study of the Effects of Engine Response Characteristics, Height Control Dynamics, and Excess Power on Nap-of-The-Earth Operations," presented at the AHS/NASA Specialists Meeting on Helicopter Handling Qualities, Palo Alto, Ca., 1982.

REFERENCES (continued)

13. A. Gessow, Aerodyanmics of The Helicoper, F. Ungar Pub. Co. 1967.

14. E. T. Vincent, Gas Turbines, McGraw Hill, 1950.

15. C. A. Skina, R. L. DeHoff, "A Practical Approach to Linear Model Analysis for Multivariable Turbine Engine Control Design." Alternatives for Linear Multivariable Control, National Engineering Consortium, 1978,

16. M. Athans. "Multivariable Control System Design Using the LQG/LTR Methodology", Slide Presentation, 1984.

17. H. Kwakernaak, R. Sivan, Linear Optimal Control Systems, Wiley, 1972.

18. M. Athans, "Multivariable Control Systems: Basic Definitions and Issues in Multivariable Feedback Systems." Lecture Notes, MIT Subject 6.232/Ref. 820208.

19. G. Stein, N. R. Sandell, Classical and Modern Methods for Control System Design. Lecture notes, MIT Subject 6.291, Spring 1979.

20. G. Strang, Linear Algebra and its Applications, Academic Press, 1976.

21. M. Athans, "Multivariable Control Systems: Model-Based Compensators for Multivariable Control Synthesis and the LQG Algorithms, "Lecture Notes MIT Subject 6.232/Ref. 820308..

22. J. Doyle, G. Stein, "Robustness with Observers", IEEE Trans. on Automatic Control, Vol. 1C-24, No. 4, August 1979.

23. G. Stein, "LQG Based Multivariable Design: Frequency Domain Interpretation", AGARD-LS-117, 1981.